UNIVERSITY OF CALIFORNIA,

IRVINE

Lyapunov Exponents and Vectors for Determining the Geometric Structure of Nonlinear Dynamical Systems

THESIS

submitted in partial satisfaction of the requirements

for the degree of

MASTER OF SCIENCE

in Mechanical and Aerospace Engineering

by

Ufuk Topcu

Thesis Committee:

Professor Kenneth D. Mease, Chair
Professor Faryar Jabbari
Professor Athanasios Sideris

2005

The thesis of Ufuk Topcu

is approved:

_____

_____

_____

Committee Chair

University of California, Irvine

2005

Dedication

To

my family.

Table of Contents

List of Figures

Acknowledgements

I would like to gratefully thank my advisor, Prof. Kenneth D. Mease, for his constant guidance and support. He introduced me to the area of geometric study of nonlinear systems and taught me most of the subjects in this thesis. I have greatly benefited from him as a role-model of an excellent teacher and researcher.

I would like to thank Prof. Athanassios Sideris for serving on the committee and helping me broaden my knowledge in the area of control and optimization. A special "thank you" goes to Prof. Faryar Jabbari for being on my committee and especially for his help and guidance from the first minute of my presence in Irvine.

Financial support from Holmes family through the Holmes Fellowship and from the National Science Foundation for this research is gratefully acknowledged.

Finally, I wish to express my gratitude to my family for their unending support and encouragement.

Abstract of the Thesis

Lyapunov Exponents and Vectors for Determining the Geometric Structure of Nonlinear Dynamical Systems

By

Ufuk Topcu

Master of Science in Mechanical and Aerospace Engineering

University of California, Irvine, 2005

Professor Kenneth D. Mease, Chair

A new methodology to analyze the timescale structure of finite dimensional nonlinear dynamical systems is developed. Our approach uses the timescale information of the linear variational dynamics associated with the nonlinear dynamics. The tools are Lyapunov exponents and vectors which were firstly defined by Lyapunov to study the asymptotic average rates of growth/decay of functions. In our study, compact regions, that are not necessarily invariant, are considered. Therefore, the finite time approximations of the Lyapunov exponents and vectors are utilized. The relations between the finite time Lyapunov exponents and vectors and their infinite time limits are studied. Conditions under which the finite time versions approximate their infinite time limits are specified.

In model order reduction and in solving a special type of optimal control problems, namely those leading to hyper-sensitive Hamiltonian boundary value problems, slow, stable and unstable manifolds play central roles. The new methodology is applied to finding these manifolds in the state space by using their invariance property. The methods are illustrated with some examples and compared with the existing methods.

Chapter 1

Introduction

1.1 Motivation

In many areas, such as aerospace, chemistry, biology and ecology, engineers and scientists need to analyze, design and control the systems of high complexity. Many of these systems evolve on multiple disparate timescales, on slow and fast timescales, or have stable and unstable modes together. Understanding the timescale structure and its associated geometric structure of the system provides the opportunity of decomposing these systems into subsystems with distinct timescales, and simplifies the analysis of the system and the synthesis of control laws. Decomposition of the original system into slow and fast subsystems enables reduced order analysis. Separate controllers can be designed for each subsystem and combined in an appropriate manner such that the performance of the controller is satisfactory for the original system. Decomposition of the original system into stable and unstable subsystems simplifies the design of controllers, and understanding the geometry associated with a possible stable-unstable decomposition in the state space enables satisfactory suboptimal solutions for some type of optimal control problems.

The aim of this research is to develop practical and accurate tools for diagnosing the multiple timescale structure, understanding the associated geometric structure, and the synthesis of control laws based on the multiple timescale structure. The main applications

presented are slow manifold determination in two-timescale dynamics, which plays a central role in model reduction, and "approximate" solutions for the so called "completely hyper-sensitive boundary value problems" associated with optimal control problems, which have to be solved in the indirect methods for solving optimal control problems. A natural extension of the combination of these two problems is using the computed slow manifold in the model reduction in "hyper-sensitive" optimal control problems, which then becomes "completely hyper-sensitive", and solving the reduced problem. This is the ultimate goal of the ongoing research.

Next section is devoted to two simple motivating examples which are representative of two main problems to which we are going to apply the tools developed in this research.

1.2 Motivating Examples

1.2.1 First Example: Two-Timescale Systems

The trajectories of systems, whose dynamics are on two or more separate timescales, quickly approach hyper-surfaces along which the motion is slower than the motion off the hyper-surface. The asymptotic behavior of the system is along the hyper-surface. This is illustrated in a 2-dimensional example from enzyme kinetics. This example is also used in [1, 2] where it is treated in the context of "singular perturbation" methods.

Example 1.2.1 *Consider 2-dimensional nonlinear dynamics*

$$\begin{aligned} \dot{x}_1 &= x_2 - (x_2 + \kappa)x_1 \\ \dot{x}_2 &= \epsilon[-x_2 + (x_2 + \kappa - \lambda)x_1] \end{aligned} \tag{1.1}$$

For $\epsilon = 0.2$, $\kappa = 1$, and $\lambda = 0.5$, trajectories starting form different initial conditions are shown in Fig. (1.1). All the trajectories approach the so called "slow manifold," which is a 1-dimensional curve in this case; then slide along it and reach the equilibrium point at the origin asymptotically. (Formal definition of a "slow manifold" will be given

in subsequent chapters. For now, it is a lower dimensional object in the state space which attracts or distracts the trajectories off it, and along which the motion is slower.) An approximation of the slow manifold is given in [1]

$$\mathcal{M}_{slow} = \{(x_1, x_2) \in \mathcal{R}^2 \ : \ x_1 = \frac{x_2}{x_2 + \kappa} + \epsilon \frac{\lambda \kappa x_2}{(x_2 + \kappa)^4}\}. \tag{1.2}$$

This 1-dimensional curve is shown in Fig.(1.1). On a representative trajectory emanating from the point $(2, 2.5)$, the elapsed times from the starting point are shown for some points. Up to 100 sec. of integration the trajectory comes to the vicinity of the equilibrium point at the origin. However, during the first second the trajectory comes close to the slow manifold and for the remaining 99 seconds it slides along it.

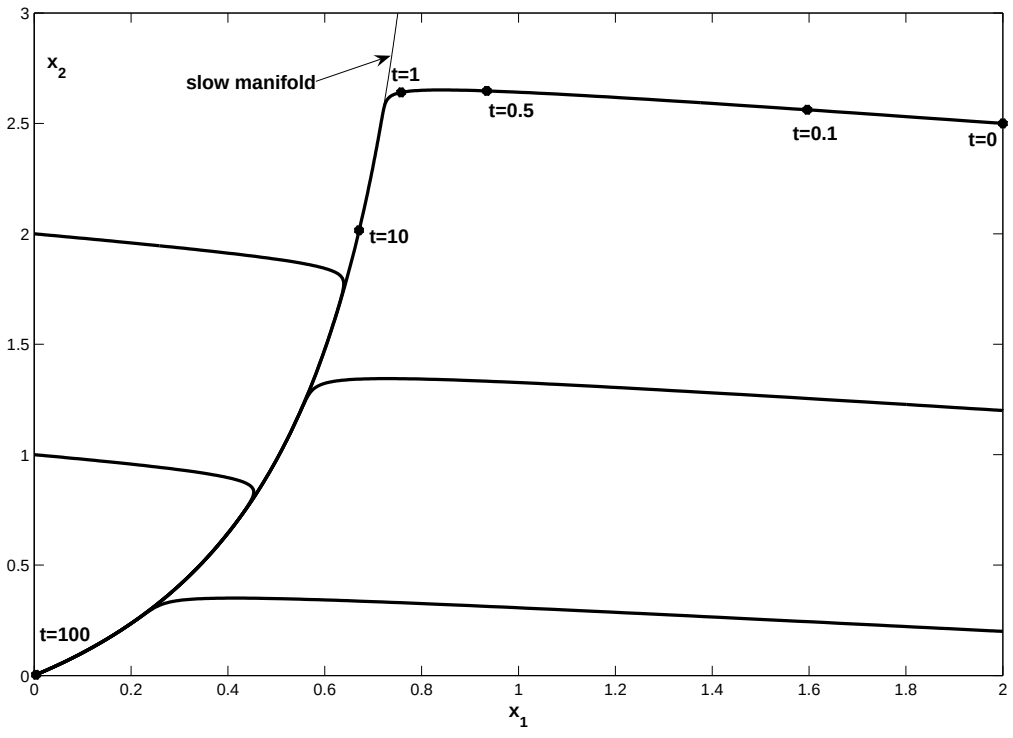

Figure 1.1: State portrait for the enzyme kinetics example.

When the asymptotic study of the system is considered, a model reduction process, treating the fast transient and the slow asymptotic parts of the motion separately, will

simplify the analysis. The "asymptotic" and "transient" parts of the trajectory can be determined separately and pasted by using appropriate matching techniques. Potentially the reduced models can be used to design controllers for slow and fast sub-systems that also provide good stability and performance features for the original system when combined appropriately. Since the core part of the system behavior takes place along the slow manifold, any model reduction procedure would require to find the slow manifold.

1.2.2 Second Example: Optimal Control Problem

Consider the following optimal control problem. Minimize the cost

$$J(x,u) = \int_0^{t_f} (x^2 + u^2) dt \tag{1.3}$$

subject to the dynamical constraint

$$\dot{x} = -x^3 + u \tag{1.4}$$

and the boundary constraints

$$\begin{aligned} x(0) &= 1 \\ x(t_f) &= 1.5 \end{aligned} \tag{1.5}$$

Applying the first-order necessary conditions for optimality leads to the following boundary value problem

$$\begin{aligned} \dot{x} &= -x^3 - \tfrac{\lambda}{2},\ x(0) = 1,\ x(t_f) = 1.5 \\ \dot{\lambda} &= -2x + 3x^2\lambda \end{aligned} \tag{1.6}$$

where $\dot{\lambda} = -\frac{\partial \mathcal{H}}{\partial x}$ and $\mathcal{H} = x^2 + u^2 + \lambda(-x^3 + u)$.

The solutions to this two-point boundary value problem computed by simple "shooting method"[3]. Figure (1.2) shows the optimal trajectories, the solutions of the boundary value problem in (1.6), for some different final times.

For the dynamics in (1.6), the origin is a saddle type equilibrium point. As the final time, t_f, increases, the solution curves in $x - \lambda$ plane approach the stable and unstable

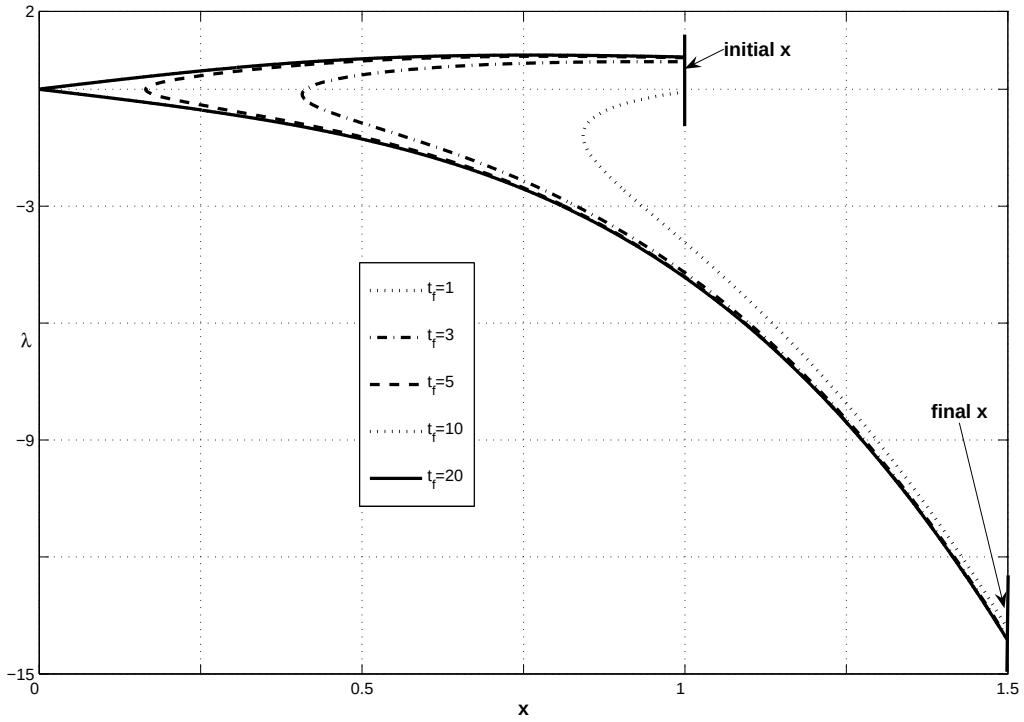

Figure 1.2: Trajectories of the boundary value problem in (1.6) for different final times in $x - \lambda$ plane.

manifolds of the equilibrium point. Figure (1.3) shows x and λ profiles versus the time elapsed along the trajectories. As the final time increases, x and λ stay around zero except the initial and final boundary layers. The solution is determined under the effect of the cost functional and the boundary constraints. Outside the boundary layer segments, the solution tends to minimize the cost functional by minimizing the magnitude of x and λ. In the boundary layers segments, the trajectory quickly goes to the boundary constraints.

Rao and Mease [4, 5] developed a methodology for solving the boundary value problems featuring the described structure. In [5] the procedure is explained as: "As the final time increases, the control objective can be viewed as transitioning from 'steering the system from the initial conditions to the terminal conditions' to 'steering the system from the initial conditions to the equilibrium and then steering the system from the equilibrium

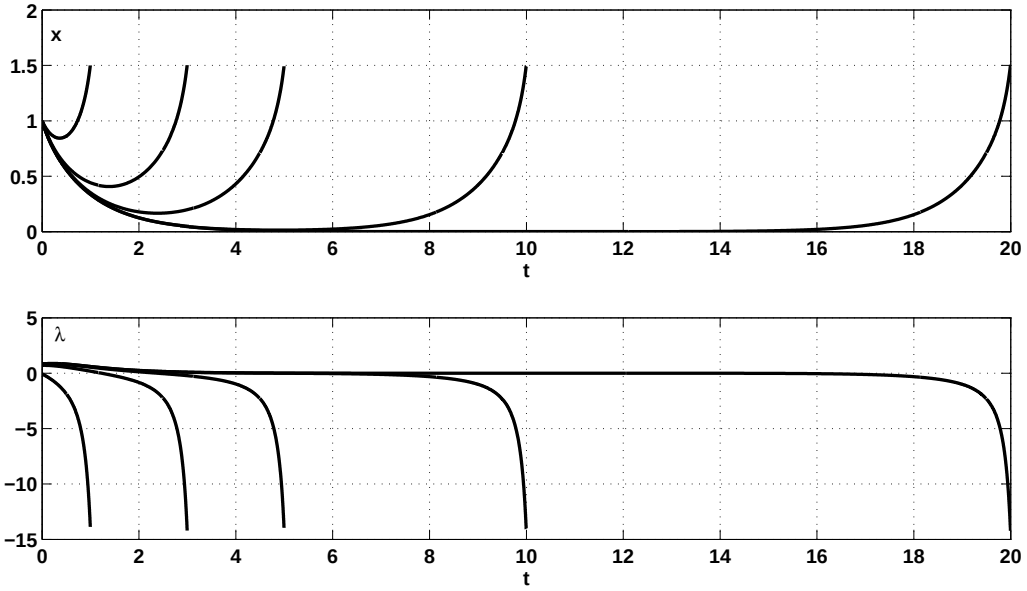

Figure 1.3: x vs. t and λ vs. t for the boundary value problem in (1.6).

to the terminal conditions'. Strictly speaking, this transition never takes place. However, assuming such a transition does occur, the problem can be decomposed into simpler subproblems; the associated error decreases as the final time increases."

Developing tools for diagnosing the existence of the aforementioned structures, slow, stable, and unstable manifolds, in the state space or in a subset of the state space and determining them, if they exist, requires the understanding of the geometric structures around invariant manifolds in the state space. The next section provides introductory information on how the geometric structure of the general nonlinear systems near compact invariant manifolds can be obtained from the study of the structure of the associated linearized problem. It starts with the trivial invariant set: isolated equilibrium point.

1.3 Geometric Structure of the Nonlinear Systems Near Equilibrium Points and Compact Invariant Manifolds

Consider the nonlinear dynamical system described by at least $\mathcal{C}^1$ vector field $f(\cdot) : \mathcal{R}^n \rightarrow T\mathcal{R}^n$

$$\dot{x} = f(x) \tag{1.7}$$

where $x \in \mathcal{R}^n$ and $f(x) \in T_x\mathcal{R}^n$. In words, the vector field $f(x)$ assigns a vector in the tangent space of $\mathcal{R}^n$ at any point $x \in \mathcal{R}^n$. The flow generated by this vector field, denoted by $\phi(t, \cdot) : \mathcal{R}^n \rightarrow \mathcal{R}^n$, satisfies the differential equations in (1.7), i.e. $\dot{\phi}(t, x) = f(\phi(t, x))$.

The nonlinear flow and vector field on $\mathcal{R}^n$ induce a linear flow and linear vector field on the tangent bundle of $\mathcal{R}^n$. When the nonlinear equations are linearized around a reference trajectory $\phi_{ref}(t, x)$, then the induced linear vector field is

$$\delta\dot{x} = \frac{\partial f}{\partial x}\delta x = A(\phi_{ref}(t, x))\delta x = A(t)\delta x, \ \textit{where} \ \ \delta x \in T_x\mathcal{R}^n. \tag{1.8}$$

The linear flow generated by the linear vector field in Eq. (1.8) is denoted by $\Phi(t, x)(\cdot) : T_x\mathcal{R}^n \rightarrow T_{\phi_{ref}(t,x)}\mathcal{R}^n$ and is a map on the tangent bundle of $\mathcal{R}^n$ that maps a vector in $T_x\mathcal{R}^n$ to a vector in $T_{\phi_{ref}(t,x)}\mathcal{R}^n$, i.e. $\delta x = \Phi(t, x)\delta x_0$, where $\delta x_0 \in T_x\mathcal{R}^n$ and $\delta x \in T_{\phi_{ref}(t,x)}\mathcal{R}^n$.

When the nonlinear system is linearized around a non-stationary reference trajectory, the induced linear vector field is linear time-varying (LTV). When the reference trajectory is stationary, i.e., an equilibrium point of the nonlinear system, x_{eq}, then the induced linear vector field is linear time-invariant (LTI), i.e., A is a constant matrix

$$\delta\dot{x} = A\delta x. \tag{1.9}$$

In general, $\Phi(t, x) \in \mathcal{R}^{n\times n}$ is the transition matrix and satisfies the LTV dynamics in

Eq. (1.8)

$$\frac{\partial \Phi(t,x)}{\partial t} = A(t)\Phi(t,x) \tag{1.10}$$

with the initial condition $\Phi(0,x) = I_n$. For the LTI dynamics the flow is determined by $\delta x = e^{At}\delta x_0$.

1.3.1 Geometric Structure of LTI Systems

For the LTI dynamics $\delta\dot{x} = A\delta x$ the eigenvalues and eigenvectors of matrix A give the information about the geometric structure of $T_x\mathcal{R}^n$. Let the eigenvalues of A be distinct for simplicity and assume that the eigenvalues are in increasing order, i.e. $\lambda_1 < ... < \lambda_n$. The eigenvectors corresponding to different eigenvalues constitute a set of basis vectors which span the different subspaces of $T_x\mathcal{R}^n$ that form invariant subbundles of $T\mathcal{R}^n$. In this context, the invariance condition can be written as $\Phi(t,x)e_i = \sigma(t)e_i$, where e_i is the eigenvector corresponding to λ_i and $\sigma_i(t) = e^{\lambda_i t}$ is a scaling factor. The invariance can be seen from the following calculation of the transition matrix, which is the matrix exponential in the LTI case

$$\Phi(t,x) = e^{At} = I + At + \frac{1}{2!}A^2t^2 + \frac{1}{3!}A^3t^3 + ... \tag{1.11}$$

Eq. (1.11) shows that the eigenvectors of e^{At} are the eigenvectors of A and

$$\Phi(t,x)e_i = Ie_i + Ae_it + \frac{1}{2!}A^2e_it^2 + \frac{1}{3!}A^3e_it^3 + ... = (1 + \lambda_it + \frac{1}{2!}{\lambda_i}^2t^2 + \frac{1}{3!}{\lambda_i}^3t^3 + ...)e_i = e^{\lambda_i t}e_i \tag{1.12}$$

gives the desired relation.

The following subspaces of $T_x\mathcal{R}^n$, called the stable eigenspace, unstable eigenspace, and center eigenspace, respectively, are defined based on the sign of the eigenvalues, λ, of

A

$$\begin{aligned}
\mathcal{E}^s &= span\{v \ : \ v \ is \ an \ eigenvector \ of \ A \ corresponding \ \lambda \ with \ Re(\lambda) < 0\} \\
\mathcal{E}^u &= span\{v \ : \ v \ is \ an \ eigenvector \ of \ A \ corresponding \ \lambda \ with \ Re(\lambda) > 0\} \\
\mathcal{E}^c &= span\{v \ : \ v \ is \ an \ eigenvector \ of \ A \ corresponding \ \lambda \ with \ Re(\lambda) = 0\}.
\end{aligned} \tag{1.13}$$

In case the eigenvectors are complex, then the generalized eigenvectors are used in the definition of eigenspaces. The vectors in the stable eigenspace contract exponentially in forward time, and the vectors in the unstable eigenspace expand exponentially in forward time whereas they contract exponentially in backward time. The vectors in the center eigenspace grow at most sub-exponentially both in forward and backward time.

These eigenspaces form a decomposition of $T_x\mathcal{R}^n$

$$T_x\mathcal{R}^n = \mathcal{E}^s \oplus \mathcal{E}^c \oplus \mathcal{E}^u. \tag{1.14}$$

Another decomposition of $T_x\mathcal{R}^n$ can be obtained by grouping the eigenvalues of A in two sets Sp_{slow} and Sp_{fast} such that $\frac{|Re\{\lambda_i\}|}{|Re\{\lambda_j\}|} << 1$ for all $\lambda_i \in Sp_{slow}$ and $\lambda_j \in Sp_{fast}$ assuming the imaginary parts of λ_i and λ_j are not much different and using the following subspaces

$$\begin{aligned}
\mathcal{E}^{slow} &= span\{v_i \ : \ \lambda_i \in Sp_{slow}\} \\
\mathcal{E}^{fast} &= span\{v_i \ : \ \lambda_i \in Sp_{fast}\}.
\end{aligned}, \tag{1.15}$$

where $Re\{\lambda\}$ is the real part of λ. Then, the decomposition can be written as

$$T_x\mathcal{R}^n = \mathcal{E}^{slow} \oplus \mathcal{E}^{fast}. \tag{1.16}$$

In this case, the rate of contraction or expansion of the vectors in $\mathcal{E}^{fast}$ is much faster than that of the vectors in $\mathcal{E}^{slow}$.

1.3.2 Geometric Structure of Nonlinear Flow Near an Equilibrium Point

Definition 1.3.1 *(Hyperbolic Equilibrium Point) An equilibrium point, x_{eq}, of the nonlinear flow determined by the vector field $\dot{x} = f(x)$ is hyperbolic provided that $\frac{\partial f(x_{eq})}{\partial x}$ has no eigenvalues with zero real part.*

Definition 1.3.2 *(Stable and Unstable Manifolds of an Equilibrium Point of a Nonlinear Flow) Let $N_{x_{eq}}$ denote a neighborhood of x_{eq}. The local stable manifold is*

$$W^s_{loc}(x_{eq}) = \{x \in N_{x_{eq}} \ : \ \phi(t,x) \in N_{x_{eq}} \ \forall t \geq 0, \ \phi(t,x) \to x_{eq} \ as \ t \to \infty\}. \tag{1.17}$$

Similarly, the local unstable manifold is

$$W^u_{loc}(x_{eq}) = \{x \in N_{x_{eq}} \ : \ \phi(t,x) \in N_{x_{eq}} \ \forall t \leq 0, \ \phi(t,x) \to x_{eq} \ as \ t \to -\infty\}. \tag{1.18}$$

The Hartman-Grobman Theorem and Stable and Unstable Manifold Theorems provide the base for the analysis of nonlinear systems near an equilibrium point by analyzing the induced linear system.

Theorem 1.3.3 *(Hartman-Grobman Theorem For Equilibrium Point) If x_{eq} is a hyperbolic equilibrium point of the nonlinear dynamics (1.7), then there exists a homeomorphism defined on some neighborhood $N_{x_{eq}}$ of x_{eq}, $h: \ N_{x_{eq}} \to T_{x_{eq}}\mathcal{R}^n$, mapping orbits of the nonlinear flow to orbits of the induced linear flow. The homeomorphism preserves the sense of orbits and can also be chosen to preserve the parametrization by time.*

Figure (1.4) illustrates the correspondence between the nonlinear and linearized flow explained by Hartman-Grobman Theorem.

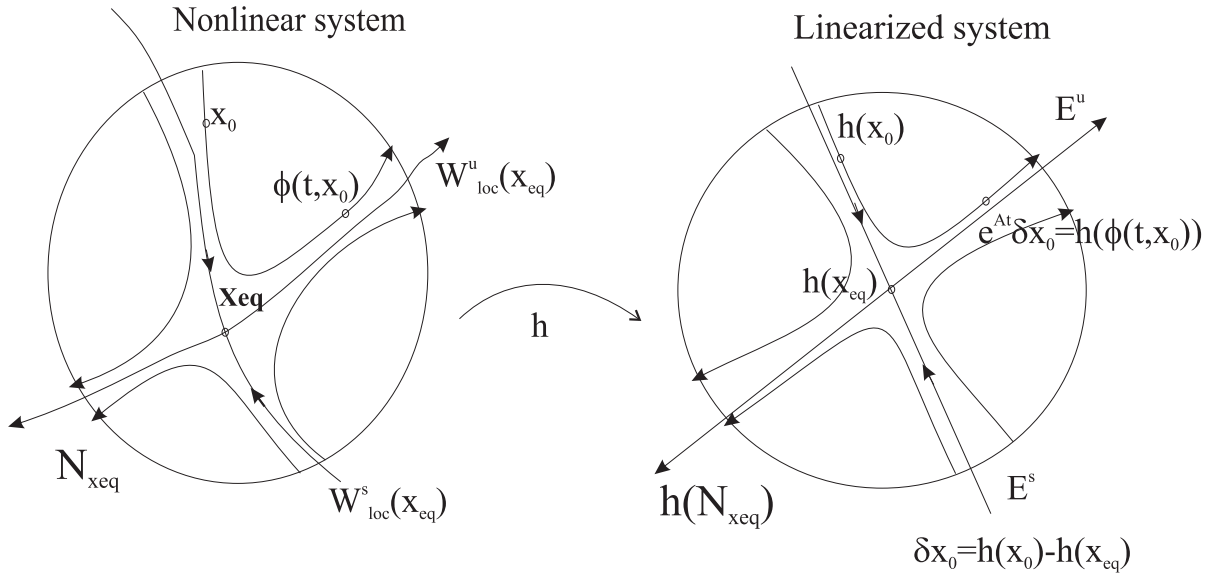

Figure 1.4: Hartman-Grobman Theorem for equilibrium points.

See [6, 7] for a detailed study of Hartman-Grobman Theorem. When $\frac{\partial f(x_{eq})}{\partial x}$ has no eigenvalues with zero real part, the asymptotic behavior of solutions of $\dot{x} = f(x)$ near x_{eq} is determined by the linearization of $\dot{x} = f(x)$ around x_{eq}. The Stable Manifold Theorem gives the relation between the stable and unstable eigenspaces of the system in (1.8) and the local stable and unstable manifolds of the system in (1.7) at the hyperbolic equilibrium point of (1.7).

Theorem 1.3.4 *(Stable Manifold Theorem for an Equilibrium Point) Suppose that $x_{eq} \in \mathcal{R}^n$ is an isolated hyperbolic equilibrium point of the nonlinear system (1.7). Then there exist local stable and unstable manifolds, $W^s_{loc}(x_{eq})$ and $W^u_{loc}(x_{eq})$, of the same dimensions as the stable and unstable eigenspaces, respectively, of the linearized dynamics (1.8). $W^s_{loc}(x_{eq})$ and $W^u_{loc}(x_{eq})$ are tangent to $\mathcal{E}^s$ and $\mathcal{E}^u$ at x_{eq}, respectively.*

Figure (1.5) illustrates the local stable and unstable manifolds of an equilibrium point and the associated eigenspaces for a 2-dimensional system.

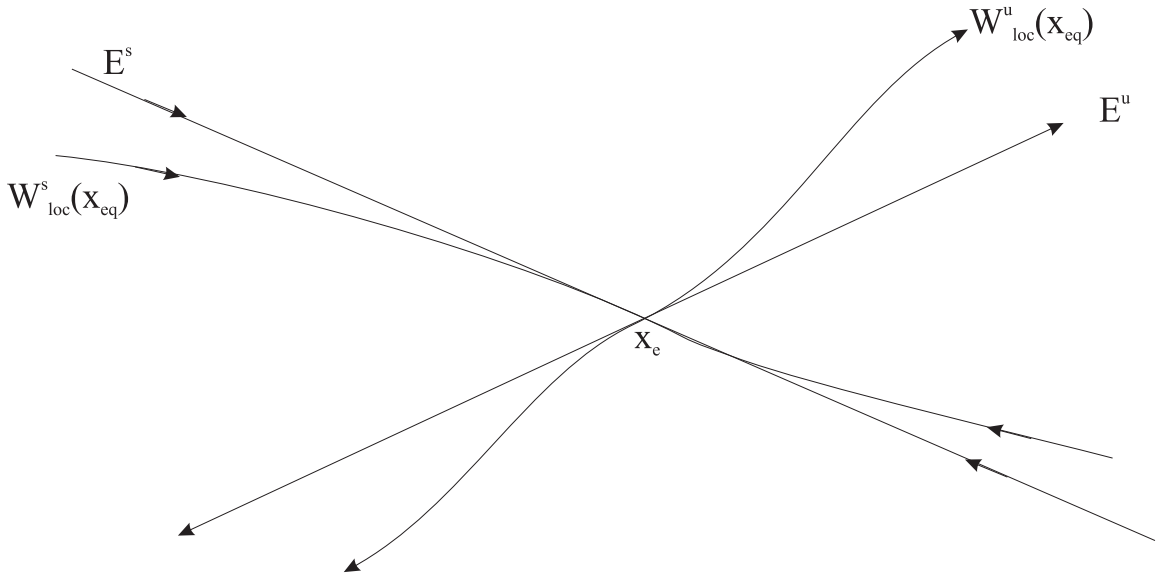

Figure 1.5: Local stable and unstable manifolds of an equilibrium point and the associated eigenspaces.

1.3.3 Geometric Structure of Nonlinear Flow Near a Compact Invariant Manifold

The geometric structure of the nonlinear flow $\phi(t, x)$ generated by the vector field $\dot{x} = f(x)$ near a compact invariant submanifold $\mathcal{M} \subset \mathcal{R}^n$ is given by the Stable Manifold Theorem for Invariant, Compact Manifolds which is the natural extension of that for equilibrium points.

Definition 1.3.5 *[8, 7](Normal Hyperbolic Manifold) The submanifold $\mathcal{M}$ is said to be normally hyperbolic if the tangent bundle $T\mathcal{R}^n$ restricted to $\mathcal{M}$, denoted as $T\mathcal{R}^n|(\mathcal{M})$, decomposes at each point $x \in \mathcal{M}$ as*

$$T_x\mathcal{R}^n = T_x\mathcal{M} \oplus \Delta^s(x) \oplus \Delta^u(x) \tag{1.19}$$

where $T_x\mathcal{M}$ denotes the tangent space to the submanifold $\mathcal{M}$ at x, $\Delta^s(x)$ and $\Delta^u(x)$ denote the stable and unstable subspace at x which are invariant under the linear variational flow $\Phi(t, x)(\cdot) : T_x\mathcal{R}^n|(\mathcal{M}) \to T_{\phi(t,x)}\mathcal{R}^n|(\mathcal{M})$ and there exist positive constants c and α such

that the properties

$$\begin{aligned} \|\Phi(t,x)\delta x\| &\leq c\|\delta x\|e^{-\alpha t} \ for\ all\ t>0,\ x\in\mathcal{M},\ \delta x\in\Delta^s(x) \\ \|\Phi(t,x)\delta x\| &\leq c\|\delta x\|e^{\alpha t} \ for\ all\ t>0,\ x\in\mathcal{M},\ \delta x\in\Delta^u(x) \end{aligned} \tag{1.20}$$

are satisfied

Theorem 1.3.6 *[9, 8, 6](Stable Manifold Theorem for Normally Hyperbolic, Invariant, Compact Manifolds) Suppose that the compact submanifold $\mathcal{M}\subset\mathcal{R}^n$ is invariant under the nonlinear flow $\phi(t,\cdot)$ generated by the vector field (1.7) and normally hyperbolic. Then in a neighborhood $N_{\mathcal{M}}$ of $\mathcal{M}$, there exist locally invariant manifolds $W^s_{loc}(\mathcal{M})$ and $W^s_{loc}(\mathcal{M})$ with the properties*

- $TW^s_{loc}(\mathcal{M}) = T\mathcal{M}\oplus\Delta^s$ *and* $TW^u_{loc}(\mathcal{M}) = T\mathcal{M}\oplus\Delta^u$,

- *Points on the local stable and unstable invariant submanifolds asymptotically approach $\mathcal{M}$ when propagated by the nonlinear flow in forward and backward time, respectively. $W^s_{loc}(\mathcal{M})$ and $W^u_{loc}(\mathcal{M})$ can be defined as the union of the local stable and unstable manifolds of the points on the invariant manifold $\mathcal{M}$*

$$\begin{aligned} W^s(\mathcal{M}) &= \textstyle\bigcup_{x\in\mathcal{M}} W^s_{loc}(\mathcal{M},x) \\ W^u(\mathcal{M}) &= \textstyle\bigcup_{x\in\mathcal{M}} W^u_{loc}(\mathcal{M},x) \end{aligned} \tag{1.21}$$

  where $W^s_{loc}(\mathcal{M},x)$ $(W^u_{loc}(\mathcal{M},x))$ is the fiber of $W^s_{loc}(\mathcal{M})$ $(W^u_{loc}(\mathcal{M}))$ at point $x\in\mathcal{M}$.

- $W^s_{loc}(\mathcal{M})$ *and* $W^u_{loc}(\mathcal{M})$ *are invariantly fibered so that each fiber has the property* $T_xW^s_{loc}(\mathcal{M}) = T_x\mathcal{M}\oplus\Delta^s(x)$ *and* $T_xW^u_{loc}(\mathcal{M}) = T_x\mathcal{M}\oplus\Delta^u(x)$ *for all* $x\in\mathcal{M}$*; and if two points* $x_1,\ x_2\in W^s_{loc}(\mathcal{M},x)$ $(\in W^u_{loc}(\mathcal{M},x))$ *for some* $x\in\mathcal{M}$*, then* $\phi(t,x_1),\ \phi(t,x_2)\in W^s_{loc}(\mathcal{M},\phi(t,x))$ $(\in W^u_{loc}(\mathcal{M},\phi(t,x)))$*, where $\phi(t,\cdot)$ is the flow generated by f.*

- *Near $\mathcal{M}$, f, is topologically conjugate to $\frac{\partial f(x)}{\partial x}|(\Delta^s\oplus\Delta^u)$, i.e., there exists an homeomorphism, defined on some neighborhood of $\mathcal{M}$, mapping orbits in $W^s_{loc}(\mathcal{M})\cup$*

$W^u_{loc}(\mathcal{M})$ to orbits of the induced linear flow in $\Delta^s \oplus \Delta^u$, preserving the sense of orbits and the parametrization by time.

Figure (1.6) shows a 1-dimensional invariant manifold $\mathcal{M}$ with its 2-dimensional stable and unstable manifolds in a 3-dimensional state space as described in Theorem (1.3.6).

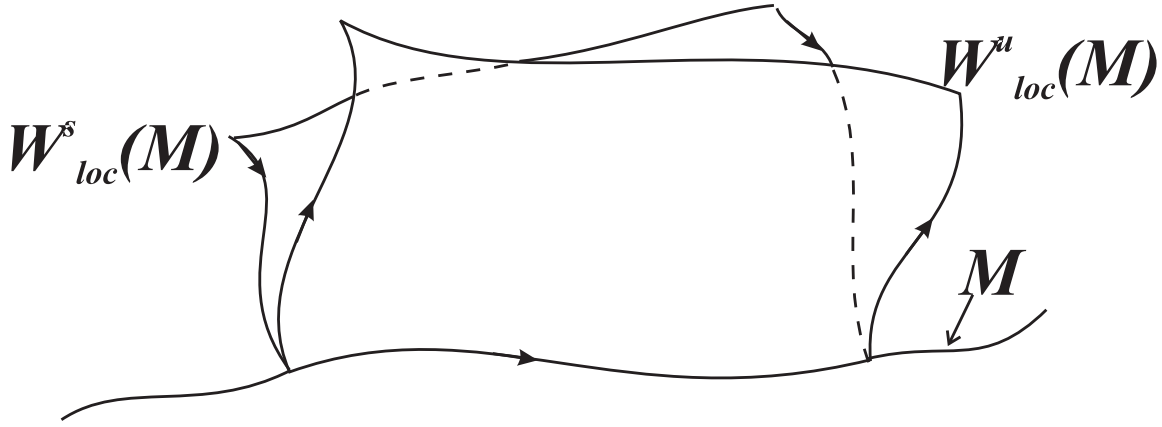

Figure 1.6: Local stable and unstable manifolds of an invariant manifold $\mathcal{M}$.

In this research, we determine this geometric structure by analyzing the geometric structure of the linearized dynamics, which is generally time-varying, using the finite time Lyapunov exponents and vectors. The second chapter gives a detailed introduction to the Lyapunov exponents and vectors.

1.4 Related Previous Work

The work reported in this thesis is the continuation of the research on the geometry of nonlinear dynamical systems done by Kenneth D. Mease and his students for the last 15 years. The work was inspired by the Computational Singular Perturbation Methodology developed by Lam.[10] The "dichotomic basis method" and "approximate dichotomic basis" method developed in the papers by Rao and Mease [4, 5] are the extension of the computational singular perturbation methodology to optimal control problems. In those papers the eigenvalues and eigenvectors of the Jacobian matrix of the Hamiltonian dynam-

ics in the optimal control problems are used in order to describe the associated geometry in state-costate space. More recently, the Lyapunov exponents and vectors have been used as the accurate tools for analyzing the geometric structure of the linearization of the nonlinear dynamical systems around non-stationary reference trajectories.[8, 11, 12] In this thesis Lyapunov exponents and vectors are used for determining the slow manifold in the state space and for the "dichotomic basis method" and "approximate dichotomic basis method" in determining the stable and unstable manifolds. The application to the slow manifold determination is a new direction in this research aimed at model order reduction. The application to the solution of the optimal control problems is an extension of the previous work providing more accurate tools.

The singular perturbation theory is a well-developed methodology for model order reduction based on the timescale separation in the dynamics. However, the tools of the singular perturbation theory is only applicable if the dynamics are given in the special form, so called "singularly perturbed form". However, there is no general way to bring a nonlinear system into singularly perturbed form. The understanding of the timescale structure and the associated geometric structure through the study of Lyapunov exponents and vectors may facilitate the applicability of the singular perturbation theory. A more detailed discussion of the singular perturbation theory is given in Chapters (3) and (4).

Any model reduction mechanism based on the timescale separation in the system dynamics requires the knowledge of a possibly existing slow manifold. Besides the singular perturbation methodology, there are other analytical and geometrical methods for determining the slow manifold. A survey on the existing methods is given in Chapter (3).

The indirect methods for solving optimal control problems suffer from the lack of a full set of boundary conditions that can be used to integrate the system dynamics and

the volume-preserving nature of the dynamics. Coordinate transformations that decouple the stable and unstable subsystems and suppress the unstable dynamics during the integration are used in literature. Our main contribution is to decouple these dynamics more accurately by using the Lyapunov exponents and vectors. More detailed discussion on the use of coordinate transformation and the use of singular perturbation theory for solving optimal control problems is given in Chapter (4).

Chapter 2

Lyapunov Exponents and Tangent Space Structure

In this chapter the tools for diagnosing the timescale structure and determining its associated tangent space structure on a compact invariant subset $\mathcal{Y}$ of $\mathcal{R}^n$ are introduced and modified in order to use them to obtain similar information for a compact non-invariant subset $\mathcal{X}$ of $\mathcal{R}^n$.

2.1 Terminology, Assumptions, and Evolution Equations

The scenario is that a dynamical system is given in a particular coordinate representation and the objective is to diagnose whether or not multiple-timescale behavior exists, and if it does, to determine the associated geometric structure, particularly the slow, stable and unstable manifolds. The state coordinate vector is $x \in \mathcal{R}^n$ and the dynamics are

$$\dot{x} = f(x), \tag{2.1}$$

where the vector field f is assumed continuously differentiable. We refer to Eq. (2.1) as the x-representation of the dynamical system. It will be important to distinguish between inherent system properties that would be observed in any coordinate representation and properties that are specific to a particular coordinate representation. We express the

solution of Eq. (2.1) for the initial condition $x(0) = x_0$ as $x(t) = \phi(t, x_0)$, where ϕ is the transition map or flow satisfying $\partial\phi/\partial t = f(\phi(t, x_0))$ and $\phi(0, x_0) = x_0$. In the state space view, ϕ maps x_0 along the trajectory (i.e., solution) through that point, t units of time to the point $x(t)$. If $t > 0$, this is forward propagation; if $t < 0$, this is backward propagation.

Controlled dynamical systems are of interest, but the explicit dependence of f on a control function is not addressed. Timescale analysis of $\dot{x} = f(x)$ is relevant for a controlled system in each of the following cases: (i) the control function is determined by a feedback law and $f(x)$ represents the closed-loop dynamics, (ii) $f(x)$ is the open-loop dynamics and the plan is to use low-gain control which would not alter the time-scale structure, or (iii) $\dot{x} = f(x)$ is the Hamiltonian system for an optimally controlled system, x being the combined state and co-state vector (see Chapter (4)).

The linearized dynamics associated with Eq. (2.1) are

$$\dot{v} = J(x)v, \tag{2.2}$$

where $J = \partial f/\partial x$. We will analyze the linearized dynamics to characterize the timescales in the nonlinear dynamics. In general, we need to consider Eqs. (2.1) and (2.2) as a coupled system, because $J(x)$ depends on x. An initial point (x, v) is mapped in time t to the point $(x(t), v(t)) = (\phi(t, x), \Phi(t, x)v)$, where Φ is the transition matrix for the linearized dynamics, defined such that $\Phi(0, x) = I$, the $n \times n$ identity matrix. Geometrically, each point x in the state space is a base point of a tangent space, in which v takes values. The coordinates for v correspond to a tangent space frame, whose axes are parallel to those of the x-frame, but with origin at x. Our analysis will concern a domain $\mathcal{Y} \subset \mathcal{R}^n$ of the state space. The tangent space at a point $x \in \mathcal{Y}$ is denoted by $T_x\mathcal{Y}$. The tangent bundle $T\mathcal{Y}$ is defined as the union of the tangent spaces over $\mathcal{Y}$, and (x, v) is a point in the tangent bundle, with v the tangent vector and x the base point. We need the

interpretation $(x, v) \in T\mathcal{Y}$ because the analysis of the linearized dynamics will define a subspace decomposition in the tangent space and the orientation of the subspaces will vary with the base point x.

If we have k linearly independent vector fields $w_1(x), \ldots, w_k(x)$ defined on $\mathcal{Y}$ that vary continuously with x, we can define at each x a k-dimensional subspace $\Lambda(x) = \text{span}\{w_1(x), \ldots, w_k(x)\}$. If $k = n$, then $\Lambda(x) = T_x\mathcal{Y}$ and for each x the vector fields provide a basis for $T_x\mathcal{Y}$. If $k < n$, then $\Lambda(x)$ is a linear subspace of $T_x\mathcal{Y}$ and Λ is called a distribution on $\mathcal{Y}$. A distribution is invariant if for any $x \in \mathcal{Y}$ and $v \in \Lambda(x)$, the property $\Phi(t, x)v \in \Lambda(\phi(t, x))$ holds for any t such that $\phi(t, x) \in \mathcal{Y}$. Distributions $\Gamma_1, \ldots, \Gamma_m$ allow a splitting of the tangent space, if $T_x\mathcal{Y} = \Gamma_1(x) \oplus \ldots \oplus \Gamma_m(x)$, where $\oplus$ denotes the direct sum of linear subspaces; in words, each vector in $T_x\mathcal{Y}$ has a unique representation as a linear combination of vectors, one from each of the subspaces $\Gamma_1(x), \ldots, \Gamma_m(x)$ and $\Gamma_i(x) \cap \Gamma_j(x) = \{\mathbf{0}\}$ for all $i \neq j$, where $\{0\}$ is the set whose only element is the zero vector. If each distribution in the splitting is invariant, then the splitting is called an invariant splitting.

If a collection of $r \leq n$ linear subspaces of $T_x\mathcal{Y}$ can be ordered such that $\Lambda_1(x) \subset \Lambda_2(x) \subset \ldots \subset \Lambda_r(x) = T_x\mathcal{Y}$, then this collection of nested proper subspaces defines a filtration of $T_x\mathcal{Y}$. Note that the subspaces of the filtration satisfy for $i = 1, \ldots, r-1$ the condition $dim\Lambda_i(x) < dim\Lambda_{i+1}(x)$.

A smooth submanifold[13] $\mathcal{M} \subset \mathcal{R}^n$ of dimension $k < n$, for which $\mathcal{M} \cap \mathcal{Y}$ is non-empty, is relatively invariant with respect to $\mathcal{Y}$ for the vector field $\dot{x} = f(x)$, if for any $x \in \mathcal{M} \cap \mathcal{Y}$, $\phi(t, x) \in \mathcal{M}$ if $\phi(t, x) \in \mathcal{Y}$. This means a trajectory emanating from any point in $\mathcal{M} \cap \mathcal{Y}$ remains on $\mathcal{M}$ in forward and backward time as long as the trajectory is in $\mathcal{Y}$. An equivalent requirement for relative invariance is that $f(x) \in T_x\mathcal{M}$ for all $x \in \mathcal{M} \cap \mathcal{Y}$,

which means that the trajectory through x is tangent to $\mathcal{M}$ and will thus stay on $\mathcal{M}$.

2.2 Lyapunov Exponents and Vectors

First introduced by Lyapunov [14] in order to study the stability of non-stationary solutions of ordinary differential equations, Lyapunov exponents are measures of the average exponential rate of growth/decay of functions. For a real valued function $g(t)$ the Lyapunov exponent is given by

$$\mu[g] = \limsup_{t\to\infty} \frac{1}{t} \ln |g(t)|. \tag{2.3}$$

Lyapunov exponents provide a generalization of the linear stability analysis using perturbations from stationary solutions to that using perturbations from non-stationary solutions. Lyapunov exponents have found extensive applications in mathematics, dynamical systems theory and physics especially in the study of chaos since they are measures of the sensitivity of solutions of dynamical systems to small perturbations from the nominal solutions. A positive exponent indicates chaotic behavior. In this context Lyapunov exponents have been extensively used in the study of fluid flow mechanisms[15, 16] and forecasting[17]. They have also been used in trajectory tracking law design[18].

Our goal is to obtain timescale information and the associated geometric structure of the nonlinear system in Eq.(2.1) by studying the linearized dynamics in Eq.(2.2). The dynamics in Eq.(2.2) are linear time-varying because of the $x(t)$ dependence of J matrix and x is the solution of the nonlinear dynamics. The Lyapunov exponents for the LTV dynamics in Eq.(2.2) are given as [19]

$$\mu^{+}(x,v) = \limsup_{T\to\infty} \frac{1}{T} ln(\frac{\|\Phi(T,x)v\|}{\|v\|}) \tag{2.4}$$

for each $x \in \mathcal{Y}$ and nonzero $v \in T_x\mathcal{Y}$, where v is a solution of Eq.(2.2). Lyapunov also identified the subclass of LTV systems called regular LTV systems, for which the Lyapunov

exponents are given by the actual limits of the exponential growth/shrinkage rates

$$\mu^+(x,v) = \lim_{T\to\infty} \frac{1}{T} ln(\frac{\|\Phi(T,x)v\|}{\|v\|}). \tag{2.5}$$

For $v = 0$, $\mu^+(x,v) = -\infty$ for each $x \in \mathcal{Y}$. LTI and periodic LTV systems are regular. The Lyapunov exponents computed for the LTI system, $\dot{x} = Ax$ reduce to the real parts of the eigenvalues of A. The Lyapunov exponents computed for the periodic LTV system, $\dot{x} = A(t)x$ where $A(t+T) = A(t)$ for some $T > 0$ and for all t, are equal to the real part of the Floquet exponents of A.[20] The following two properties of the Lyapunov exponents are easy to show

1. $\mu^+(x,\alpha v) = \mu^+(x,v)$ for each $v \in T_x\mathcal{Y}$ and $\alpha \in \mathcal{R}\backslash\{0\}$;

2. $\mu^+(x,v+w) \leq \max\{\mu^+(x,v), \mu^+(x,w)\}$ for each $v,\ w \in T_x\mathcal{Y}$

and are used in the proof of the following theorem. [19] Note that given sets S_1 and S_2 with $S_1 \subset S_2$, the notation $S_2\backslash S_1$ refers to the set containing all the elements in S_2 except for those that are also elements of S_1; in this sense, it is S_2 minus S_1.

Theorem 2.2.1 *The Lyapunov exponents have the following properties:*

1. *if $v, w \in T_x\mathcal{Y}$ are such that $\mu^+(x,v) \neq \mu^+(x,w)$ then $\mu^+(x,v+w) = \max\{\mu^+(x,v), \mu^+(x,w)\}$;*

2. *if $v_1, ..., v_m \in T_x\mathcal{Y}$ and $\alpha_1, ..., \alpha_m \in \mathcal{R}\backslash\{0\}$ then $\mu^+(x, \alpha_1 v_1 + ... + \alpha_m v_m) \leq \max\{\mu^+(x,v_i),\ i = 1:m\}$, and if, in addition, there exists i such that $\mu^+(x,v_i) > \mu^+(x,v_j)$ for all $j \neq i$ then $\mu^+(x, \alpha_1 v_1 + ... + \alpha_m v_m) = \mu^+(x,v_i)$;*

3. *if for some $v_1, ..., v_m \in T_x\mathcal{Y}\backslash\{0\}$ the Lyapunov exponents $\mu^+(x,v_1), ...\mu^+(x,v_m)$ are distinct, then the vectors $v_1, ..., v_m$ are linearly independent;*

4. the function (Lyapunov exponent) μ^+ attains no more than n distinct finite values.

By statement 4 of Thm.(2.2.1) the forward Lyapunov exponents can take on at most n distinct values on $T_x\mathcal{Y}\backslash\{0\}$. For simplicity we assume that μ^+ takes on exactly n distinct values on $T_x\mathcal{Y}\backslash\{0\}$, i.e. there is no repeated Lyapunov exponent. We further assume that these distinct values of Lyapunov exponents are ordered as

$$\mu_1^+ \ < \ ... \ < \ \mu_n^+. \tag{2.6}$$

It is important to note that for a given trajectory of a regular dynamical system the Lyapunov exponents are independent of the starting point, because they are asymptotic measures of the average exponential rate of growth/decay of functions.

The linear subspaces $L_i^+(x)$, defined as

$$L_i^+(x) = \{v \in T_x\mathcal{Y} \ : \ \mu^+(x,v) \leq \mu_i^+\}, \quad i = 1, 2, ..., n \tag{2.7}$$

with $L_0^+ = \{0\}$, form the following filtration of $T_x\mathcal{Y}$

$$\{0\} = L_0^+ \subset L_1^+(x) \subset L_2^+(x) \subset ... \subset L_n^+(x) = T_x\mathcal{Y}. \tag{2.8}$$

Theorem 2.2.2 *[19] Let $\{L_i^+(x), \ i = 1, ..., n\}$ be the filtration defined in (2.7) and (2.8). Then the following properties hold:*

1. $\mu^+(x,v) \leq \mu_i^+$ for every $v \in L_i^+(x)$;

2. $\mu^+(x,v) = \mu_i^+$ for every $v \in L_i^+(x)\backslash L_{i-1}^+(x)$.

Another representation of the $L_i^+(x)$ subspaces can be constructed as follows: Let the one dimensional subspace $L_1^+(x)$ be spanned by the unit vector $l_1^+(x)$, a vector in $\mathcal{R}^n$ called the Lyapunov vector corresponding to μ_1^+ at x. Then, define another unit vector $l_2^+(x)$, called the Lyapunov vector corresponding to μ_2^+ at x, orthogonal to $l_1^+(x)$ such that

$L_2^+(x) = span\{l_1^+(x), l_2^+(x)\}$. Continuing this procedure creates a new representation of the subspaces in (2.7):

$$\begin{aligned} L_1^+(x) &= span\{l_1^+(x)\}, \\ L_2^+(x) &= span\{l_1^+(x),\ l_2^+(x)\}, \\ &\vdots \\ L_i^+(x) &= span\{l_1^+(x),\ l_2^+(x),\ ...,\ l_i^+(x)\}, \\ &\vdots \\ L_n^+(x) &= span\{l_1^+(x),\ l_2^+(x),\ ...,\ l_n^+(x)\}. \end{aligned} \tag{2.9}$$

Example 2.2.3 *To gain more insight into the filtration in (2.8), consider a two-dimensional nonlinear system with $\mathcal{Y} = \{x_{eq}\}$, x_{eq} an equilibrium point. Assume the linearized dynamics at x_{eq} are characterized by distinct eigenvalues λ_f and λ_s, with $\lambda_f << \lambda_s < 0$, and corresponding eigenvectors e_f and e_s. The Lyapunov exponents are equal to the eigenvalues, i.e., $\mu_1^+ = \lambda_f$ and $\mu_2^+ = \lambda_s$, and the Lyapunov vector $l_1^+(x_{eq})$ corresponding to μ_1^+ aligns with the eigenvector e_f corresponding to λ_f. The second Lyapunov vector l_2^+ is in the direction of $e_f^\perp$, the vector perpendicular to e_f. The subspace $L_1^+(x_{eq})$ is $E^f(x_{eq}) = span\{e_f\}$, the eigenspace for λ_f, whereas $L_2^+(x_{eq}) = T_{x_{eq}}\mathcal{X}$. It would be desirable instead to obtain the decomposition $T_{x_{eq}}\mathcal{X} = E^f(x_{eq}) \oplus E^s(x_{eq})$ where $E^s(x_{eq}) = span\{e_s\}$. However, as the averaging time T goes to ∞, all the vectors not in $L_1^+(x_{eq})$ have the Lyapunov exponent $\mu_2^+ = \lambda_s$; thus the Lyapunov exponents for forward time propagation do not distinguish E^s. The way to obtain E^s is by repeating the same analysis for backward time propagation; in this case, the situation is reversed and E^s can be distinguished, whereas E^f cannot.[21] Eigenspaces are invariant under the linear dynamics in that an initial tangent vector in an eigenspace will remain in that eigenspace under forward or backward propagation, and $T_{x_{eq}}\mathcal{X} = E^f(x_{eq}) \oplus E^s(x_{eq})$ is an example of an invariant splitting.*

In order to define a new filtration to be able to capture E^s, let's first define the backward

Lyapunov exponents

$$\mu^-(x,v) = \lim_{T\to\infty} \frac{1}{T} ln(\frac{\|\Phi(-T,x)v\|}{\|v\|}). \tag{2.10}$$

For $v = 0$, $\mu^-(x,v) = -\infty$ for each $x \in \mathcal{Y}$. The backward Lyapunov exponents satisfy all the properties stated for the forward Lyapunov exponents in Thm. (2.2.1). Assume that they are distinct and the distinct values are ordered as

$$\mu_n^- \ < \ ... \ < \ \mu_1^-. \tag{2.11}$$

Then similar to the filtration defined in terms of the forward Lyapunov exponents, the subspaces

$$L_i^-(x) = \{v \in T_x Y \ : \ \mu^-(x,v) \leq \mu_i^-\}, \quad i = 1,2,...,n \tag{2.12}$$

comprise another filtration of $T_x\mathcal{Y}$ with $L_{n+1}^+ = \{0\}$

$$\{0\} = L_{n+1}^- \subset L_n^-(x) \subset L_{n-1}^-(x) \subset ... \subset L_1^-(x) = T_x\mathcal{Y}. \tag{2.13}$$

Theorem 2.2.4 *Let $\{L_i^-(x),\ i = 1,...,n\}$ be the filtration defined in (2.12) and (2.13). Then the following properties hold:*

1. *$\mu^-(x,v) \leq \mu_i^-$ for every $v \in L_i^-(x)$;*

2. *$\mu^-(x,v) = \mu_i^-$ for every $v \in L_i^-(x) \backslash L_{i-1}^-(x)$.*

Similar to the forward subspaces, another representation of the backward subspaces can be generated by setting $L_n^-(x) = span\{l_n^-(x)\}$, where $l_n^-(x)$ is the backward Lyapunov vector corresponding to μ_n^- at x, and repeating the procedure in (2.9) in the reverse direction

$$\begin{aligned}
L_n^-(x) &= span\{l_n^-(x)\}, \\
L_{n-1}^-(x) &= span\{l_n^-(x),\ l_{n-1}^-(x)\}, \\
&\vdots \\
L_i^-(x) &= span\{l_n^-(x),\ l_{n-1}^-(x),\ ...,\ l_i^-(x)\}, \\
&\vdots \\
L_1^-(x) &= span\{l_n^-(x),\ l_{n-1}^-(x),\ ...,\ l_1^-(x)\}.
\end{aligned} \tag{2.14}$$

Now back to the Example (2.2.3), $E^s(x_{eq})$ can be identified as $L_2^-(x_{eq})$, and e^s and $l_2^-(x_{eq})$ are in the same direction. Fig.(2.1) shows the eigenvectors and Lyapunov vectors for the Example (2.2.3).

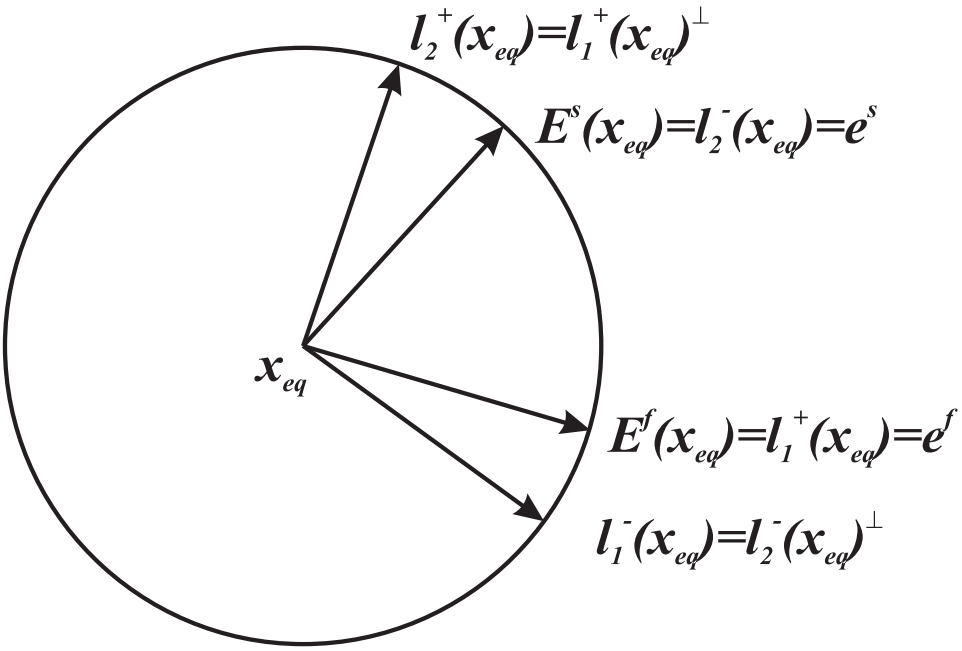

Figure 2.1: Eigenvectors and Lyapunov vectors of the systems in Example (2.2.3).

Having defined the forward and backward Lyapunov exponents and filtration in terms of the Lyapunov exponents we are ready to state the following characterization of the regularity.

Definition 2.2.5 *[11, 19] The system is regular at x, if and only if*

i) the forward and backward Lyapunov exponents exist as the limits,

ii) $\mu_i^+ = -\mu_i^-,\ i = 1, ...n;$

iii) the forward and backward filtrations have the same dimension;

iv) there exists a decomposition $T_x\mathcal{Y} = E_1(x) \oplus ... \oplus E_n(x)$ *into invariant sub-bundles such that* $L_i^+(x) = E_1(x) \oplus ... \oplus E_i(x)$ *and* $L_i^-(x) = E_i(x) \oplus ... \oplus E_n(x)$, $i = 1, ..., n;$

v) for any $v \in E_i(x)\backslash\{0\}$, $\lim_{T\to\infty} ln\frac{\|\Phi(\pm T,x)v\|}{\|v\|} = \pm\mu_i^+$.

Note that in dynamical system literature and particularly in [19, 20] equivalent definitions are given in terms of the Lyapunov exponents of the adjoint linear system, $\dot{\hat{v}} = -J^T(x)\hat{v}$. This equivalence will be shown in the following section after the finite time Lyapunov exponents and vectors are introduced.

Computation of the Lyapunov Exponents: By the definition of the subspaces $L_i^+(x)$ any unit vector in the subspace $L_i^+(x)\backslash L_{i-1}^+(x)$ has the Lyapunov exponent μ_i^+, i.e. for $v \in L_i^+(x)\backslash L_{i-1}^+(x)$

$$\mu^+(v,x) = \lim_{T\to\infty} \frac{1}{T} ln\|\Phi(T,x)v\| = \mu_i^+. \tag{2.15}$$

The claim is that *most* of the tangent vectors in the tangent space at x are in the subspace $v \in L_i^+(x)\backslash L_{i-1}^+(x)$. Let's try to visualize this in a 2-dimensional setting. In 2-dimensions all the vectors except $l_1^+(x)$ are in the subspace $v \in L_2^+(x)\backslash L_1^+(x)$. If by chance it is not in $L_2^+(x)\backslash L_1^+(x)$, then a vector in $L_2^+(x)\backslash L_1^+(x)$ can be found with at most 2 trials by keeping one component and changing the other one. Similarly, in the n dimensional case any arbitrarily chosen vector is most probably in $L_n^+(x)\backslash L_{n-1}^+(x)$. If it is not, a vector in $L_n^+(x)\backslash L_{n-1}^+(x)$ can be found with at most n trials. Consequently, the largest Lyapunov exponent can be computed by Eq.(2.15) by taking an arbitrary tangent vector $v \in T_x\mathcal{Y}$ assuming that it is not in $L_n^+(x)\backslash L_{n-1}^+(x)$. The calculation of the next Lyapunov exponent is not straightforward since any arbitrary vector chosen will not be in the subspace $L_{n-1}^+(x)\backslash L_{n-2}^+(x)$. However, most of the subspaces spanned by any two linearly independent unit vectors will be in the subspace $L_n^+(x)\backslash L_{n-2}^+(x)$. Let two unit tangent vectors v_n and v_{n-1} at x be arbitrarily chosen. Then, the sum of the greatest two Lyapunov

exponents is given by

$$\mu_n^+ + \mu_{n-1}^+ = \lim_{T\to\infty} \frac{1}{T} \ln(A_{n,n-1}) \tag{2.16}$$

where $A_{n,n-1}$ is the area of the parallelogram determined by $\Phi(T,x)v_n$ and $\Phi(T,x)v_{n-1}$. Once the largest Lyapunov exponent is known the second largest can be calculated from Eq.(2.16). Repeating this computation the i^{th} Lyapunov exponent can computed from

$$\mu_n^+ + \mu_{n-1}^+ + ... + \mu_i^+ = \lim_{T\to\infty} \frac{1}{T} \ln(A_{n,i}) \tag{2.17}$$

where $A_{n,i}$ is the volume of the parallelogram determined by

$$\Phi(T,x)v_n,\ \Phi(T,x)v_{n-1},\ ...,\ \Phi(T,x)v_i, \tag{2.18}$$

and $v_n,\ v_{n-1}, ..., v_i$ are $n-i+1$ arbitrarily chosen tangent vectors at x.

The backward Lyapunov exponents can be computed by following the same procedure in backward time. However, once again note that the computation of the Lyapunov exponents requires infinite averaging time, which is not feasible in practical applications.

Theorem 2.2.6 *[22] The distributions*

$$\begin{aligned} \Lambda_i^+(x) &= span\{l_1^+(x), ..., l_i^+(x)\} \\ \Lambda_i^-(x) &= span\{l_n^-(x), ..., l_i^-(x)\}, \end{aligned} \tag{2.19}$$

where $l_1^+(x), ..., l_i^+(x)$ are the column vectors of $L_i^+(x)$, and $l_n^-(x), ..., l_i^-(x)$ are the column vectors of $L_i^-(x)$, are invariant distributions, i.e., for any $v \in \Lambda_i^+(x)$, $\Phi(t,x)v \in \Lambda_i^+(\phi(t,x))$, and for any $v \in \Lambda_i^-(x)$, $\Phi(t,x)v \in \Lambda_i^-(\phi(t,x))$ for all t.

The proof of the theorem is based on the property that the Lyapunov exponents are constants on trajectories of Eq.(2.1) and can be found in [22]. We do not repeat the proof; but give a sketch of the proof in order to clarify what the invariance of the subspaces means. The proof equivalently shows the following: For any $x \in \mathcal{Y}$ and $t \in \mathcal{R}$

$$\langle \Phi(t,x)l_i^+(x), l_j^+(\phi(t,x))\rangle = \begin{cases} 0, & if\ i < j \\ nonzero, & if\ i \geq j \end{cases} \tag{2.20}$$

where $\langle \cdot, \cdot \rangle$ denotes the inner product and $1 \leq i,\ j \leq n$. In words, it says when a vector $v \in span\{l_1^+(x), l_2^+(x), ..., l_i^+(x)\}$ is propagated by the transition matrix $\Phi(t, x)$, then the propagated vector will not have a component in the direction of $l_j^+(\phi(t, x))$ for any $j > i$. Thus, the distributions spanned by the basis vectors of the subspaces $L_i^+(x),\ i = 1, ..., n$ are invariant distributions on $\mathcal{R}^n$. Similarly for the backward Lyapunov vectors, for any $x \in \mathcal{Y}$ and $t \in \mathcal{R}$

$$\langle \Phi(t, x) l_i^-(x), l_j^-(\phi(t, x)) \rangle = \begin{cases} 0, & if\ i > j \\ nonzero, & if\ i \leq j \end{cases} \tag{2.21}$$

where $1 \leq i,\ j \leq n$. Therefore, the distributions spanned by the basis vectors of the subspaces $L_i^-(x),\ i = 1, ..., n$ are invariant distributions on $\mathcal{R}^n$.

The Lyapunov exponents and vectors provide tools for correctly analyzing the timescale structure and the associated tangent space geometry in LTV systems [19, 21, 11]. Example (2.2.7), which is from [12], compares the timescale information obtained by using the Lyapunov exponents and vectors and that obtained by the eigenvalues and eigenvectors of Jacobian and transition matrices.

Example 2.2.7 *The purpose of this example is to distinguish clearly between the timescale information provided by the Lyapunov exponents and vectors and the information from the eigenvalues and eigenvectors of the transition matrix and the local Jacobian matrix. Consider the linear, time-invariant system*

$$\dot{w} = \Lambda w = \begin{bmatrix} \lambda_f & 0 \\ 0 & \lambda_s \end{bmatrix} w \tag{2.22}$$

where $w = (w_1, w_2)^T$ and the eigenvalues of Λ are real with $\lambda_f << \lambda_s < 0$. We introduce the coordinate transformation

$$x = R(t)w = \begin{bmatrix} \cos\theta(t) & -\sin\theta(t) \\ \sin\theta(t) & \cos\theta(t) \end{bmatrix} w \tag{2.23}$$

where $\theta = \omega t$ and ω is a constant. In terms of x, the system is

$$\dot{x} = A(t)x = (\dot{R}R^T + R\Lambda R^T)x = R(R^T\dot{R} + \Lambda)R^T x \tag{2.24}$$

The transition matrix for the w-system is $e^{\Lambda t}$, whereas the transition matrix for the x-system is

$$\Phi = R(t)e^{\Lambda t} \tag{2.25}$$

In the w-representation the behavior is composed of fast and slow exponentially contracting modes with fixed directions given by the eigenvectors of Λ. In the x-representation there are also fast and slow exponentially contracting modes, but the fast and slow directions are rotating. From the SVD of Φ, we will show that the Lyapunov exponents and vectors identify the slow and fast exponential modes. In contrast, we will show that eigenvalues and eigenvectors for $A(t)$ and Φ do not. Our interest is not directly in linear time-varying systems, but this example serves as an idealization of the linearized dynamics of a nonlinear system whose slow and fast directions rotate as one traverses the state space along a trajectory, as would be the case along a trajectory on a slow manifold with curvature.

Φ has the SVD: $\Phi = L^-\Sigma^+(L^+)^T = R(t)\exp(\Lambda t)I$, where I is the 2×2 identity matrix. The singular values are the positive square roots of the eigenvalues of $\Phi^T\Phi = \exp(2\Lambda t)$, and clearly the rotational motion does not influence them. The Lyapunov exponents are $\mu_1^+ = \lambda_f$ and $\mu_2^+ = \lambda_s$ and are independent of t for this example, so any averaging time will give the same Lyapunov exponents. For the time interval (t_1, t_2), the SVD is $\Phi = R(t_2)\exp(\Lambda(t_2 - t_1))R^T(t_1)$; thus we have $L^+(t) = L^-(t) = R(t)$. Note that here t is not an averaging time argument. If there were some underlying nonlinear dynamics, whose linearization gives the LTV dynamics in Eq.(2.23), then t would be an argument that indicates the base point in the state space at which the Lyapunov vectors are computed. The SVD of Φ identifies the exponential rates of the two modes in Σ^+ and the rotating directions

of these modes in L^+ and L^-. Specifically we have the fast subspace $E^f(t) = L_1^+(t) = span\{l_1^+(t)\}$ and the slow subspace $E^s(t) = L_2^-(t) = span\{l_2^-(t)\}$, where the fast direction is $l_1^+(t) = [\cos\theta(t) \quad \sin\theta(t)]^T$ and the slow direction is $l_2^-(t) = [-\sin\theta(t) \quad \cos\theta(t)]^T$. In this example the rotational motion is periodic and Floquet theory is applicable; but, the SVD would also characterize different and irregular rotations of the fast and slow directions.

The eigenvalues of $A(t) = (\dot{R}R^T + R\Lambda R^T)$ are[23] the same as the eigenvalues of the matrix

$$(R^T\dot{R} + \Lambda) = \begin{bmatrix} \lambda_f & -\omega \\ \omega & \lambda_s \end{bmatrix} \tag{2.26}$$

because the two matrices are related by a similarity transformation. The two eigenvalues are

$$\lambda(A(t)) = \frac{1}{2}\left(\lambda_f + \lambda_s \pm \left((\lambda_f - \lambda_s)^2 - 4\omega^2\right)^{1/2}\right) \tag{2.27}$$

and are denoted by λ_+ and λ_- based on which sign is taken. The corresponding eigenvectors of $A(t)$ are

$$v_+(A(t)) = R(t)\begin{bmatrix} -\omega \\ \lambda_+(A(t)) - \lambda_f \end{bmatrix} \qquad v_-(A(t)) = R(t)\begin{bmatrix} \lambda_-(A(t)) - \lambda_s \\ \omega \end{bmatrix} \tag{2.28}$$

The eigenvalues of $\Phi(t)$ are

$$\lambda(\Phi(t)) = \frac{1}{2}\left(cos(\omega t)(e^{\lambda_f t} + e^{\lambda_s t}) \pm \left(cos^2(\omega t)(e^{\lambda_f t} + e^{\lambda_s t})^2 - 4e^{(\lambda_f + \lambda_s)t}\right)^{1/2}\right) \tag{2.29}$$

The eigenvalues of $A(t)$ and $\Phi(t)$ depend on the rotation rate ω. For $A(t)$, the eigenvalues are independent of t for this example. As ω increases from zero the eigenvalues approach each other, becoming equal when $\omega = (\lambda_s - \lambda_f)/2$, and then split as a complex conjugate pair. For a given value of ω, the eigenvalues of Φ depend on $\cos\omega t$. At times for which $\cos\omega t = 0$, the eigenvalues are pure imaginary. Only at times for which $\cos\omega t = 1$ are the eigenvalues $\lambda_- = e^{\lambda_f t}$ and $\lambda_+ = e^{\lambda_s t}$. Hence, in general, neither the eigenvalues of A nor Φ are reliable indicators of the fast and slow exponential modes.

The main purpose of this work is to compute the slow, stable and unstable manifolds associated with the timescale structure, if such structure exists. When the Lyapunov vectors (more specifically the subspaces spanned by the appropriate Lyapunov vectors) are used, then these manifolds can be calculated with no error, as we will show on a 2-dimensional example in the next chapter. However, no practical method to determine Lyapunov exponents and vectors emerges from the previous analysis because existing theory considers asymptotic behavior using infinite time limits on an invariant subset of the phase space. Furthermore, it assumes the regularity of the system. On the other hand, most of the problems motivating this research, e.g. guidance problems often formulated as optimal control problems, are posed for a finite time interval and on a compact subset that is not necessarily invariant. Even if longer averaging times are available, the sampling will be outside of the region of interest because of the region is non-invariant. The timescale information outside of the region may be different than that inside of the region and change the computed timescale information. Moreover, on non-invariant sets it is not possible to assume that the system under consideration is regular. The techniques we will develop do not require a strict compatibility between the forward and backward Lyapunov exponents as in the second property in the Definition (2.2.5).

When the subset is not invariant, the timescales and the associated geometric structure characteristics of the flow on the subset must be computable on finite-time trajectory segments. In the next section, a method for extracting the timescale information and its associated tangent space structure on a compact non-invariant subset is presented.

2.3 Finite Time Lyapunov Exponents and Vectors

Existing dynamical systems theory[19] for manifold structure in the state space considers an invariant set and is based on asymptotic properties. Rates of tangent vector contraction and expansion are characterized by Lyapunov exponents defined as limits when $t \to \infty$ or $t \to -\infty$. In sharp contrast, our interest is in timescale structure on a compact region $\mathcal{X}$ that is not invariant and thus only accommodates finite averaging times. The behavior outside of $\mathcal{X}$ may be different than that inside $\mathcal{X}$, so we do not want the Lyapunov exponents to be influenced by behavior outside of $\mathcal{X}$. Hence we use finite-time Lyapunov exponents to characterize the rates of contraction and expansion and finite-time Lyapunov vectors to characterize the tangent space structure. Fortunately, a timescale gap that induces tangent space structure also ensures that structure is computable.

We consider in particular the system behavior on an n-dimensional compact subset $\mathcal{X} \subset \mathcal{Y}$. For example, $\mathcal{X}$ could be generated by choosing a closed sphere $\Omega \in \mathcal{Y}$ of initial conditions for x, centered on the initial point in the state space for a nominal trajectory, and then integrating Eq. (2.1) for time T_c to yield $\mathcal{X} = \{x \in \mathcal{Y} : x = \phi(t, x_0)$ for some $t \in [0, T_c]$ and $x_0 \in \Omega\}$. For each $x \in \mathcal{X}$, there is a maximal time interval $\mathcal{T}(x) = [\underline{t}(x), \bar{t}(x)]$ which includes zero, such that $\phi(t, x) \in \mathcal{X}$ for all $t \in \mathcal{T}(x)$. The minimum time to reach transversely the boundary of $\mathcal{X}$ from x is $\bar{t}(x)$ for forward time propagation and $\underline{t}(x)$ for backward time propagation. If x is on the boundary of $\mathcal{X}$, then one of these times can be zero. If the trajectory never leaves $\mathcal{X}$ in forward time, then $\bar{t}(x)$ is taken to be infinite, and similarly for backward time. If $\bar{t}(x) = \infty$ for all $x \in \mathcal{X}$, then $\mathcal{X}$ is a positively invariant set for the dynamics under consideration; if $\underline{t}(x) = -\infty$ for all $x \in \mathcal{X}$, then $\mathcal{X}$ is a negatively invariant set; and if $\mathcal{T}(x) = (-\infty, \infty)$ for all $x \in \mathcal{X}$ then $\mathcal{X}$ is an invariant set. We include the possibility of $\mathcal{X}$ being an invariant set, even though our interest is in the non-invariant

case, because we want to connect our developments to existing dynamical systems theory.

A sphere of initial conditions for $v \in T_x\mathcal{X}$, propagated along a trajectory of the nonlinear system for time T according to the linearized dynamics, evolves into an ellipsoid. A vector $v_0 \in T_{x_0}\mathcal{X}$, propagated for T units of time along the trajectory $\phi(t, x_0)$, evolves to the vector $v_T = \Phi(T, x_0)v_0$ in the tangent space $T_{\phi(T,x_0)}\mathcal{X}$. To simplify the notation, the subscript "0" will not be used further; rather x and v will be used to denote the initial state and tangent vectors.

The ratio of the Euclidean lengths of an initial non-zero vector and its corresponding final vector, $\sigma = \|v_T\|/\|v\|$, is a multiplier that characterizes the net expansion (growth), if $\sigma > 1$, or contraction, if $\sigma < 1$, of the vector over the time interval $(0, T)$. The propagation time T is always taken to be positive whether forward or backward. The forward and backward finite-time Lyapunov exponents are given by

$$\begin{aligned} \mu^+(T, x, v) &= \tfrac{1}{T} \ln \sigma^+(T, x, v) = \tfrac{1}{T} \ln \tfrac{\|\Phi(T,x)v\|}{\|v\|} \\ \mu^-(T, x, v) &= \tfrac{1}{T} \ln \sigma^-(T, x, v) = \tfrac{1}{T} \ln \tfrac{\|\Phi(-T,x)v\|}{\|v\|} \end{aligned} \tag{2.30}$$

for propagation time $T > 0$. For $v = 0$, define $\mu^+(T, x, 0) = \mu^-(T, x, 0) = -\infty$. A Lyapunov exponent allows the corresponding multiplier to be interpreted as an average exponential rate, i.e., $\sigma = exp(\mu \cdot T)$.

Discrete forward and backward Lyapunov spectra, for each (T, x), can be defined in terms of the extremal values of the forward and backward exponents, respectively. For forward propagation, these extremal values are the exponents for the unit vectors in $T_x\mathcal{X}$ that map to the principal axes of an ellipsoid in $T_{\phi(T,x)}\mathcal{X}$, and there are at most n distinct extremal values for each (T, x).

One way to obtain the extremal exponents is to compute the singular value decompo-

sition (SVD) of $\Phi(T,x) = N^+(T,\phi(T,x))\Sigma^+(T,x)L^+(T,x)^T$, where

$$\Sigma^+(T,x) = \begin{pmatrix} \sigma_1^+(T,x) & & \\ & \ddots & \\ & & \sigma_n^+(T,x) \end{pmatrix} \tag{2.31}$$

contains the singular values and the ordering is such that $\sigma_1^+(T,x) \leq \sigma_2^+(T,x) \leq \ldots \leq \sigma_n^+(T,x)$, and to compute the extremal Lyapunov exponents as $\mu_i^+(T,x) = (1/T)\ln\sigma_i^+(T,x)$, $i = 1,\ldots,n$. The column vectors of $L^+(T,x)$ are denoted $l_i^+(T,x), i = 1,\ldots,n$ are the finite time Lyapunov vectors and the column vectors of $N^+(T,\phi(T,x))$ are denoted $n_i^+(T,\phi(T,x)), i = 1,\ldots,n$ are the principal axes of the ellipsoid in $T_{\phi(T,x)}\mathcal{X}$. Rearranging the SVD of $\Phi(T,x)$, we can write $\Phi(T,x)l_i^+(T,x) = \exp(\mu_i^+(T,x)T)n_i^+(T,\phi(T,x))$ which indicates that $l_i^+(T,x) \in T_x\mathcal{X}$ whereas $n_i^+(T,\phi(T,x)) \in T_{\phi(T,x)}\mathcal{X}$.

Similarly for backward propagation, the extremal values are the exponents for the unit vectors in $T_x\mathcal{X}$ that map to principal axes of an ellipsoid in $T_{\phi(-T,x)}\mathcal{X}$. The backward extremal exponents can be obtained from the singular value decomposition $\Phi(-T,x) = N^-(T,\phi(-T,x))\Sigma^-(T,x)L^-(T,x)^T$, assuming the ordering on the diagonal of $\Sigma^-(T,x)$ is such that $\sigma_1^-(T,x) \geq \ldots \geq \sigma_n^-(T,x)$, by $\mu_i^-(T,x) = (1/T)\ln\sigma_i^-(T,x)$, $i = 1,\ldots,n$. The column vectors of $L^-(T,x)$ denoted by $l_i^-(T,x)$, $i = 1,\ldots,n$ are backward finite time Lyapunov vectors. For the column vectors of $L^-(T,x)$ and $N^-(T,\phi(-T,x))$, we have $l_i^-(T,x) \in T_x\mathcal{X}$ whereas $n_i^-(T,\phi(-T,x)) \in T_{\phi(-T,x)}\mathcal{X}$.

In summary, a sphere of tangent vectors in $T_x\mathcal{X}$ is propagated T units of time forward to an ellipsoid in $T_{\phi(T,x)}\mathcal{X}$ and backward to another ellipsoid in $T_{\phi(-T,x)}\mathcal{X}$. In $T_x\mathcal{X}$, the $l_i^+(T,x)$ vectors propagate to the principal axes of the forward ellipse, whereas the $l_i^-(T,x)$ vectors propagate to the principal axes of the backward ellipse. See Fig.(2.2) for the case of $n = 1$. The finite time Lyapunov vectors, will be used to define subspaces in $T_x\mathcal{X}$ with different exponential rates.

Figure 2.2: Trajectory of nonlinear system and associated tangent spaces, illustrating the role of the Lyapunov exponents and vectors in the forward and backward propagation of a sphere of tangent vectors.

A note on the uniqueness of the singular value decomposition: The assumption that the Lyapunov exponents are ordered as $\mu_1^+(T,x) \leq ... \leq \mu_n^+(T,x)$ is not only for simplicity, but it is also required for the uniqueness of singular value decomposition of the transition matrix. An assumption for the ordering of the exponents, i.e., entries of Σ in $\Phi = N\Sigma L^T$, assures the uniqueness of N, Σ, and L.

Relations between the forward and backward exponents and vectors over the same trajectory segment: It is known that for the LTV systems the transition matrix has the property $[\Phi(t,t_0)]^{-1} = \Phi(t_0,t)$ where t_0 is the time at which the propagation begins and t is the time at which the propagation ends. In our notation, this relation can be written as $\Phi(T,x) = \Phi(-T,\phi(T,x))^{-1}$. Using this relation and the SVD of each transition matrix as

$$\begin{aligned} \Phi(T,x) &= N^+(T,\phi(T,x))\Sigma^+(T,x)L^+(T,x)^T \\ \Phi(-T,\phi(T,x)) &= N^-(T,x)\Sigma^-(T,\phi(T,x))L^-(T,\phi(T,x))^T, \end{aligned} \tag{2.32}$$

the following relations between forward and backward exponents and vectors over the same trajectory segment can be written

$$\begin{aligned} n_i^+(T,\phi(T,x)) &= l_i^-(T,\phi(T,x)); \\ \mu_i^+(T,x) &= -\mu_i^-(T,\phi(T,x)); \\ l_i^+(T,x) &= n_i^-(T,x). \end{aligned} \tag{2.33}$$

Figure (2.3) illustrates these relations.

Relations between the backward exponents and the exponents of the adjoint system over the same trajectory segment: The adjoint system of a linear system, $\delta\dot{x} = A\delta x$, is $\delta\dot{\hat{x}} = -A^T\delta\hat{x}$. It can be shown that $\Phi(t,t_0;-A^T) = [\Phi(t,t_0;A)]^{-T}$ [20]. Let $\Phi(t,t_0;-A^T)$ be denoted by $\Phi_*(t,t_0)$. Thus, $\Phi_*(T,x) = \Phi(T,x)^{-T} = \Phi(-T,\phi(T,x))^T$. By equating the SVDs of $\Phi_*(T,x)$ and $\Phi(-T,\phi(T,x))^T$, the following relations can be

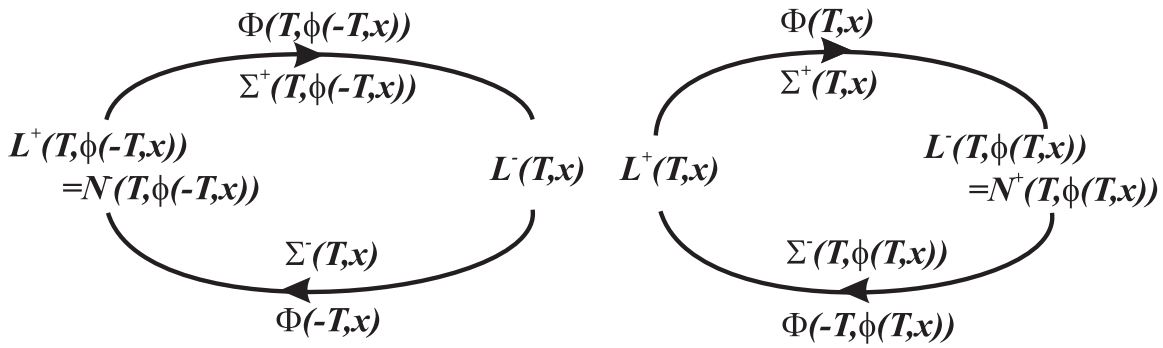

Figure 2.3: Correspondence between the backward and forward N and L matrices computed from the SVD of the transition matrix.

obtained

$$\begin{aligned} \Sigma_*(T,x) &= \Sigma^-(T,\phi(T,x)) \\ L_*(T,x) &= N^-(T,x) \\ N_*(T,\phi(T,x)) &= L^-(T,\phi(T,x)). \end{aligned} \tag{2.34}$$

Using these relations and the fact that the infinite time Lyapunov exponents are constant along the trajectories, we can verify that in the definition of regularity we stated earlier the backward exponents and the exponents of the adjoint systems can be used equivalently.

Optimization problem interpretation of the Lyapunov exponents and vectors: It can be shown that the columns of $L^+(T,x)$, the vectors that map to the principal axes of the ellipsoid at the point $\phi(T,x)$, are the right singular vectors of $\Phi(T,x)$ by solving the following constrained optimization problem.

$$\begin{gathered} extremize \;\; v^T\Phi(T,x)^T\Phi(T,x)v \;\; over \;\; v \\ subject\ to \;\; v^Tv = 1 \end{gathered} \tag{2.35}$$

By using a Lagrange multiplier λ, the Lagrangian can be written as

$$\mathcal{L}(v,\lambda) = v^T\Phi(T,x)^T\Phi(T,x)v + \lambda(1 - v^Tv).$$

Differentiating $\mathcal{L}$ with respect to v, $\Phi(T,x)^T\Phi(T,x)v^* = \lambda v^*$, where v^* is the optimizing solution, can be written. Thus, the optimizing solution v^* is an eigenvector of $\Phi(T,x)^T\Phi(T,x)$. Consequently, it is a right singular vector of $\Phi(T,x)$ [24]. The solution

to the following extremization problem gives the columns of $L^-(T,x)$

$$\begin{array}{c} extremize \;\; v^T\Phi(-T,x)^T\Phi(-T,x)v \;\; over \;\; v \\ subject\ to \;\; v^Tv = 1. \end{array} \tag{2.36}$$

Similar extremization problems can be used in order to define the infinite time Lyapunov exponents and vectors for regular systems. For example, the solution to the problem

$$\begin{array}{c} extremize \;\; \lim_{T\to\infty} \frac{1}{T} \ln \|\Phi(T,x)v\| \qquad over \;\; v \\ subject\ to \;\; \|v\| = 1 \end{array} \tag{2.37}$$

is the vectors $l_i^+(x),\ i = 1, ..., n$. The regularity assures that the following limits exists and the vectors $l_i^+(x),\ i = 1, ..., n$ and the Lyapunov exponents μ_i^+ can be computed as the eigenvectors and the eigenvalues of

$$\lim_{T\to\infty} [\Phi(T,x)^T\Phi(T,x)]^{1/2T}. \tag{2.38}$$

Despite the fact that Lyapunov exponents are constant along the trajectories and Lyapunov vectors are only functions of the base point $x \in \mathcal{X}$, the finite time Lyapunov exponents and vectors depend on both the base point and the averaging time.

To simplify the presentation, we assume that the forward and backward extremal exponents are distinct for all T and x. The column vectors of $L^+(T,x)$ and the column vectors of $L^-(T,x)$ finite time Lyapunov vectors each provide orthonormal bases for $T_x\mathcal{X}$. The following subspaces, for $i = 1, \ldots, n$, can be defined by the Lyapunov vectors

$$\begin{aligned} L_i^+(T,x) &= span\{l_1^+(T,x), \ldots, l_i^+(T,x)\} \\ L_i^-(T,x) &= span\{l_i^-(T,x), \ldots, l_n^-(T,x)\}. \end{aligned} \tag{2.39}$$

Proposition 2.3.1 *The subspaces $L_i^+(T,x)$ and $L_i^-(T,x)$ have the properties:*

i) $v \in L_i^+(T,x)\backslash\{0\} \Rightarrow \mu^+(T,x,v) \le \mu_i^+(T,x)$

ii) $v \in L_i^-(T,x)\backslash\{0\} \Rightarrow \mu^-(T,x,v) \le \mu_i^-(T,x)$.

Proof: Let v be a unit vector in $span\{l_1^+(T,x),\ldots,l_i^+(T,x)\}$. v can be decomposed as $v = a_1 l_1^+(T,x) + ... + a_i l_i^+(T,x)$ where $a_1^2 + ... + a_i^2 = 1$. The finite time Lyapunov exponent of v can be written as $\mu^+(T,x,v) = \frac{1}{T}\ln\left(a_1^2 e^{2\mu_1^+(T,x)T} + ... + a_i^2 e^{2\mu_i^+(T,x)T}\right)^{1/2}$ by using the orthogonality of the Lyapunov vectors, the property of the Lyapunov vectors that they are unit length by definition, and the equality $\Phi(T,x)l_i^+(T,x) = e^{\mu_i^+(T,x)T} n_i^+(T,\phi(T,x))$. Since $a_1^2 e^{2\mu_1^+(T,x)T} + ... + a_i^2 e^{2\mu_i^+(T,x)T}$ is a convex combination of $e^{2\mu_1^+(T,x)T}, ..., e^{2\mu_i^+(T,x)T}$, $\mu^+(T,x,v)$ is less than $\mu_i^+(T,x)$. The proof of the second property in the proposition is similar to the proof of the first property just T is replaced by $-T$. □

Similar to the filtrations formed by Lyapunov vectors, the subspaces defined in terms of the finite time Lyapunov vectors form filtrations as

$$\begin{aligned} \{0\} = L_0^+ \subset L_1^+(T,x) \subset L_2^+(T,x) \subset ... \subset L_n^+(T,x) = T_x\mathcal{X} \\ T_x\mathcal{X} = L_n^-(T,x) \supset L_{n-1}^-(T,x) \supset ... \supset L_n^-(T,x) \supset L_{n+1}^- = \{0\} \end{aligned} \tag{2.40}$$

The feasibility of determining timescale structure depends on whether the structure of primary interest converges, as the averaging time increases, within the available range of averaging times. Next section is devoted to the convergence properties of the finite time Lyapunov exponents and vectors. The convergence of the finite time Lyapunov vectors is based on the existence of a sufficiently large spectral gap.

2.4 Convergence Properties of the Finite Time Lyapunov Exponents and Vectors

The finite time Lyapunov exponents do not converge to the Lyapunov exponents in general. The discussion in the section (2.2) is given for the Lyapunov regular systems. For the Lyapunov regular systems the forward and backward finite time Lyapunov exponents converge with the increasing averaging time and are of opposite signs. The relations be-

tween the finite time Lyapunov exponents and their infinite time limits for the forward and backward cases are

$$\begin{aligned} &\lim_{T\to\infty} \mu_i^+(T,x) = \mu_i^+, \quad i = 1, ..., n, \\ &\lim_{T\to\infty} \mu_i^-(T,x) = \mu_i^- = -\mu_i^+, \quad i = 1, ..., n. \end{aligned} \tag{2.41}$$

A less restrictive requirement is the convergence of the backward and forward finite time Lyapunov exponents as the averaging time tends to ∞, but not necessarily to the values of opposite sign. If the forward and backward finite time Lyapunov exponents converge, then the system is called forward and backward regular, respectively. In this case the relations between the finite time Lyapunov exponents and Lyapunov exponents are

$$\begin{aligned} &\lim_{T\to\infty} \mu_i^+(T,x) = \mu_i^+, \quad i = 1, ..., n, \\ &\lim_{T\to\infty} \mu_i^-(T,x) = \mu_i^-, \quad i = 1, ..., n. \end{aligned} \tag{2.42}$$

2.4.1 Differential equations of the finite time Lyapunov exponents and vectors with respect to the averaging time

Goldhirsch et al.[25] developed the evolution equations for the finite time Lyapunov exponents $\mu_i^+(T,x)$ and the finite time Lyapunov vectors $l_i^+(T,x)$.

Lemma 2.4.1 *[11] Over intervals of the averaging time T during which the finite time Lyapunov exponents are distinct, the finite time Lyapunov exponents and vectors at $x \in \mathcal{X}$ evolve with the averaging time T according to the differential equations*

$$\frac{\partial}{\partial T} e^{2\mu_i^+(T,x)T} = e^{2\mu_i^+(T,x)T} l_i^+(T,x)^T Q^T [J(T)^T + J(T)] Q l_i^+(T,x), \tag{2.43}$$

$$\begin{aligned} \frac{\partial}{\partial T} l_i^+(T,x) = &\sum_{k=1}^{i-1} \frac{l_k^+(T,x)^T Q^T [J(T)^T + J(T)] Q l_i^+(T,x)}{e^{(\mu_i^+(T,x) - \mu_k^+(T,x))T} - e^{(\mu_k^+(T,x) - \mu_i^+(T,x))T}} l_k^+(T,x) + c_{ii} l_i^+(T,x) \\ &+ \sum_{k=i+1}^{n} \frac{l_k^+(T,x)^T Q^T [J(T)^T + J(T)] Q l_i^+(T,x)}{e^{(\mu_i^+(T,x) - \mu_k^+(T,x))T} - e^{(\mu_k^+(T,x) - \mu_i^+(T,x))T}} l_k^+(T,x). \end{aligned} \tag{2.44}$$

where $J(T) = J(x(T))$ and $Q = Q(T,x) = N^+(T, \phi(T,x)) L^+(T,x)^T$ are function of averaging time T and the state x. The coefficient c_{ii} is determined such that $l_i^+(T,x)$ evolves continuously with unit length.

Note that replacing Q by $Q(T,x) = N^+(T,\phi(T,x))L^+(T,x)^T$ gives

$$Ql_i^+(T,x) = n_i^+(T,\phi(T,x)). \tag{2.45}$$

because of the mutual orthogonality and unit length properties of the Lyapunov vectors.

A similar result for backward finite time Lyapunov exponents and vectors can be derived. It is given in the next lemma.

Lemma 2.4.2 *Over intervals of the averaging time T during which the finite time Lyapunov exponents are distinct, the finite time Lyapunov exponents and vectors at $x \in \mathcal{X}$ evolve with the averaging time T according to the differential equations*

$$\frac{\partial}{\partial T}e^{2\mu_i^-(T,x)T} = -e^{2\mu_i^-(T,x)T}l_-^+(T,x)^T\tilde{Q}^T[J(-T)^T + J(-T)]\tilde{Q}l_i^-(T,x), \tag{2.46}$$

$$\begin{aligned}\tfrac{\partial}{\partial T}l_i^-(T,x) = &-\textstyle\sum_{k=1}^{i-1}\frac{l_k^-(T,x)^T\tilde{Q}^T[J(-T)^T+J(-T)]\tilde{Q}l_i^-(T,x)}{e^{(\mu_i^-(T,x)-\mu_k^-(T,x))T}-e^{(\mu_k^-(T,x)-\mu_i^-(T,x))T}}l_k^-(T,x) - c_{ii}l_i^-(T,x)\\ &-\textstyle\sum_{k=i+1}^{n}\frac{l_k^-(T,x)^T\tilde{Q}^T[J(-T)^T+J(-T)]\tilde{Q}l_i^-(T,x)}{e^{(\mu_i^-(T,x)-\mu_k^-(T,x))T}-e^{(\mu_k^-(T,x)-\mu_i^-(T,x))T}}l_k^+(T,x)\end{aligned} \tag{2.47}$$

where $J(-T) = J(x(-T))$ and $\tilde{Q} = \tilde{Q}(T,x) = N^-(T,\phi(T,x))L^-(T,x)^T$ are function of averaging time T and the state x. The coefficient c_{ii} is determined such that $l_i^-(T,x)$ evolves continuously with unit length.

2.4.2 Convergence properties

Definition 2.4.3 *For an n-dimensional dynamical system on a compact set $\mathcal{X}$ with finite-time Lyapunov exponents ordered as $\mu_1^+(T,x) < \mu_2^+(T,x) < \ldots < \mu_n^+(T,x)$, neighboring exponents $\mu_j^+(T,x)$ and $\mu_{j+1}^+(T,x)$ for a particular value j are temporally uniformly distinct at x, if there exists a T independent spectral gap $\Delta\mu^+(x) > 0$ and an averaging time $T_{min}(x)$ such that $\mu_{j+1}^+(T,x) - \mu_j^+(T,x) > \Delta\mu^+(x)$ for all $T \in \mathcal{T}(x)\backslash[-T_{min}(x), T_{min}(x)]$. $T_{min}(x)$ is introduced to eliminate any initial transient period that is not representative of the subsequent behavior and should be small relative to the available averaging time. If*

μ_j^+ and μ_{j+1}^+ are temporally uniformly distinct for all $x \in \mathcal{X}$ and there exists a positive constant $\Delta\mu$ such that $\Delta\mu < \Delta\mu(x)$ for all $x \in \mathcal{X}$, then we say there is a uniform spectral gap on $\mathcal{X}$. A uniform spectral gap for the neighboring backward time exponents μ_{k-1}^- and μ_k^- is similarly defined.

Theorem 2.4.4 *[11]If the neighboring Lyapunov exponents $\mu_j^+(T,x)$ and $\mu_{j+1}^+(T,x)$ are temporally uniformly distinct at the point x, then as T increases, the subspace $L_j^+(T,x)$ converges toward a fixed subspace $L_j^+(x)$ at least at the rate $1/(e^{\Delta\mu^+\cdot T} - e^{-\Delta\mu^+\cdot T})$ where $\Delta\mu^+(x)$ is the spectral gap. Similarly, if $\mu_{k-1}^-(T,x)$ and $\mu_k^-(T,x)$ are temporally uniformly distinct at x, then as T increases, the $L_k^-(T,x)$ converges toward a fixed subspace $L_k^-(x)$ at least at the rate $1/(e^{\Delta\mu^-\cdot T} - e^{-\Delta\mu^-\cdot T})$ where $\Delta\mu^-(x)$ is a bound on $\mu_{k-1}^- - \mu_k^-$ over T.*

The proof of Theorem (2.4.4) given in [11, 25]. It is based on Lemma (2.4.1) and Lemma (2.4.2). The term $l_k^+(T,x)^T Q[F(T)^T + F(T)]Ql_i^+(T,x)$ in Eq.(2.4.1) can be bounded using the continuity of $F(T)^T + F(T)$ on the compact set $\mathcal{X}$ and the fact that the Lyapunov vectors have unit length. Thus, the coefficients of $l_j^+(T,x), ..., l_n^+(T,x)$ for the rates of change of $l_1^+(T,x), ..., l_j^+(T,x)$ are bounded by a function which decays at the rate $1/(e^{\Delta\mu^+\cdot T} - e^{-\Delta\mu^+\cdot T})$. To see this, let $l_k^+(T,x)^T Q[F(T)^T + F(T)]Ql_i^+(T,x)$ be bounded by $B > 0$ for all T, i.e., $\|l_k^+(T,x)^T Q[F(T)^T + F(T)]Ql_i^+(T,x)\| \leq B$. Then, for $k > i$

$$\frac{l_k^+(T,x)^T Q^T[J(T)^T + J(T)]Ql_i^+(T,x)}{e^{(\mu_i^+(T,x)-\mu_k^+(T,x))T} - e^{(\mu_k^+(T,x)-\mu_i^+(T,x))T}} \leq \frac{B}{(e^{\Delta\mu^+\cdot T} - e^{-\Delta\mu^+\cdot T})}, \tag{2.48}$$

which decays at the rate $1/(e^{\Delta\mu^+\cdot T} - e^{-\Delta\mu^+\cdot T})$.

Summarizing, the subspaces $L_i^+(T,x)$ converge to fixed subspaces at the rate $1/(e^{\Delta\mu^+\cdot T} - e^{-\Delta\mu^+\cdot T})$, meaning that the components of the vectors in $L_i^+(T,x)$ in the directions that are not in the converged fixed subspace decay at that rate. The finite time Lyapunov vectors may or may not converge. If they converge, their convergence is slower than the

rate $1/(e^{\Delta\mu^+ \cdot T} - e^{-\Delta\mu^+ \cdot T})$; in fact $l_j^+(T,x),\ j = 1,...,i$ converge at a rate related to the difference of $\mu_j^+(T,x)$ from $\mu_{j-1}^+(T,x)$ and $\mu_{j+1}^+(T,x)$. If $\mu_j^+(T,x),\ j = 1,...,n$ are uniformly distinct with a spectral gap $\Delta\mu_j^+$, then the individual finite time Lyapunov vectors converge at the rate $1/(e^{\Delta\mu_j^+ \cdot T} - e^{-\Delta\mu_j^+ \cdot T})$.

The question whether the converged fixed subspaces are the subspaces spanned by the (infinite time) Lyapunov vectors has been raised by Goldhirsch et al. [25] and answered that the finite time subspaces converge to the infinite time subspaces by showing that the relation $\Phi(t,x)l_i^+(\infty,x) \propto e^{\mu_i^+ \cdot t}$ holds for large t. Therefore, when the subspaces $L_i^+(T,x),\ i = 1,...,n$ spanned by the finite time Lyapunov vectors converge the following limits can be written

$$\lim_{T\to\infty} L_i^+(T,x) = L_i^+(x),\ i = 1,...,n, \tag{2.49}$$

and when the individual finite time Lyapunov vectors converge

$$\lim_{T\to\infty} l_i^+(T,x) = l_i^+(x),\ i = 1,...,n. \tag{2.50}$$

For the systems whose finite time Lyapunov exponents converge, the following relation is conjectured and tested numerically in [25]

$$\mu_i^\pm(T,x) = \mu_i^\pm + \frac{b_i + \xi_i(T)}{T}, \tag{2.51}$$

where b_i is constant and $\xi_i(T)$ is the "noise" term whose time average is zero. Thus, although the convergence rate of the finite time Lyapunov vectors (or the subspaces spanned by the finite time Lyapunov vectors) is exponential, the convergence of the finite time Lyapunov exponents, when they converge, is at a slower rate $1/T$. The convergence of the finite time Lyapunov exponents and vectors is illustrated in the next example.

Example 2.4.5 *Consider the second order nonlinear differential equations*

$$\dot{x}_1 = (1 + 2a(x_1 + x_2))\lambda_s(x_1 - a(x_1 + x_2)^2) + 2a(x_1 + x_2)\lambda_f(x_2 + a(x_1 + x_2)^2).$$

$$\dot{x}_2 = -2a(x_1 + x_2)\lambda_s(x_1 - a(x_1 + x_2)^2) + (1 - 2a(x_1 + x_2))\lambda_f(x_2 + a(x_1 + x_2)^2). \tag{2.52}$$

where $a = 0.01$*, and* λ_s *and* λ_f *are constants. This nonlinear system has been used in [11, 26] and it has been shown that the finite time Lyapunov exponents converge for* $\lambda_s = -1$ *and* $\lambda_f = -10$*. Figure (2.4) shows the Lyapunov exponents and the angles between* $l_i^+(T, x),\ i = 1, 2$*, and* $l_i^-(T, x),\ i = 1, 2$ *and the horizontal axis for* $\lambda_s = -1$ *and* $\lambda_f = -10,\ -3$*. For both cases, the finite time Lyapunov exponents converge. For* $\lambda_f = -10$*, they converge to* -10 *and* -1 *and the gap is* 9*, whereas for* $\lambda_f = -3$*, they converge to* -3 *and* -1 *and the gap is* 2*. Since the gap is smaller in the case of* $\lambda_f = -3$ *than that in the case of* $\lambda_f = -10$*, a slower convergence of the finite time Lyapunov vectors in the case of* $\lambda_f = -3$ *is expected. The last two plots in Fig. (2.4) show indeed that the finite time Lyapunov vectors in the case of* $\lambda_f = -3$ *converge at a slower rate.*

2.5 Practical Invariance of Finite Time Distributions

Definition 2.5.1 *(Practically Invariant Distribution) Let* $\xi_1(x), \xi_2(x), ..., \xi_n(x)$ *be a basis for* $T_x\mathcal{X}$*, and* $\xi_1(x), \xi_2(x), ..., \xi_m(x)$*,* $m \leq n$ *span a distribution* $\Lambda(x)$ *on* $T\mathcal{X}$*. In general,* $\Phi(t, x)\Lambda(x)$ *is spanned by* $\xi_i(\phi(t, x)),\ i = 1, ..., n$*. Let* v *be any nonzero vector in* $\Lambda(x)$*. If these exist* $\epsilon > 0$ *and* $t_1,\ t_2 > 0$ *such that*

$$\max_{v \in \Lambda(x)} \frac{\|\Phi(t, x)\, v - \Pi_\Lambda(\Phi(t, x)\, v)\|}{\|\Phi(t, x)\, v\|} \leq \epsilon \tag{2.53}$$

for all $t \in [-t_1, t_2]$*, and* Π_Λ *is the projection on the subspace* $\Lambda(\phi(t, x))$*, then* $\Lambda(x)$ *is a practically invariant distribution of the order of* ϵ *on* $[-t_1, t_2]$ *under the linear flow.*

ϵ is the level of accuracy with which the subspace $\Lambda(T, \phi(t, x))$ is required to approximate the subspace $\Phi(t, x)\Lambda(x)$.

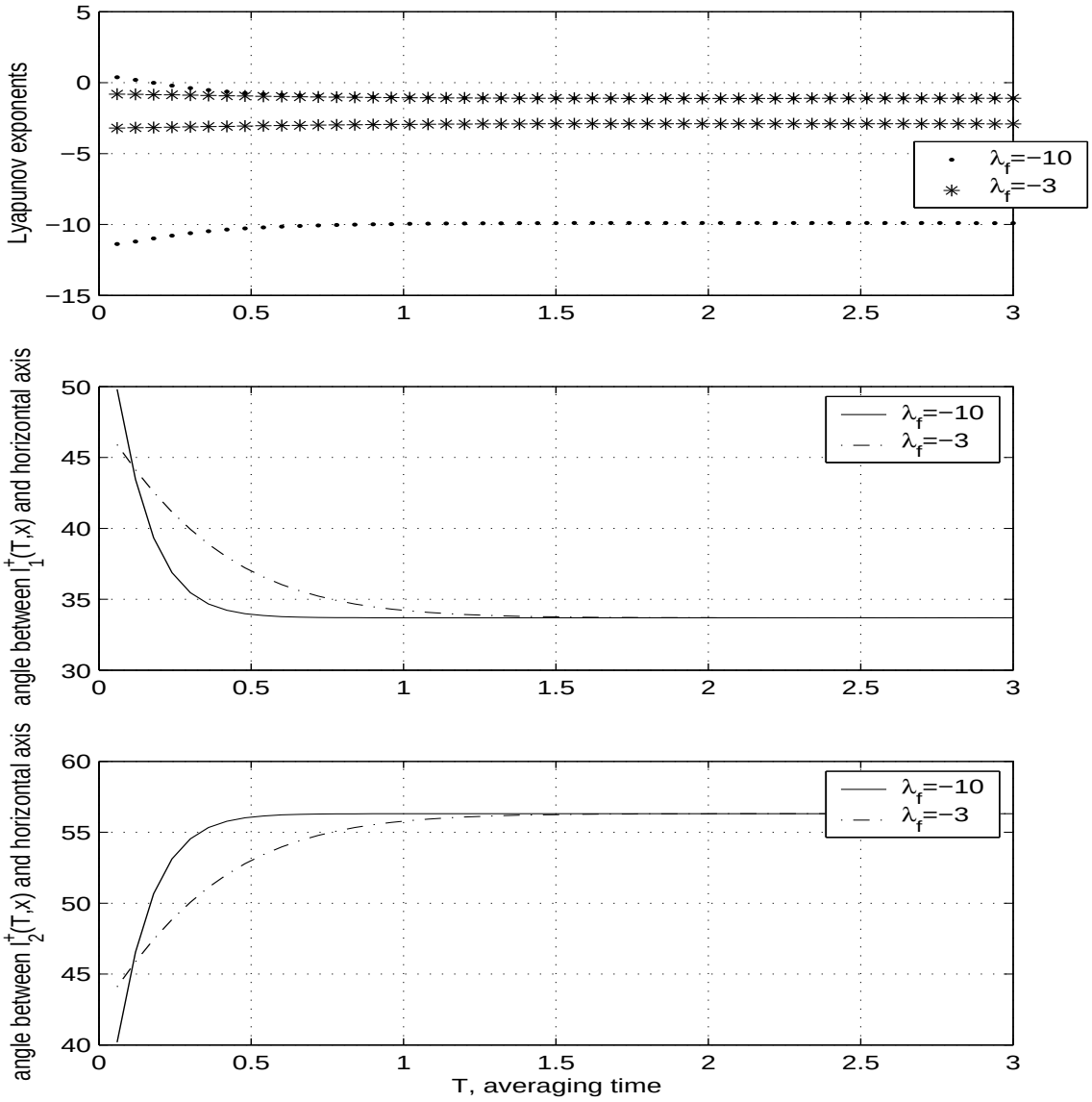

Figure 2.4: The effect of the spectral gap on the convergence rate of the finite time Lyapunov vectors.

Proposition 2.5.2 *If the condition*

$$\frac{(\Delta\mu_i)^{-1}}{T_c - T_{min}} \ll 1 \tag{2.54}$$

is satisfied, the distributions $L_i^+(T,x) = span\{l_1^+(T,x), ..., l_i^+(T,x)\}$ *are practically invariant under the propagation of the transition matrix* $\Phi(t,x)$.

Note that the distribution $L_i^+(T,\cdot)$ assigns a subspace to each point $x \in \mathcal{X}$ which coincides the subspace defined in terms of the finite time Lyapunov vectors in previous sections.

Proof: The proof will be given only for $n = 2$ and only for the distribution $L_1^+(T,x)$. The distribution $L_2^+(T,x) = T_x\mathcal{X} = \mathcal{R}^2$ is trivially invariant. A generalization for higher dimensions will be explained. In the 2-dimensional case the practically invariant distribution is the span of $l_1^+(T,x)$. Since it is a linear subspace at each point x, the practical invariance of $l_1^+(T,x)$ suffices the practical invariance of its span. Pre-multiplication of $\Phi(-T,\phi(T,x))l_1^-(T,\phi(T,x)) = e^{\mu_1^-(T,\phi(T,x))T}l_1^+(T,x)$ by $\Phi(t,x)$ yields to

$$\Phi(-(T-t),\phi(T,x))l_1^-(T,\phi(T,x)) = e^{\mu_1^-(T,\phi(T,x))T}\Phi(t,x)l_1^+(T,x). \tag{2.55}$$

By using the singular value decomposition of $\Phi(-(T-t),\phi(T,x))$ one can write the following equation.

$$\begin{aligned}\begin{bmatrix} l_1^+((T-t),\phi(t,x))^T \\ l_2^+((T-t),\phi(t,x))^T \end{bmatrix}^T diag(e^{\mu_i^-((T-t),\phi(T,x))(T-t)}) \begin{bmatrix} l_1^-((T-t),\phi(T,x))^T \\ l_2^-((T-t),\phi(t,x))^T \end{bmatrix} l_1^-(T,\phi(T,x)) \\ = e^{\mu_1^-(T,\phi(T,x))T}\Phi(t,x)l_1^+(T,x).\end{aligned} \tag{2.56}$$

Now let θ be the angle between $l_1^-(T-t,\phi(T,x))$ and $l_1^-(T,\phi(T,x))$

$$\theta = \angle(l_1^-(T-t,\phi(T,x)), l_1^-(T,\phi(T,x))). \tag{2.57}$$

Since $l_1^-((T-t),\phi(T,x))^T l_1^-(T,\phi(T,x)) = cos\theta$ and $l_2^-((T-t),\phi(T,x))^T l_1^-(T,\phi(T,x)) = sin\theta$ one can write the following equation by doing the multiplications in the last equation.

$$\begin{aligned}e^{\mu_1^-(T,\phi(T,x))T}\Phi(t,x)l_1^+(T,x) \quad &= cos\theta e^{\mu_1^-((T-t),\phi(T,x))(T-t)}l_1^+((T-t),\phi(t,x)) \\ &+ sin\theta e^{\mu_2^-((T-t),\phi(T,x))(T-t)}l_2^+((T-t),\phi(t,x)).\end{aligned} \tag{2.58}$$

Now let α be the angle $\angle(\Phi(t,x)l_1^+(T,x), l_1^+((T-t),\phi(t,x)))$. From Eq. (2.58)

$$\tan\alpha = \frac{sin\theta}{cos\theta}\frac{e^{\mu_2^-((T-t),\phi(T,x))(T-t)}}{e^{\mu_1^-((T-t),\phi(T,x))(T-t)}} \leq \frac{sin\theta}{cos\theta}e^{-\Delta\mu(T-t)}. \tag{2.59}$$

By Theorem (2.4.4), the Lyapunov vector $l_1^-(T,\phi(T,x))$ converges exponentially fast. Thus, there exists $T > t^* > 0$ such that $\frac{sin\theta}{cos\theta} \leq 1$ for all $t \in [0,t^*]$. Consequently, $tan\alpha \leq$

$e^{-\Delta\mu(T-t)}$ for all $t \in [0, t^*]$. The exponential decay in the angle between $l_1^-(T, \phi(T, x))$ and its infinite time limit actually shows that t^* is not much less than T. Due to the trigonometric relation $sin\alpha \leq tan\alpha$ in the first quadrant and the fact that $l_1^+(T, x)$ was arbitrary in the span of itself, the condition in Eq. (2.53) is satisfied with $\epsilon = e^{-\Delta\mu(T-t)}$.□

The propagation time can either be positive or negative, corresponding to forward propagation and backward propagation, respectively. Although $e^{-\Delta\mu(T-t)}$ provides a tight bound in the case of the distribution spanned by the forward Lyapunov vectors for all negative times, it grows exponentially in forward time. Thus, practical invariance of forward distributions under the propagation of the transition matrix makes sense in the interval $t \in [\underline{t}(x), t_2]$, where t_2 depends on the accuracy level, ϵ, required and the available averaging time. The averaging time, T, the forward propagation duration, t_2, should be such that $e^{-\Delta\mu(T-t)} \leq \epsilon,\ for\ all\ t \in [\underline{t}(x), t_2]$, i.e., $e^{-\Delta\mu(T-t_2)} \leq \epsilon$.

In higher dimensions the proof follows the same with an arbitrary unit vector v in $L_i^+(T, x)$. In this case bounds for $tan\alpha_j$ are exponentially decaying with increasing T and exponentially growing with increasing propagation time t, where

$$\alpha_j = \angle \left(\Pi_{ij}(\Phi(t, x)v), l_j^+(T - t, \phi(t, x))\right),\ j = 1, ..., i,\ i = i + 1, ..., n, \tag{2.60}$$

and $\Pi_{ij}(\cdot)$ is the projection on the subspace spanned by $l_j^+(T - t, \phi(t, x))$ and $l_i^+(T - t, \phi(t, x))$. These angles decay exponentially with increasing T and $\Phi(t, x)v$ converges to a vector in the subspace $L_i(T - t, \phi(t, x))$ exponentially with T, if the condition in Eq.(2.54) is satisfied.

Figure (2.5) visualizes the proof for the 3 dimensional case where the practically invariant distribution is 2 dimensional, i.e., the spectral gap is between the largest and second largest exponent.In this case the decay of α_1 and α_2 is enough to show that $\Phi(t, x)v$ is close to the subspace spanned by $l_1^+(T - t, \phi(t, x))$ and $l_2^+(T - t, \phi(t, x))$. A similar result

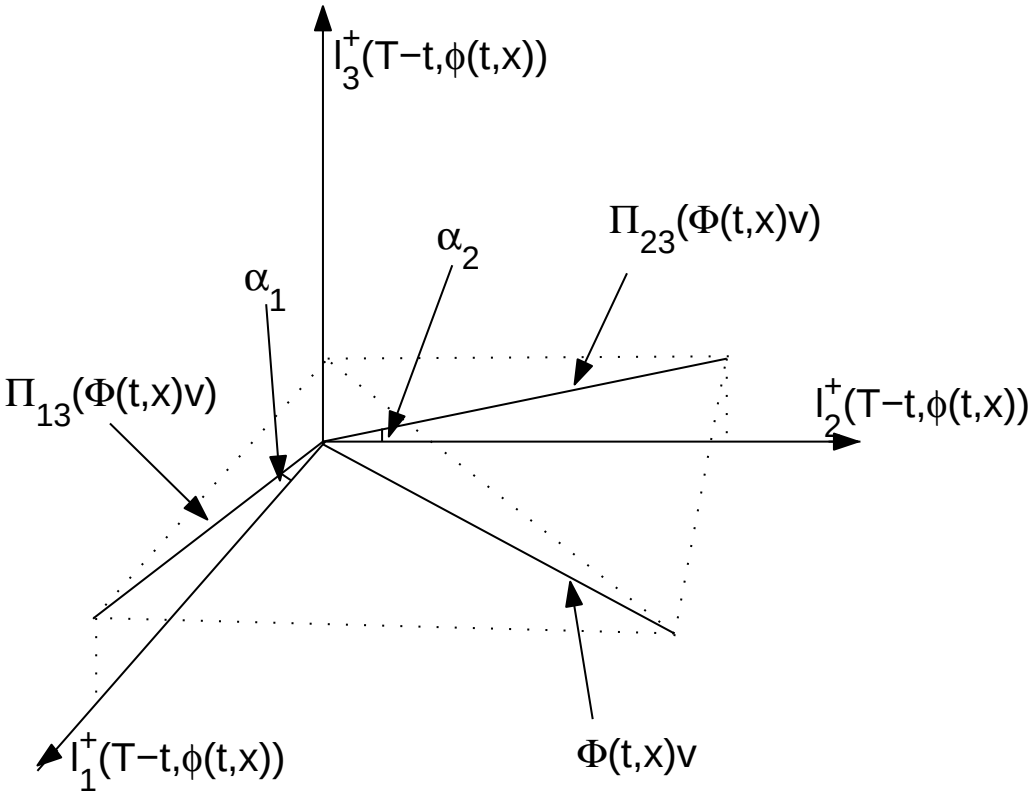

Figure 2.5: Illustration of the proof of the practical invariance for a 3 dimensional system with a spectral gap between μ_2^+ and μ_3^+.

can be stated for the distributions spanned by the backward time Lyapunov vectors.

Proposition 2.5.3 *If the condition in Eq.(2.54) is satisfied, the distributions* $L_i^-(T,x)$, $i = 1,...,n$ *are practically invariant under the propagation of the transition matrix* $\Phi(t,x)$.

Although $e^{-\Delta\mu(T-t)}$ provides a tight bound in the case of the distribution spanned by the backward time. Thus, practical invariance of backward distributions under the propagation of the transition matrix makes sense in the interval $t \in [-t_1, \bar{t}(x)]$, where t_1 depends on the accuracy level, ϵ, required and the available averaging time.

The practical invariance of $L_1^+(T,x) = span\{l_1^+(T,x)\}$ is illustrated in a 2-dimensional example (2.5.4).

Example 2.5.4 *Consider again the system in Example (2.4.5). By the equation*

$$\Phi(T,x)l_1^+(T,x) = e^{\mu_1^+(T,x)T} n_1^+(T,\phi(T,x)) = e^{\mu_1^+(T,x)T} l_1^-(T,\phi(T,x)), \tag{2.61}$$

if the vector $l_1^+(T,x)$ *is propagated by* $\Phi(t,x)$ *for* T *units of time* $\Phi(T,x)l_1^+(T,x)$ *and* $l_1^-(T,\phi(T,x))$ *are in the same direction. For the propagation times between* 0 *and* T*,* $\Phi(T,x)l_1^+(T,x)$ *cannot in general be written equal to the finite time Lyapunov vectors at* $\phi(t,x)$ *with an averaging time* T*. However, by Proposition (2.5.2) the propagated Lyapunov vector* $\Phi(T,x)l_1^+(T,x)$ *should be close to the Lyapunov vector at that point* $l_1^+(T,\phi(T,x))$ *for the propagation times that constitute a large fraction of the available averaging time. This is what we call the practical invariance and the span of* $l_1^+(T,x)$ *is the practically invariant subspace. The first plot in Fig.(2.6) shows that the direction of* $\Phi(T,x)l_1^+(T,x_0)$ *is very close to the direction of* $l_1^+(T,\phi(t,x_0))$ *for the initial* 2.5 *units of propagation time of* 3 *units of averaging time. Then, it quickly diverges from that direction and aligns with* $l_1^-(T,\phi(T,x_0))$ *at the final time. The second plot in Fig.(2.6) shows that the angle between* $\Phi(T,x)l_1^+(T,x_0)$ *and* $l_1^+(T,\phi(t,x_0))$ *is relatively small for the initial* 2.5 *units of propagation time compared to that in the rest of the* 3 *units of time .*

2.6 Computation of Lyapunov Exponents and Vectors

The most widely used methods for the computation of the Lyapunov exponents and vectors are based on two matrix decompositions of the transition matrix $\Phi(T,x)$ namely

- Singular value decomposition (SVD),
- QR decomposition.

Each method is subclassified as

- Continuous method,
- Discrete method.

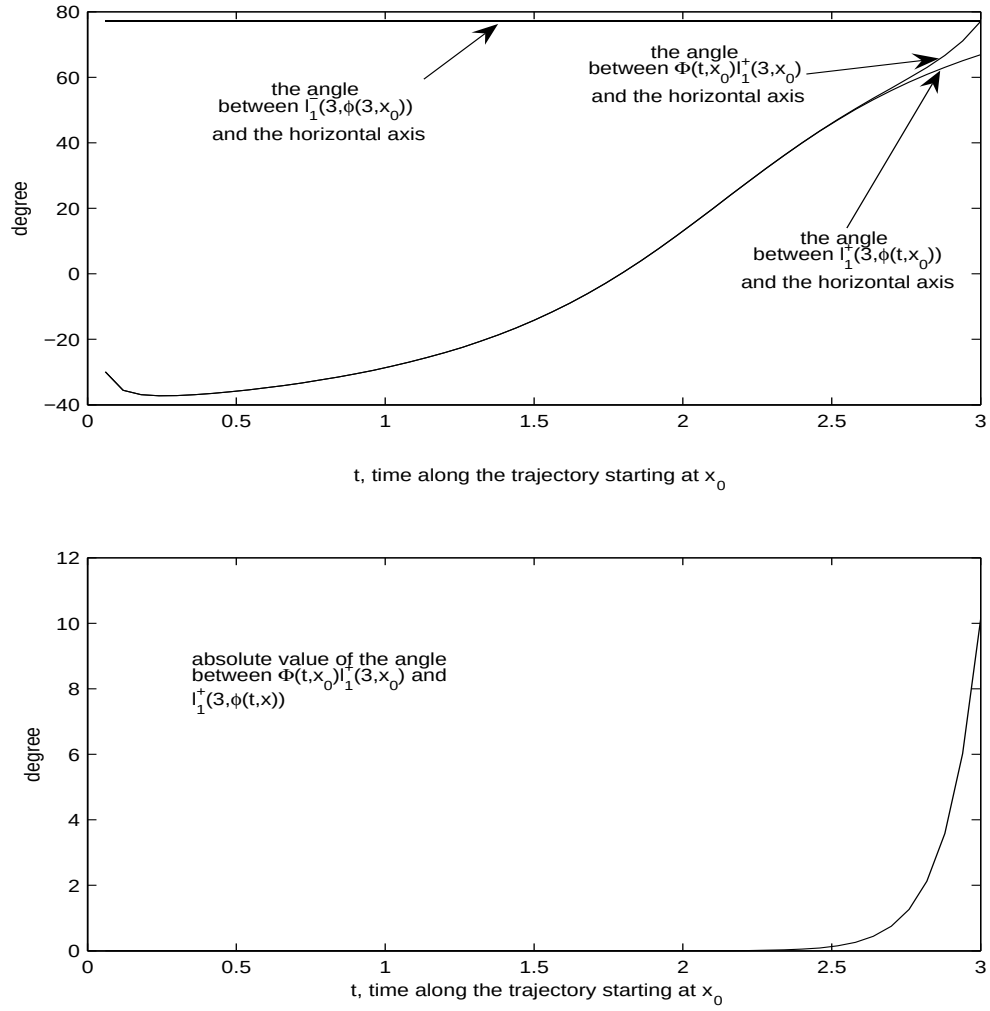

Figure 2.6: Illustration of the practical invariance in a 2 dimensional nonlinear example.

The SVD and its use in the computation of the Lyapunov exponents and vectors are studied in section (2.3). In summary, the SVD of the transition matrix

$$\Phi(T,x) = N^+(T,\Phi(T,x))\Sigma^+(T,x)L^+(T,x) \tag{2.62}$$

gives the information of which directions in a unit sphere in the tangent space at point x evolve to the principal axes of an ellipsoid in the tangent space at point $\phi(T,x)$ and the length of the principal axes of the ellipsoid. The columns of $L^+(T,x)$ are the directions in the tangent space at x that have extremal average expansion/shrinkage rates over the

period $0 - T$. Note that these directions are not necessarily the directions of extremal expansion/shrinkage for the averaging times less than T. However, they quickly converge to some fixed directions as T increases under certain circumstances given in section (2.4). The columns of $N^+(T, \phi(T, x))$ are the directions of the principal axes of the ellipsoid in the tangent space at $\phi(T, x)$.

Another matrix decomposition used for the computation of Lyapunov exponents is the QR decomposition of the transition matrix. It provides the information how the volumes V_k of k-dimensional parallelepipeds in the tangent space $T_{\phi(t,x)}\mathcal{X} \subset \mathcal{R}^n$, where $k \leq n$, change. Consider n arbitrarily chosen orthogonal unit vectors $\{u_1, ..., u_n\}$ in $T_x\mathcal{X}$. The choice of $u_i = (0, ..., 0, 1, 0, ..., 0)^T$, where the i-th element is one, is almost standard. Let $p_i \in T_{\phi(T,x)}\mathcal{X}$ be $p_i = \Phi(T, x)u_i$. Then, the QR decomposition of the transition matrix $\Phi(T, x)$ is given by [27]

$$\begin{aligned} \Phi(T,x) &= Q(T,x)R(T,x) \\ &= [q_1 \ ... \ q_n] \begin{pmatrix} R_{11} & * & \dots & * \\ 0 & R_{22} & \ddots & \vdots \\ \vdots & \ddots & \ddots & * \\ 0 & \dots & 0 & R_{nn} \end{pmatrix}, \end{aligned} \tag{2.63}$$

where R is an upper triangular matrix and Q is an orthogonal matrix such that $Q = [q_1 \ ..., \ q_n]$. $q_1, ..., q_n$ are obtained by applying a Gram-Schmidt orthogonalization to $p_1, ..., p_n$ such that p_1 and q_1 are in the same direction. Figure(2.7) illustrates this geometry in 2-dimensional case. Then, the volume of the parallelepiped at point $\phi(T, x)$ is

$$V_k = \prod_{i=1}^{k} R_{i \times i}, \tag{2.64}$$

since the volume at x is one.

Note that the SVD and the QR decomposition do not give the same information for finite times. Thus, the finite time Lyapunov exponents are not accessible from the Q and R

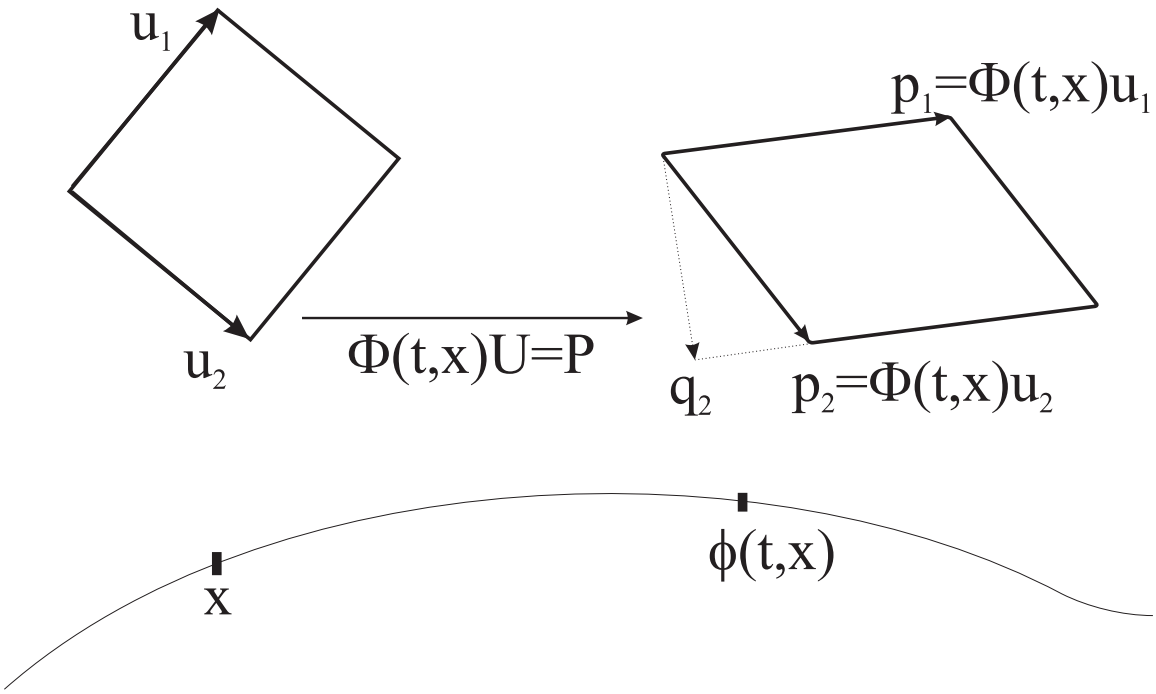

Figure 2.7: Illustration of the QR decomposition method for a 2 dimensional system.

matrices. However, some further manipulation of Q and R yields the finite time exponents and vectors. To see this, start with the SVD and QRD of the transition matrix

$$\Phi = QR = N\Sigma L^T. \tag{2.65}$$

Using the orthogonality of L and N matrices, $\Sigma = N^T QRL$. By the orthogonality of Q and N, $\Sigma^T\Sigma$ gives

$$\Sigma^T\Sigma = L^T(R^T R)L. \tag{2.66}$$

Consequently, the eigenvalues of $R^T R$ are σ_i^2 and the columns of L are the eigenvectors of $R^T R$.

When the finite time Lyapunov exponents converge, then the Lyapunov exponents are given by

$$\mu_i^+ = \lim_{T\to\infty} \frac{1}{T} \ln(R_{n-i+1\times n-i+1}). \tag{2.67}$$

Roughly speaking, the difference between the discrete and continuous methods is the order of integration and matrix decomposition. In discrete methods, Eqs. (2.1) and (2.2)

are integrated with the given initial conditions and the matrix decomposition is performed at the averaging times of interest. In continuous methods, the differential equations for the appropriate matrices among Q, R, N, Σ, and L or the entries of these matrices are integrated in order to obtain the timescale information at the averaging times of interest. Detailed information on the continuous methods can be found in [26, 28, 27, 29, 30, 31].

In the numerical computation of the transition matrix the columns of the transition matrix become linearly dependent as T increases. Therefore, it is necessary to re-initialize the integration of the Eq. (2.2) periodically and use the composition property of the transition matrix

$$\Phi(T + \Delta T, x) = \Phi(\Delta T, \phi(T, x))\Phi(T, x). \tag{2.68}$$

In order to compute $\Phi(T, x)$, the time interval $0 - T$ is discretized as $0 = T_0 < T_1 < T_2 < ... < T_i < ... < T_N = T$ and the Eqs. (2.1) and (2.2) are integrated with the conditions $x(T_i) = x_i$ and $\Phi(0, \phi(T_i, x(0))) = \Phi(0, x_i) = I_{n\times n}$. Then, the transition matrix is calculated by

$$\Phi(T, x) = \Phi(T_N - T_{N-1}, \phi(T_{N-1}, x(0))\Phi(T_{N-1} - T_{N-2}, \phi(T_{N-2}, x(0)) \ ... \ \Phi(T_1 - T_0, x(0)). \tag{2.69}$$

The re-initialization of the integration of the linearized equations reduces the accumulation of the integration error.

For the computation of the Lyapunov exponents, when the finite time Lyapunov exponents converge, let ΔT be such that $T_j - T_{j-1} = \Delta T, \ j = 1, 2, ...$ where T_j are the times at which the integration of the linearized equations is re-initialized and let the QRD of the transition matrix from T_{j-1} to T_j be

$$\Phi(T_j - T_{j-1}, \phi(T_{j-1}, x(0)) = Q_j R_j. \tag{2.70}$$

Then, the Lyapunov exponents can be calculated as [26, 28]

$$\mu_i^+ = \lim_{j\to\infty} \frac{1}{T_j} \ln |(R_j)_{ii}...(R_1)_{ii}|. \tag{2.71}$$

More detail on the implementation of the QRD based discrete method can be found in [26, 28, 27]. Although the exponents computed using the QRD based method are not the same as the exponents using the SVD based method for finite times, they become the same asymptotically [27, 32].

Comments on the methods for computing the Lyapunov exponents and vectors

- The integration of the differential equations in the continuous methods should be done by using special integrators (e.g. unitary integrators) that preserve the orthogonality [28].

- The differential equations in case of the continuous SVD method become singular when there exist repeated Lyapunov exponents. This can be seen from the differential equations (2.43) and (2.44). Although we assumed that the Lyapunov exponents are distinct in our work, this may still cause numerical problems when the Lyapunov exponents are close to each other but not equal.

- Continuous methods are computationally more costly [27].

- Discrete methods have difficulties in computing the large negative Lyapunov exponents as the averaging time increases.

Chapter 3

Slow Manifold Determination in Two-Timescale Nonlinear Dynamical Systems

3.1 Introduction to the problem and literature

Disparate timescales in the behavior of a dynamical system can induce a manifold structure in the state space – an organizational structure for the trajectories of the system. In a two-timescale system which has fast and slow behaviors, there may be an invariant slow manifold which attracts trajectories emanating from initial states off this manifold. A slow manifold may also be repelling in that trajectories from initial states off the manifold are attracted to it in backward time, i.e., they depart in forward time. In fact the existence of a slow manifold only requires that each trajectory in the neighborhood of the manifold either depart from or approach the manifold at a rate that is significantly faster than the rates at which trajectories on the manifold evolve [33]. When a slow manifold is attracting for some initial conditions in forward time and attracting for other initial conditions in backward time, it is called normally hyperbolic [21].

The existence of a slow manifold presents an opportunity for reduced-order analysis and design. For example, in the case of an attracting slow manifold, the long-term behavior of the system is governed by the dynamics on the slow manifold, because the trajectory

through any point off the slow manifold quickly approaches the slow manifold and then stays on it. More precisely, the trajectory asymptotically approaches a trajectory on the slow manifold, but in a practical sense the two trajectories are indistinguishable after a fast initial transient phase.

Let us say that the slow manifold exists for a particular choice of state variables (i.e., system coordinates). In a different set of coordinates, obtained by a transformation that does not alter the timescales [11], the same qualitative state space structure would exist with certain properties the same and others altered – for example, there would be a slow manifold of the same dimension, but it could be more or less curved and have a different orientation relative to its counterpart in the original set of coordinates. A limitation of most methods for the analysis of two-timescale systems is the requirement for a coordinate representation in which the slow manifold can be represented as a graph, meaning that the values of some of the coordinates on the slow manifold can be expressed as functions of the remaining coordinates, and that one knows how to separate the coordinates appropriately for this purpose.

The analytical singular perturbation method [34] is an approach for decomposing a dynamical system on the basis of timescale separation. To apply the singular perturbation method, the dynamical system must be expressed in terms of coordinates that correspond to the different timescales, and, through scaling, small parameters corresponding to the different timescales must be identified; that is, the system must be expressed in standard singularly perturbed form. When this form can be obtained, reduced-order analysis and design are possible.

Many examples of the beneficial use of singular perturbations in flight mechanics are given in the survey by Naidu and Calise [35]. A prominent example is the energy state

approximation [36, 37, 38]. Certain aircraft in certain situations are incapable of increasing total mechanical energy quickly, though they are capable of changing altitude and velocity quickly [36] – picture gaining speed and losing altitude in a dive or losing speed and gaining altitude in a climb. Fast conversion of potential energy into kinetic energy or vice-versa is possible, even though the sum of the two can only change slowly. To minimize the time for this energy increase, the aircraft should be flown at the altitude that maximizes the excess power $V(T - D)$. This optimum altitude depends on the thrust model and in general varies with energy; thus there is an optimum energy climb path in the (h, V) plane. If the initial and final (h, V) points are not on this path, the optimum energy climb is preceded and followed by instantaneous "zoom" climbs or dives to meet the boundary conditions on altitude and speed; these occur along nearly constant energy curves at the initial and final values of energy as determined by the boundary conditions.

Unfortunately, a systematic procedure for transforming a multiple timescale nonlinear system in general form to singularly perturbed form is not available, nor is a means of diagnosing multiple timescale behavior. Kelley [38] said "Between singular perturbation theory and applications to flight mechanics and control, there is a gap, in that the theory requires the system of differential equations to come equipped with one or more parameters whose vanishing reduces the system order. Such parameters occurred quite naturally in the original applications of the theory (e.g., viscosity in flow problems), but they must be introduced artificially in many, if not most, of the situations [in flight mechanics], i.e., they are parameters merely of interpolation between the original and simplified systems." The lack of diagnostic and modeling capabilities motivates the present research. We address specifically two-timescale behavior, but the approach can be extended to multiple timescales.

Fenichel [33, 1] characterized the underlying manifold structure of a two-timescale system as described in the first paragraph. His formulation is coordinate-free, i.e., geometric, but it is based on *a priori* knowledge of an ϵ-dependent slow manifold, where ϵ is a small parameter, that is a manifold of equilibrium points when $\epsilon = 0$. Thus although the characterization exposed the geometry of a two-timescale system in a general way, a general model reduction procedure did not emerge directly from Fenichel's results.

Fenichel's[33] more general approach to invariant manifolds is based on Lyapunov exponents as has been much of the work on hyperbolic sets and manifolds in dynamical systems theory [21, 19]. In [11] Lyapunov exponents and vectors were employed to determine the timescales and associated tangent space structure, synthesizing the methodology and supporting theory from a number of sources cited in the literature. A step was taken toward linking the geometry of singularly perturbed systems to the use of Lyapunov exponents by Mease [39]. In a recent paper[12], a definition of, and a means of diagnosing, two-timescale behavior in a nonlinear, finite-dimensional, time-invariant dynamical system were presented. This lead to a new method of computing a slow manifold, when one exists. The presentation in this chapter is parallel to that paper.

3.2 Slow manifold

A dynamical system has boundary-layer type, two-timescale behavior in $\mathcal{X}$, if there exists a reduced-order (dimension less than n) slow manifold $\mathcal{S}$ that intersects $\mathcal{X}$ and is relatively invariant with respect to $\mathcal{X}$, and if each neighboring trajectory approaches $\mathcal{S}$ in either forward or backward time at a rate significantly faster than the rate at which trajectories evolve on $\mathcal{S}$. A precise definition of rates will be given later in terms of Lyapunov exponents.

We mention three representations of a smooth, relatively-invariant slow manifold $\mathcal{S}$ in

$\mathcal{X}$, assuming that $\mathcal{S}$ is n^s-dimensional with $n^s < n$.

1. Algebraic constraints: $\mathcal{S} = \{x \in \mathcal{X} : h_1(x) = \ldots = h_{n-n^s}(x) = 0\}$ where h_i, $i = 1, \ldots, n - n^s$ are independent constraints and smooth functions of x.

2. Graph: At least locally, the coordinates of x can be separated into a vector x_{indep} of n^s independent variables and a vector x_{dep} of $n-n^s$ dependent variables and there exists a function $\psi : \mathcal{R}^{n^s} \to \mathcal{R}^{n-n^s}$ such that $\mathcal{S} = \{(x_{indep}, x_{dep}) \in \mathcal{X} : x_{dep} = \psi(x_{indep})\}$.

3. Invariance-based orthogonality conditions: For each $x \in \mathcal{X}$, suppose there is an invariant splitting of the tangent space $T_x\mathcal{X} = E^s(x) \oplus E^f(x)$ into slow and fast subspaces of dimensions n^s and n^f respectively. Precise definitions of these subspaces are given later. For points on $\mathcal{S}$, we should have $T_x\mathcal{S} = E^s(x)$ and $x \in \mathcal{S} \cap \mathcal{X}$. Given a basis $\{w_1(x), \ldots, w_{n-n^s}(x)\}$ for $(E^s(x))^\perp$, the orthogonal complement to $E^s(x)$, the n^s-dimensional slow manifold can be defined implicitly by

$$\mathcal{S} = \{x \in \mathcal{X} : \langle w_i(x), f(x) \rangle = 0, i = 1, ..., n - n^s\}. \tag{3.1}$$

These orthogonality conditions for f in representation 3 can be viewed as partial-equilibrium conditions, partial in the sense that the vector field f need only be zero in certain directions. If one has constraint functions h_i, $i = 1, \ldots, n-n^s$ for representation 1, then $(E^s(x))^\perp = span\{\frac{\partial h_1}{\partial x}(x), \ldots, \frac{\partial h_{n-n^s}}{\partial x}(x)\}$. It may be easier however to find a basis for $(E^s(x))^\perp$ directly without first finding constraint functions. Not every basis of $(E^s(x))^\perp$ can be related to a set of constraint functions. Both representations 1 and 3 are implicit; $n - n^s$ algebraic equations, nonlinear in general, must be solved to compute points on the slow manifold.

3.3 Existing Methods for Slow Manifold Determination in Two-Timescale Systems

3.3.1 Graph via Singular Perturbation Method

The standard form is by far the most common and best understood starting point for the analysis of a two time-scale system [34]. The singularly perturbed form (on the fast timescale) is

$$\begin{aligned} \dot{y} &= p(y,z,\varepsilon) \\ \varepsilon\dot{z} &= q(y,z,\varepsilon) \end{aligned} \tag{3.2}$$

where $y \in \mathcal{R}^{n^s}$ and $z \in \mathcal{R}^{n^f}$ with $n^s + n^f = n$, ε is a small constant parameter and both p and q are of $O(1)$ with respect to ε. The vector y is composed of the slow state variables and the vector z is composed of the fast state variables. The terms slow and fast are appropriate here because $\dot{y} = O(1)$ and $\dot{z} = O(1/\varepsilon)$.

Suppose that for $\varepsilon = 0$ there is a manifold of equilibrium points given as the set $\mathcal{S}(0) = \{(y,z) : q(y,z;0) = 0\}$. Assuming that $\partial q/\partial z$ is nonsingular for all points in $\mathcal{S}(0)$, $\mathcal{S}(0)$ is a normally hyperbolic manifold, a trivial case of a slow manifold, since points on $\mathcal{S}(0)$ do not move at all. For the case where the $\varepsilon = 0$ system has a normally hyperbolic slow manifold, Fenichel has shown that for sufficiently small values of ε, the system will also have a normally hyperbolic manifold, we denote by $\mathcal{S}(\varepsilon)$, and the motion on this manifold will be slow compared to the motion off the manifold.

Now suppose that when $\varepsilon = \varepsilon_1$ the (y,z) coordinates are related to the x coordinates by the transformation $(y,z) = h(x)$ and that $\varepsilon = \varepsilon_1$ is small enough that the slow manifold $\mathcal{S}(\varepsilon_\infty)$ exists, then the slow manifold for the system given by Eq. (2.1) can be determined via the (y,z) representation as follows: The slow manifold can be expressed[34] in terms of a graph of the form $z = \psi(y,\varepsilon)$ as the set of points $\mathcal{S}(\varepsilon_1) = \{(y,z) : z = \psi(y,\varepsilon_1)\}$ with

$\psi(y, \varepsilon)$ satisfying the partial differential equation

$$\varepsilon \frac{\partial \psi}{\partial y} p(y, \psi, \varepsilon) = q(y, \psi, \varepsilon). \tag{3.3}$$

The solution ψ can be obtained as an asymptotic expansion in ε of the form

$$\psi(y, \varepsilon) = \psi_0(y) + \varepsilon \psi_1(y) + \varepsilon^2 \psi_2(y) + \dots \tag{3.4}$$

beginning with computing the zeroth-order term implicitly defined by $q(y, \psi_0(y), 0) = 0$. The zeroth-order term $\psi_0(y)$ exists by the implicit function theorem and the nonsingularity of $\partial q / \partial z$.

3.3.2 Graph via Invariance Partial Differential Equation

Alternatively, Fraser and Roussel[40, 41] start with a system in the form

$$\begin{aligned} \dot{u} &= U(u, w), \\ \dot{w} &= W(u, w), \end{aligned} \tag{3.5}$$

and assume the slow manifold can be expressed as $\mathcal{S} = \{(u, w) : w = k(u)\}$. Differentiating $w = k(u)$ with respect to time yields the partial differential equation

$$\frac{dk}{du} U(u, k) = W(u, k) \tag{3.6}$$

To this point the method is similar to the singular perturbation method. The difference is in the approach for solving the invariance PDE. Rather than use an asymptotic expansion in ε, Fraser and Roussel use a successive approximation approach. For example, when W is of the special form $W = k + \tau(u)$, they construct the solution via the successive approximation formula

$$k_{i+1} = -\tau(u) + \frac{dk_i}{du} U(u, k_i), \tag{3.7}$$

which under certain conditions is a contraction mapping and converges.

The requirements for special model forms limit the applicability of this method and the singular perturbation method. In both cases, the dimension of the slow manifold must be known, the coordinates must allow the slow manifold to be represented as a graph, and it must be known how to separate the coordinates for this purpose. Given a system representation in the general form of Eq. (2.1) that has two-timescale behavior, there is not a general approach to converting it to a representation with the form and properties required for either method.

3.3.3 Invariance-Based Orthogonality Conditions via Eigenanalysis: ILDM Method

In the intrinsic low-dimensional manifold (ILDM) method of Maas and Pope[42], the basis for $E^s(x)$ is approximated by the appropriate (real, generalized) eigenvectors of the Jacobian matrix $F(x)$ (or the corresponding Schur vectors) and the $n - n^s$ orthogonality conditions in Eq. (3.1) are constructed and solved to compute points on the slow manifold. The eigenvalues and eigenvectors of the Jacobian matrix, F in Eq. (2.2), a matrix which varies along a trajectory, are not in general reliable indicators of the timescales and associated directions. Kaper and Kaper[43] have analyzed this method in application to a two-timescale system in standard singularly perturbed form with small parameter ε characterizing the timescale separation and shown that the error in determining the slow manifold is of order ε^2 and increases proportionally with the curvature of the slow manifold. The attributes of the ILDM method are that it is in principle applicable to any finite-dimensional dynamical system of the general form in Eq. (2.1) with a hyperbolic slow manifold and that the basis vector computations do not require integration.

3.3.4 Numerical Simulation

If the slow manifold is attracting for all initial conditions in $\mathcal{X}$, then the slow manifold can be determined by forward time simulation from many initial conditions. Similarly, if the slow manifold is repelling for all initial conditions in $\mathcal{X}$, then it can be determined by backward time simulation from many initial conditions. If the slow manifold is attracting for some initial conditions and repelling for other initial conditions, i.e., normally hyperbolic, then simulation is not a viable approach.

3.3.5 Computational Singular Perturbation Method

The aim of the computational singular perturbation (CSP) method, developed by Lam and Goussis [10, 44], is to produce essentially the same results as the analytical singular perturbation method, but to operate directly on the nonlinear dynamical system as given, that is, with no requirement for the singularly perturbed form. From an initial state, generally off the slow manifold, the dynamical system is integrated to compute the trajectory. When the trajectory reaches the vicinity of the slow manifold, as indicated by essentially an application of the ILDM method, an iterative method is activated that corrects the local eigenvectors to basis vectors that more accurately represent the manifold structure. A geometric interpretation of CSP was presented by Mease[45], where it was also recognized that the basis vector refinement procedure in the CSP method is essentially a Lyapunov transformation used previously for the decoupling of linear time-varying systems [34]. Because the slow and fast subspaces E^s and E^f are invariant, it follows that in tangent vector coordinates adapted to these subspaces, the linearized dynamics must have a block diagonal structure such that the slow and fast dynamics are uncoupled [46, 45]. Zagaris et al [46] have analyzed the accuracy of the CSP method applied to a two-timescale system in

standard singularly perturbed form and found that the error in determining the slow manifold is of order ε^{q+1} after q applications of the CSP basis vector refinement algorithm [46]. However, refinement requires computing derivatives of basis vectors which can be difficult to do accurately [47]. Another limitation of the CSP method is that the slow manifold is initially found via simulation, which only works for either an attracting or a repelling slow manifold and not the general hyperbolic case. Instead of using simulation, the ILDM method could be applied to obtain an initial approximation of the slow manifold $\mathcal{S}$ and then the CSP refinement used to improve the basis vectors and more accurately locate $\mathcal{S}$. Also the timescale information and basis vector initialization rely on local eigenvalues and eigenvectors which we shall demonstrate are, in general, unreliable except at equilibrium points.

3.4 Two-Timescale Behavior

We define two-timescale behavior by first defining a uniform two-timescale set. A two-timescale set has a special tangent space structure and allows us to formulate conditions that would be satisfied at points of a slow manifold. If a slow manifold exists, then the nonlinear system has two-timescale behavior of the boundary-layer type and there is an opportunity for system decomposition and reduced-order analysis.

In the following definition and propositions, the relative terms "fast" and "slow" are interpreted with respect to the characteristic time T_c that it takes for an trajectory to traverse $\mathcal{X}$. T_c should be thought of as an average value of $\bar{t}(x) - \underline{t}(x)$ over $\mathcal{X}$. We assume that the Lyapunov exponents are always distinct in characterizing two-timescale structure of the tangent space. The results can be adapted to the non-distinct case, but the notation is more cumbersome.

Definition 3.4.1 *(Two-Timescale Set) A set $\mathcal{X} \in \mathcal{R}^n$, with characteristic time T_c, is a uniform two-timescale set for Eq. (2.1), with respect to the Euclidean metric, if there exist positive real numbers μ^f, μ^s and T_{min}, with $0 < \mu^s < \mu^f$ and $T_{min} < T_c$, and positive integers n^{fc}, n^s and n^{fe}, with $n^{fc} + n^s + n^{fe} = n$, such that the following properties are satisfied:*

1. $\frac{(\Delta\mu)^{-1}}{T_c - T_{min}} = \frac{(\mu^f - \mu^s)^{-1}}{T_c - T_{min}} << 1$
2. *For each $x \in \mathcal{X}$, $\mu^+_{n^{fc}}(T,x) \leq -\mu^f$, $-\mu^s \leq \mu^+_{n^{fc}+1}(T,x)$, $\mu^+_{n^{fc}+n^s}(T,x) \leq \mu^s$, and $\mu^f \leq \mu^+_{n^{fc}+n^s+1}(T,x)$ for all $T \in (T_{min}, \bar{t}(x)]$*
3. *For each $x \in \mathcal{X}$, $-\mu^-_{n^{fc}}(T,x) \leq -\mu^f$, $-\mu^s \leq -\mu^-_{n^{fc}+1}(T,x)$, $-\mu^-_{n^{fc}+n^s}(T,x) \leq \mu^s$, and $\mu^f \leq -\mu^-_{n^{fc}+n^s+1}(T,x)$ for all T such that $-T \in [\underline{t}(x), -T_{min})$.*

Either n^{fc} or n^{fe} is allowed to be zero, but not both. For $n^{fe} = 0$, the condition on $\mu^-_{n^{fc}+n^s+1}$ does not apply; similarly, for $n^{fc} = 0$, the condition on $\mu^+_{n^{fc}}$ does not apply.

Properties 2 and 3 are illustrated in Fig.(3.1) where the bounds and forward and backward exponents are each plotted on different copies of the real line for clarity. The exponents for particular values of T and $\mathbf{x}$ are pictured, but Properties 2 and 3 require this structure for all the specified values of T and $\mathbf{x}$. Definition (3.4.1) is adapted from the definition of a uniform partially hyperbolic invariant set in dynamical systems theory [19].

In Definition (3.4.1), the fast and slow behaviors are characterized by the exponential rates μ^f and μ^s respectively. The properties in Definition (3.4.1) ensure that, uniformly in T and $\mathbf{x}$, there is a significant timescale gap with respect to T_c (Property 1), the fast contracting behavior dies out quickly in forward time relative to T_c (Property 2), and the fast expanding behavior dies out quickly in backward time relative to T_c (Property 3).

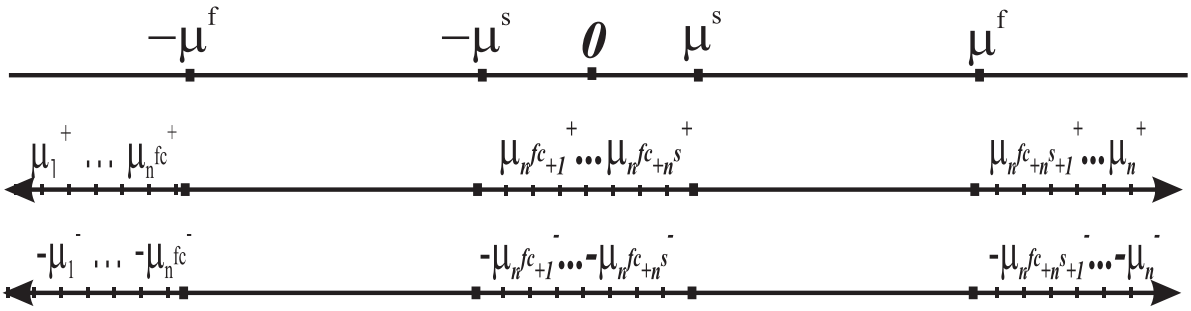

Figure 3.1: Spectra of forward and backward Lyapunov exponents illustrating the gaps.

Definition (3.4.1) ensures that the fast behavior is fast relative to T_c and that the slow behavior is slow relative to the fast behavior. For the slow behavior to actually be slow relative to T_c we could require $(\mu^s)^{-1} \geq T_c$, but we do not make this restriction. Properties 2 and 3 also ensure that consistent gaps in the forward and backward Lyapunov spectra not only exist, but also separate the spectrum in a dimensionally consistent manner. T_{min} provides a grace period over which the bounds on the exponents do not have to be satisfied, while Property 1 ensures that the remaining averaging time $T_c - T_{min}$ is sufficiently large. The grace period accommodates initial transients which could otherwise violate the bounds. For cases of additional gaps in the spectrum, multiple timescale systems can be defined similarly.

Proposition 3.4.2 *When $\mathcal{X}$ is a uniform two-timescale set, the subspaces*

$$\begin{aligned} E^{fc}(T,x) &= L^+_{n^{fc}}(T,x), \\ E^{s}(T,x) &= L^+_{n^{fc}+n^s}(T,x) \cap L^-_{n^{fc}+1}(T,x), \\ E^{fe}(T,x) &= L^-_{n^{fc}+n^s+1}(T,x) \end{aligned} \tag{3.8}$$

have the properties:

$$\begin{aligned} v \in E^{fc}(T,x)\backslash\{0\} &\Rightarrow \mu^+(T,x,v) \leq -\mu^f \ \textit{for all}\ T \in (T_{min}, \bar{t}(x)], \\ v \in E^{s}(T,x)\backslash\{0\} &\Rightarrow -\mu^s \leq -\mu^-(T,x,v) \ \textit{for all}\ -T \in [\underline{t}(x), -T_{min}), \\ v \in E^{s}(T,x)\backslash\{0\} &\Rightarrow \mu^+(T,x,v) \leq \mu^s \ \textit{for all}\ T \in (T_{min}, \bar{t}(x)], \\ v \in E^{fe}(T,x)\backslash\{0\} &\Rightarrow -\mu^f \leq -\mu^-(T,x,v) \ \textit{for all}\ -T \in [\underline{t}(x), -T_{min}). \end{aligned} \tag{3.9}$$

If x is near the boundary of $\mathcal{X}$ such that either $\underline{t}(\mathbf{x}) \geq -T_{min}$ or $T_{min} \geq \bar{t}(\mathbf{x})$, then the properties and bounds are only applicable in one direction.

Proof: The four properties in Eq. (3.9) follow directly from the definitions of the subspaces $L^+_{n^{fc}}$, $L^-_{n^{fc}+1}$, $L^+_{n^{fc}+n^s}$, and $L^-_{n^{fc}+n^s+1}$ (see Eq. (2.39)) and of a uniform two-timescale set (see Definition (3.4.1)).□

Proposition (3.4.2) says that there is tangent space structure associated with the slow and fast exponential rates. Definition (3.4.1) has established that the gaps in the exponential rates are temporally and spatially uniform. However the subspaces $E^{fc}(T,x)$, $E^s(T,x)$ and $E^{fe}(T,x)$ in Proposition (3.4.2) depend on T. Which value of T should we use, i.e., which subspace structure is appropriate?

Consider the hypothetical situation in which $\mathcal{X}$ is contained in a larger set $\mathcal{Y}$ and the uniform two-timescale set properties for $\mathcal{X}$ (with the same constants μ^f, μ^s, T_{min}, n^{fc}, n^s and n^{fe}) are satisfied on all of $\mathcal{Y}$. Moreover, assume $\mathcal{Y}$ is invariant under the dynamics of Eq. (2.1). We can now compute E^{fc}, E^s and E^{fe} at each point of $\mathcal{X}$ for arbitrarily large averaging times T and these subspaces will converge to subspaces that depend only on $\mathbf{x}$. The supporting theory[19] shows that these T-independent subspaces are invariant.

Proposition (3.4.2) has been adapted from a result [19] saying that an invariant set $\mathcal{X}$ is a two-timescale set, if there exists an invariant splitting at each $x \in \mathcal{X}$

$$T_x\mathcal{X} = E^{fc}(x) \oplus E^s(x) \oplus E^{fe}(x) \tag{3.10}$$

and constants μ^s and μ^f, with $\mu^s < \mu^f$, and $C > 0$ such that

$$\begin{aligned}
v \in E^{fc}(x) &\Rightarrow \|\Phi(t,x)v\| \leq Ce^{-\mu^f t}\|v\|, t > 0,\\
v \in E^{s}(x) &\Rightarrow C^{-1}e^{-\mu^s t}\|v\| \leq \|\Phi(t,x)v\|, t < 0,\\
v \in E^{s}(x) &\Rightarrow \|\Phi(t,x)v\| \leq Ce^{\mu^s t}\|v\|, t > 0,\\
v \in E^{fe}(x) &\Rightarrow \|\Phi(t,x)v\| \leq Ce^{\mu^f t}\|v\|, t < 0.
\end{aligned} \tag{3.11}$$

For an invariant two-timescale set, $T_c \to \infty$ and Property 1 of Definition (3.4.2) is satisfied for any $\Delta\mu > 0$. When the two-timescale set is not invariant, T_c is finite and Property 1, though imprecise, indicates that we can average over at least several time constants and converge within some tolerance, based on the following proposition.

Proposition 3.4.3 *When $\mathcal{X}$ is a uniform two-timescale set, at each $x \in \mathcal{X}$ the subspaces $E^{fc}(T,x)$, $E^{s}(T,x)$ and $E^{fe}(T,x)$ converge toward fixed subspaces, with increasing T, at least at the rate $1/(e^{\Delta\mu T} - e^{-\Delta\mu T})$, where $\Delta\mu = \mu^f - \mu^s$.*

Proof: Given the properties of uniform two-timescale set in Definition (3.4.1), Theorem (2.4.4) allows us to conclude that $L^+_{n^{fc}}$, $L^-_{n^{fc}+1}$, $L^+_{n^{fc}+n^s}$, and $L^-_{n^{fc}+n^s+1}$ converge with increasing T toward fixed subspaces at least at the rate $1/(e^{\Delta\mu T} - e^{-\Delta\mu T})$. Because of the relationships in Eq. (3.8), it follows that E^{fc}, E^s and E^{fe} converge at the same rate.□

Proposition 3.4.4 *$E^{fc}(T,x)$, $E^{s}(T,x)$, and $E^{fe}(T,x)$ are linearly independent subspaces at each point $x \in \mathcal{X}$, i.e., the intersection of any two of them is the set consisting only of the zero vector.*

Proof: We prove that $E^{fc}(T,x) \cap E^{s}(T,x) = \{0\}$; the other two cases follow from the same procedure.

$$\begin{aligned} E^{fc}(T,x) \cap E^{s}(T,x) &= L^+_{n^{fc}}(T,x) \cap (L^+_{n^{fc}+n^s}(T,x) \cap L^-_{n^{fc}+1}(T,x)) \\ &= (L^+_{n^{fc}}(T,x) \cap (L^+_{n^{fc}+n^s}(T,x)) \cap L^-_{n^{fc}+1}(T,x) \qquad (3.12) \\ &= L^+_{n^{fc}}(T,x) \cap L^-_{n^{fc}+1}(T,x). \end{aligned}$$

Assume there exists a unit vector $v \in L^+_{n^{fc}}(T,x) \cap L^-_{n^{fc}+1}(T,x)$. Because $v \in L^-_{n^{fc}+1}(T,x)$, $v \in span\left\{l^-_{n^{fc}+1}(T,x), ..., l^-_n(T,x)\right\}$. When v is propagated backward in time for T units of time, the resulting vector $\Phi(-T,x)v \in span\left\{l^+_{n^{fc}+1}(T,\phi(-T,x)), ..., l^+_n(T,\phi(-T,x))\right\}$.

On the other hand, since $v \in L^+_{n^{fc}}(T,x)$, it can be decomposed as $v = b_1 l^+_1(T,x) + ... + b_{n^{fc}} l^+_{n^{fc}}(T,x)$. Since

$$\Phi(-T,x)v \in span\left\{l^+_{n^{fc}+1}(T,\phi(-T,x)),...,l^+_n(T,\phi(-T,x))\right\}, \tag{3.13}$$

$\Phi(-T,x)l^+_i(T,x) \in span\left\{l^+_{n^{fc}+1}(T,\phi(-T,x)),...,l^+_n(T,\phi(-T,x))\right\}$ for $i = 1,...,n^{fc}$. However, note that the distribution $L^+_{n^{fc}}(T,x)$ is practically invariant. Thus, for any $i = 1,...,n^{fc}$

$$\Phi(-T,x)l^+_i(T,x) = a_1 l^+_1(T,\phi(-T,x)) + ... + a_n l^+_{n^{fc}}(T,\phi(-T,x)), \tag{3.14}$$

where $\frac{a_j}{a_k}$, $k = n^{fc}+1,...,n$ and $j = 1,..,n^{fc}$, is a function that exponentially decays with the averaging time, exponentially grows with the propagation time, and is finite for finite averaging and propagation times. However, if $\Phi(-T,x)l^+_i(T,x)$ is confined in $span\left\{l^-_{n^{fc}+1}(T,x),...,l^-_n(T,x)\right\}$ for any $i = 1,...,n^{fc}$, then this ratio becomes indefinite. This leads to a contradiction. Thus, there is no non-zero vector in $L^+_{n^{fc}}(T,x) \cap L^-_{n^{fc}+1}(T,x)$.□

Proposition 3.4.5 $dimE^s(T,x) = n^s$

Proof: Because $E^s(T,x)$ is constructed by intersecting two linear subspaces whose dimensions sum to $n+1$, they have to intersect at least in a line. Thus

$$\begin{aligned} dimE^s(T,x) &\geq dimL^+_{n^{fc}+n^s}(T,x) + dimL^-_{n^{fc}+1}(T,x) - n \\ &= n^{fc} + n^s + n - n^{fc} - n = n^s \end{aligned} \tag{3.15}$$

From Proposition (3.4.4) asserting the linear independence of $E^{fc}(T,x)$, $E^s(T,x)$, and $E^{fe}(T,x)$ and the facts that $dimE^{fc}(T,x) = n^{fc}$ and $dimE^{fe}(T,x) = n^{fe}$, it follows that $dimE^s(T,x) = n^s$. □

3.5 Procedure for diagnosing a two-timescale set and computing the slow manifold

$\mathcal{X}$ being a uniform two-timescale set establishes the potential for the existence of a normally hyperbolic, slow manifold.

Definition 3.5.1 *Let (i) $\mathcal{Y} \subset \mathcal{R}^n$ be an invariant two-timescale set with $\mathcal{X} \subset \mathcal{Y}$, (ii) $E^s(x)$ be the subspace to which the subspace $E^s(T, x)$ defined in Proposition 1 converges, (iii) $\mathcal{S} \subset \mathcal{Y}$ be an invariant n^s-dimensional manifold, and (iv) $\mathcal{S} \cap \mathcal{X}$ be non-empty. In $\mathcal{X}$, $\mathcal{S}$ is a relatively invariant slow manifold if $T_x\mathcal{S} = E^s(x)$ for all $x \in \mathcal{S} \cap \mathcal{X}$.*

The motion on $\mathcal{S}$ is slow in $\mathcal{X}$, because at any point on $\mathcal{S}$ we have $f(x) \in E^s(x)$, and thus there is no fast motion because the components of $f(x)$ in $E^{fc}(x)$ and $E^{fe}(x)$ are zero.

3.5.1 Procedure for diagnosing a two-timescale set

Lyapunov exponents are computed at points of $\mathcal{X}$ to determine if $\mathcal{X}$ is a two-timescale set according to Definition (3.4.1). One needs to see a pattern as illustrated in Fig. (3.1) uniformly in $\mathbf{x}$ and T and to verify that the timescale gap is sufficiently large relative to T_c. Assuming the properties of Definition (3.4.1) are satisfied, we look for a slow manifold in $\mathcal{X}$.

3.5.2 Procedure for computing the slow manifold

Within $\mathcal{X}$, the points on a slow manifold $\mathcal{S}$ are defined implicitly by the orthogonality conditions in Eq. (3.1). Rather than use local eigenvectors to form an approximate basis for the orthogonal complement to E^s as in the ILDM method, we propose using the appropriate Lyapunov vectors to form the basis for $(E^s(x))^\perp$ as given by the following proposition.

Proposition 3.5.2

$$(E^s(T,x))^\perp = span\{l_1^-(T,x),\ldots,l_{n^{fc}}^-(T,x),l_{n^{fc}+n^s+1}^+(T,x),\ldots,l_n^+(T,x)\} \tag{3.16}$$

Proof: From Proposition (3.4.2) and Definition (3.4.1), we have $E^s(T,x) = L^+_{n^{fc}+n^s} \cap L^-_{n^{fc}+1}$. Using an identity from [13], we have $(E^s(T,x))^\perp = (L^-_{n^{fc}+1})^\perp \oplus (L^+_{n^{fc}+n^s})^\perp$. The proposition then follows from the facts that $(L^-_{n^{fc}+1}(T,x))^\perp = span\{l_1^-(T,x),\ldots,l_{n^{fc}}^-(T,x)\}$ and $(L^+_{n^{fc}+n^s}(T,x))^\perp = span\{l^+_{n^{fc}+n^s+1}(T,x),\ldots,l_n^+(T,x)\}$. □

For $x \in \mathcal{S} \cap \mathcal{X}$, $E^s(T,x)$ approximates $T_x\mathcal{S}$ more and more accurately as T increases. The invariant superset $\mathcal{Y}$ we have introduced to allow precise statements is assumed to be fictitious; only trajectory segments in $\mathcal{X}$ can be integrated along to compute timescale information. The bounds on T, $T \le \bar{t}(x)$ for forward integration and $\underline{t}(x) \le -T$ for backward integration, limit the accuracy, but as pointed out earlier, Property 1 in Definition (3.4.1) ensures that significant progress toward convergence can be achieved with the available averaging time. Via numerical experimentation a value of the averaging time T is determined that allows the Lyapunov vectors to be computed to sufficient accuracy.

In order to obtain a solution of the algebraic equations, we designate n^s components of x as independent variables, fix their values, and determine the values of the remaining $n - n^s$ components, the dependent variables, that minimize

$$J = \langle l_1^-(T,x), f(x)\rangle^2 + \ldots + \langle l^-_{n^{fc}}(T,x), f(x)\rangle^2 + \langle l^+_{n^{fc}+n^s+1}(T,x), f(x)\rangle^2 + \ldots + \langle l_n^+(T,x), f(x)\rangle^2 \tag{3.17}$$

for the dependent variables with fixed independent variables. This is repeated for a grid on the independent variable space. The directions of the Lyapunov vectors indicate how to separate the coordinates of x into independent and dependent variables. The independent variables must be chosen such that their coordinate axes are not parallel to any directions

in $(E^s)^\perp$. (Lyapunov vectors could also serve this same purpose in the approach of Fraser and Roussel.) Within $\mathcal{X}$, there could be zero, one, or more than one slow manifold. Hence, for fixed values of the independent variables, there could be zero, one or several minima.

This procedure for determining a slow manifold is essentially the same as the ILDM method, except that Lyapunov exponents and vectors are used instead of eigenvalues and eigenvectors. Determining the Lyapunov vector basis for $(E^s)^\perp$ requires considerably more computation compared to determining the eigenvectors, but the greater accuracy may be needed, if the timescale separation is modest or if the slow manifold has significant curvature, since these are the conditions [1] for which the accuracy of the eigenvector-based ILDM is reduced.

3.6 Two-Dimensional Nonlinear Example

Consider the nonlinear, time-invariant (NTI) system

$$\begin{aligned} \dot{x}_1 &= \lambda_s x_1 \\ \dot{x}_2 &= \alpha(\lambda_f - 2\lambda_s)x_1^2 + \lambda_f x_2 \end{aligned} \tag{3.18}$$

In order to clearly illustrate the nature of the timescale information and its use in computing the slow manifold, we have constructed this system to be simple enough that we can analytically compute the transition matrix and its SVD to obtain the Lyapunov exponents and vectors. The nonlinear system was obtained by applying a nonlinear transformation to the linear, time-invariant (LTI) system

$$\begin{aligned} \dot{w}_1 &= \lambda_s w_1 \\ \dot{w}_2 &= \lambda_f w_2 \end{aligned} \tag{3.19}$$

or $\dot{w} = \Lambda w$ where $w = (w_1, w_2)^T$ and $\Lambda = diag(\lambda_s, \lambda_f)$. The nonlinear coordinate transformation that relates these two representations is

$$\begin{aligned} x_1 &= w_1 \\ x_2 &= -\alpha w_1^2 + w_2 \end{aligned} \tag{3.20}$$

A similar nonlinear system has been used by others [48, 1]. We assume that the linear system has a two-timescale structure, with λ_s and λ_f denoting the slow and fast eigenvalues. The nonlinear system may have two-timescale structure, depending on whether the state transformation does or does not significantly modify the timescales. In this example, the nonlinear system in Eq. (3.18) does have two-timescale structure. From Fenichel's geometric perspective [33], the trajectories of a two-timescale system are organized in the state space by a slow manifold and a family of fast manifolds. In the (w_1, w_2) space, the slow manifold is the w_1 axis and the vertical line through each point on the slow manifold is a fast manifold. Consider the case $\lambda_f << -|\lambda_s|$. Trajectories from initial points off the slow manifold proceed quickly in the vertical direction, i.e., along the fast manifold through the initial point, toward the slow manifold at the fast rate $e^{\lambda_f t}$ and subsequently proceed along the slow manifold at the slower rate $e^{\lambda_s t}$. This description is only approximate for finite timescale separation, because motion in the slow direction does occur during the approach to the slow manifold and thus the trajectory does not exactly follow the fast manifold on which it begins. At each point in the state space, the timescales for the LTI system are given by the eigenvalues of the matrix Λ, and the fast and slow directions of the motion are given by the corresponding eigenvectors.

The trajectories of the NTI system are shown in the (x_1, x_2) space in Fig. (3.2) for $\alpha = 0.02$, $\lambda_s = -1$ and $\lambda_f = -10$. The two-timescale structure is still present, but the slow manifold is now curved rather than straight. In fact it is the image of the slow manifold for the **w**-representation under the transformation, Eq. (3.20), given explicitly as the set

$$\mathcal{S} = \{x \in \mathcal{R}^2 : \alpha x_1^2 + x_2 = 0\} \tag{3.21}$$

If λ_f were positive, with $\lambda_f >> |\lambda_s|$, then the description just given would apply to the

backward time evolution; in forward time the slow manifold would be repelling. The sign of λ_s determines the direction of the slow motion, but does not affect the basic geometry. We focus our attention on a region in the right half-plane, to be defined precisely later, that trajectories traverse in finite time, and consider the computation of the two-timescale structure. In this contrived example we have the luxury of having an analytical representation for the slow manifold, Eq. (3.21), and thus it follows that for any $x \in \mathcal{S}$ the tangent space is

$$T_x\mathcal{S} = span\{(1 \quad -2\alpha x_1)^T\}. \tag{3.22}$$

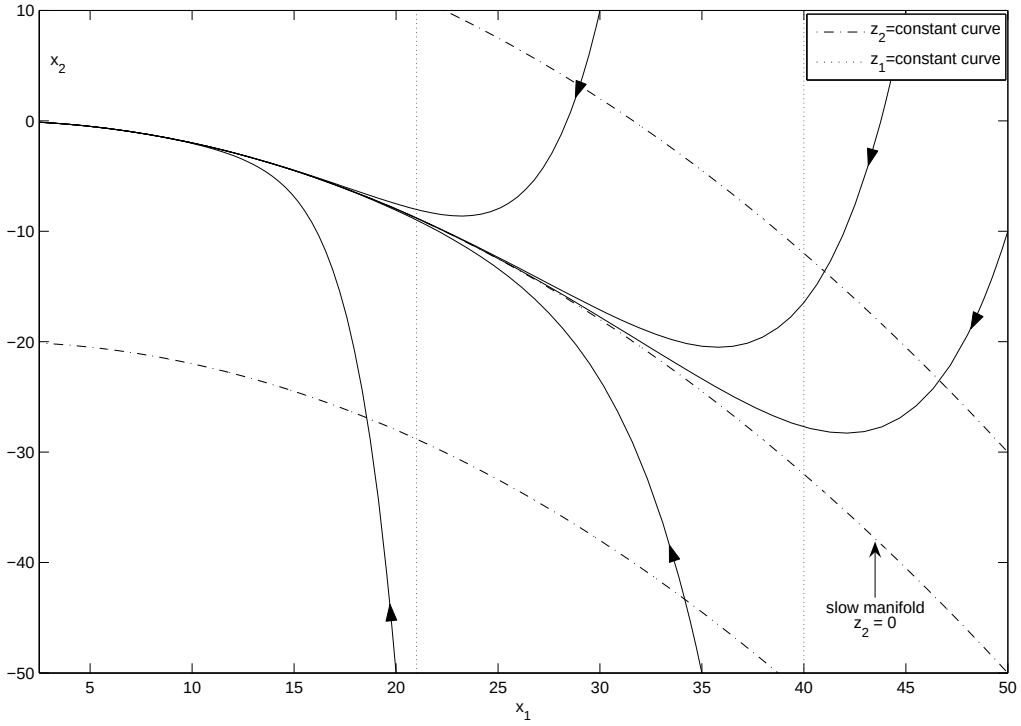

Figure 3.2: State portrait for nonlinear system given by Eq. (3.18).

Linear Timescale Analysis

The solution of the nonlinear system for initial conditions $x_1(0) = x_{10}$ and $x_2(0) = x_{20}$ can be obtained by first solving the linear system and then converting its solution to that of

the nonlinear system, using the transformation given in Eqs. (3.20). The result is

$$\begin{aligned} x_1(t) &= e^{\lambda_s t} x_{10} \\ x_2(t) &= \alpha(e^{\lambda_f t} - e^{2\lambda_s t}) x_{10}^2 + e^{\lambda_f t} x_{20}. \end{aligned} \tag{3.23}$$

This is the transition map $\phi(t, x_0)$ for the nonlinear system. The transition matrix for the linearized dynamics can be obtained by differentiating the transition map with respect to the initial conditions. This yields

$$\Phi = \frac{\partial \phi}{\partial x_0} = \begin{bmatrix} e^{\lambda_s t} & 0 \\ 2\alpha(e^{\lambda_f t} - e^{2\lambda_s t}) x_{10} & e^{\lambda_f t}. \end{bmatrix} \tag{3.24}$$

We obtain the Lyapunov exponents by first computing the eigenvalues of either $\Phi^T\Phi$ or $\Phi\Phi^T$ and neglecting, for sufficiently large times relative to $(\lambda_s - \lambda_f)^{-1}$, terms proportional to $exp((\lambda_f - \lambda_s)t)$ in comparison to terms that are either not exponentially decaying or exponentially decaying at a much slower rate. The two eigenvalues, which are the squares of the singular values σ of Φ, are given by

$$\begin{aligned} \sigma_1^2 &= e^{2\lambda_f t}(1 + 4\alpha^2 e^{2\lambda_s t} x_{10}^2)^{-1}, \\ \sigma_2^2 &= e^{2\lambda_s t}(1 + 4\alpha^2 e^{2\lambda_s t} x_{10}^2). \end{aligned} \tag{3.25}$$

The forward Lyapunov exponents are

$$\begin{aligned} \mu_1^+ = \tfrac{1}{2t} \ln \sigma_1^2 &= \lambda_f - \tfrac{1}{2t} \ln(1 + 4\alpha^2 e^{2\lambda_s t} x_{10}^2), \\ \mu_2^+ = \tfrac{1}{2t} \ln \sigma_2^2 &= \lambda_s + \tfrac{1}{2t} \ln(1 + 4\alpha^2 e^{2\lambda_s t} x_{10}^2). \end{aligned} \tag{3.26}$$

The infinite time limits, which depend on the sign of λ_s, are

$$\begin{aligned} (\mu_1^+, \mu_2^+) &= (\lambda_f, \lambda_s) \qquad \text{if} \qquad \lambda_s < 0, \\ (\mu_1^+, \mu_2^+) &= (\lambda_f - \lambda_s, 2\lambda_s) \qquad \text{if} \qquad \lambda_s > 0. \end{aligned} \tag{3.27}$$

A similar derivation leads to the backward infinite time limits $(\mu_1^-, \mu_2^-) = (-\lambda_f, -\lambda_s)$. Comparing these results with the eigenvalues of the linear system, Eq. (3.19), we see that the coordinate transformation does effect on the timescales if $\lambda_s > 0$; however, if λ_s is small relative to $|\lambda_f|$ there is still two-timescale behavior.

The Lyapunov vectors that define the fast and slow directions are l_1^+ and l_2^-. We obtain l_2^- as the eigenvector of $\Phi^T\Phi$ corresponding to the eigenvalue σ_2^2. The vector l_2^- can be shown to converge to

$$l_2^- = \begin{bmatrix} 1 \\ -2\alpha x_{10} \end{bmatrix} \tag{3.28}$$

as $t \to -\infty$. Note that although we have defined the Lyapunov vectors to be unit vectors, we are omitting the scaling factor here to simplify the appearance; also, only the direction of the Lyapunov vectors is relevant in determining the tangent space structure. Similarly we can show that the Lyapunov vector l_1^+ converges as $t \to \infty$ to

$$l_1^+ = \begin{bmatrix} 0 \\ 1 \end{bmatrix} \tag{3.29}$$

for all x.

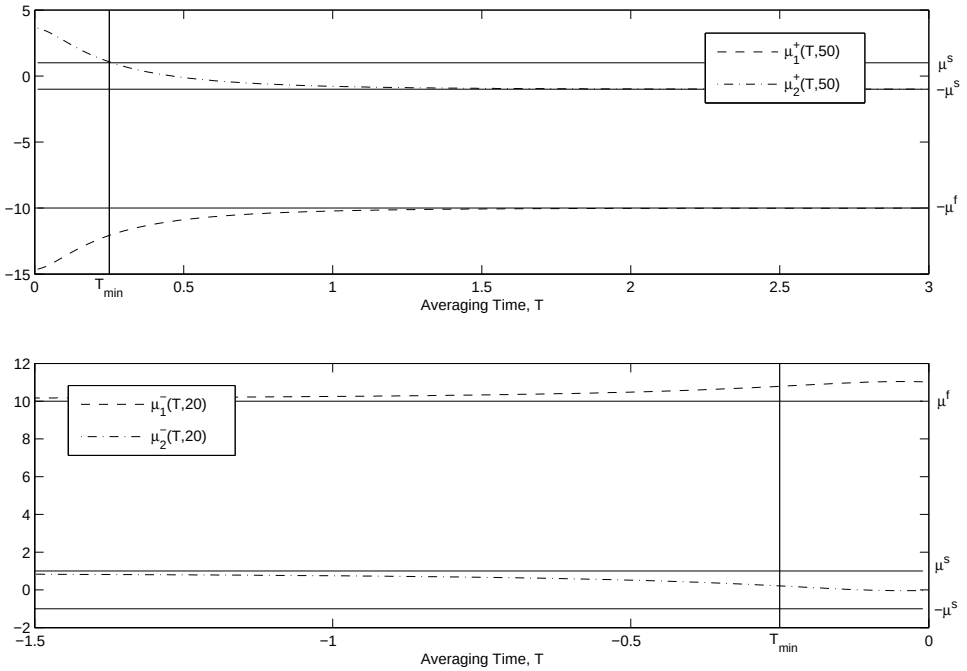

Figure 3.3: Forward and backward Lyapunov exponents versus averaging time and constants μ^s, μ^f and T_{min}.

We now consider the region $\mathcal{X} = \{(x_1, x_2) \in \mathcal{R}^2 : 2.5 \leq x_1 \leq 50 \quad \text{and} \quad -50 \leq x_2 \leq 10\}$ and check if the system satisfies the conditions of Definition (3.4.1) for a uniform

two-timescale set. Figure (3.2) shows this region and several trajectories. Taking $\mu^s = 1.0$, $\mu^f = 10.0$, $n^{fc} = 1$, $n^s = 1$, $n^{fe} = 0$, $T_{min} = 0.25$, and $T_c = 3.0$, we find that the Definition (3.4.1) conditions are satisfied and we conclude that $\mathcal{X}$ is uniform two-timescale set. Thus the gap in the spectrum induces the computable tangent space structure

$$T_x\mathcal{X} = E^{fc}(x) \oplus E^s(x) = span\{l_1^+(x)\} \oplus span\{l_2^-(x)\}. \tag{3.30}$$

We have indicated dependence of l_1^+ and l_2^- on x even though in this example l_1^+ is the same for all x and l_2^- depends only on x_1. Figure (3.3) shows the forward and backward exponents at particular points in $\mathcal{X}$ as functions of T, illustrating adherence to the bounds μ^s and μ^f and the minimum averaging time T_{min}. Figure (3.4) shows for $x_{10} = 15.0$ that the convergence of l_1^+ and l_2^- to the limiting values given in Eqs. (3.28) and (3.29) is rapid relative to T_c; this convergence behavior is representative of that at all points in $\mathcal{X}$. Observe that for $x \in \mathcal{S} \cap \mathcal{X}$, $E^s(x) = T_x\mathcal{S}$. Further $(E^s(x))^\perp = span\{l_1^-\}$ where l_1^- is deduced directly from l_2^- to be $[2\alpha x_1 \quad 1]^T$.

Slow Manifold via Orthogonality Conditions using Eigenvectors (ILDM Method)

In the ILDM method the direction orthogonal to the slow manifold is derived approximately from the local eigenvectors. The system matrix for the linearized dynamics is

$$F = \begin{bmatrix} \lambda_s & 0 \\ 2\alpha(\lambda_f - 2\lambda_s)x_1 & \lambda_f \end{bmatrix}. \tag{3.31}$$

The eigenvalues are λ_s and λ_f; in this case they indicate the two-timescale behavior correctly. Denoting the eigenvector corresponding to λ_s by v_s, the orthogonality condition is

$$\begin{aligned} 0 &= \langle v_s^\perp(x), f(x)\rangle \\ &= -2\alpha(\lambda_f - 2\lambda_s)x_1(\lambda_s x_1) + (\lambda_s - \lambda_f)(\alpha(\lambda_f - 2\lambda_s)x_1^2 + \lambda_f x_2). \end{aligned} \tag{3.32}$$

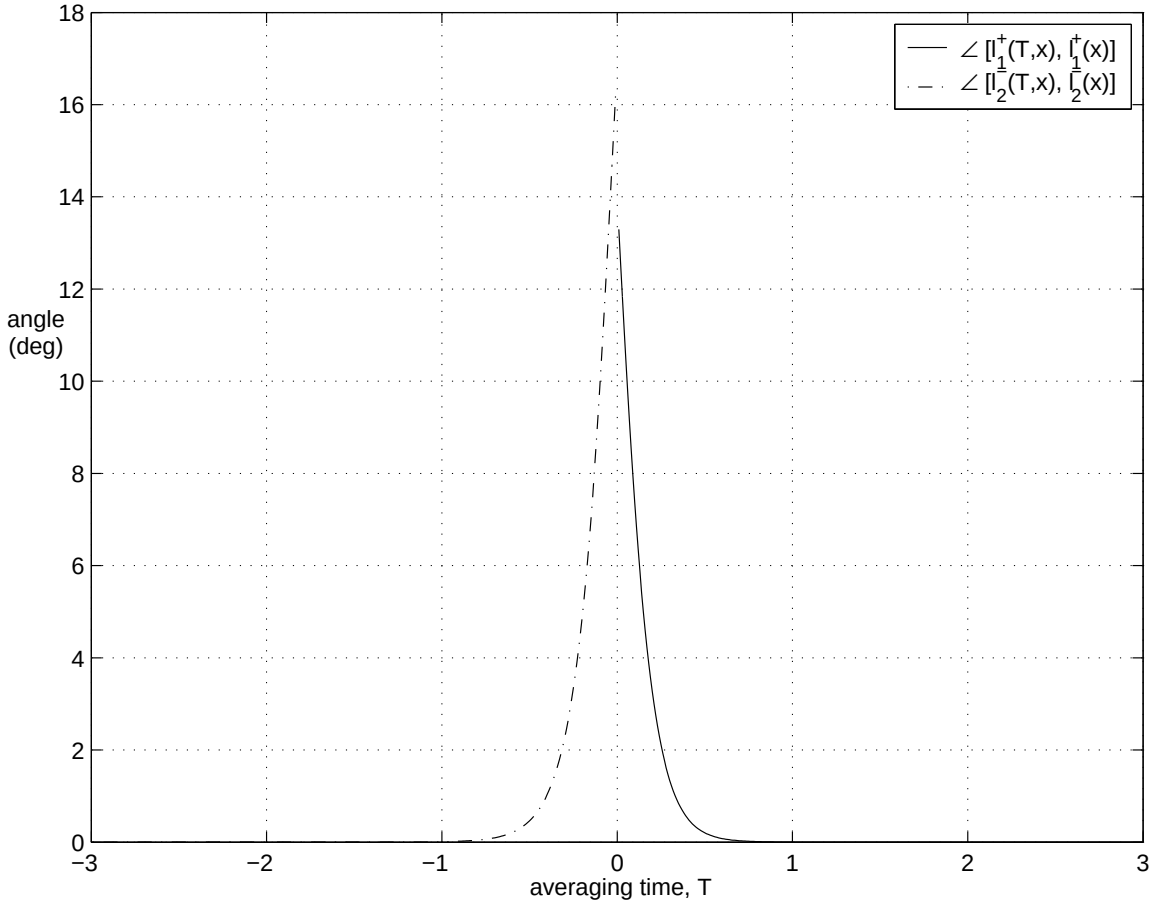

Figure 3.4: Convergence of Lyapunov vectors l_1^+ and l_2^- to their infinite time limits.

Letting $\varepsilon = |\lambda_s/\lambda_f|$, we find after some algebraic manipulation the approximation for the slow manifold given by $\hat{\mathcal{S}} = \{(x_1, x_2) : x_2 = -(1 - 2\varepsilon^2 + O(\varepsilon^3))\alpha x_1^2\}$. Thus the error in the x_2 direction is of order $O(\varepsilon^2)$ and proportional to the parameter α which is a measure of the curvature of the slow manifold. There is no error in the limit of infinite timescale separation ($\varepsilon \to 0$) or in the case of no curvature $\alpha = 0$. This is an illustration of the more general result obtained by Kaper and Kaper[1] in their analysis of the ILDM method.

Slow Manifold via Orthogonality Conditions using Lyapunov Vectors

The orthogonality condition, using the Lyapunov vector $(l_2^-)^\perp = l_1^-$ in the $t \to -\infty$ limit, is

$$\begin{aligned} 0 &= \langle l_1^-(x), f(x) \rangle \\ &= 2\alpha x_1(\lambda_s x_1) + (\alpha(\lambda_f - 2\lambda_s)x_1^2 + \lambda_f x_2) \\ &= \lambda_f(\alpha x_1^2 + x_2). \end{aligned} \tag{3.33}$$

Thus, the correct slow manifold, restricted to $\mathcal{X}$, $\mathcal{S} = \{(x_1, x_2) \in \mathcal{X} : \alpha x_1^2 + x_2 = 0\}$ is obtained.

Figure (3.5) shows the error in the x_2 coordinate of the slow manifold as a function of x_1 for the ILDM method and for the Lyapunov vector method with finite averaging times $T = 0.5, 1.0$ and 3.0. For both methods, the Matlab function "fminsearch" from the Optimization Toolbox was used to solve the algebraic equations in the form of a minimization problem as posed explicitly for the Lyapunov vector method in Eq. (3.17). Both plots in Fig. (3.5) show a pair of curves for each case: the higher one for $\alpha = 0.2$ and the lower one for $\alpha = 0.02$. At least for this example, the errors for the Lyapunov vector method are proportional to α. The Lyapunov vector method provides greater accuracy than the ILDM method and the accuracy increases with averaging time. Relative to the ILDM method errors, the Lyapunov vector method errors are 1, 3 and 10 orders of magnitude less for averaging times of 0.5, 1.0 and 3.0.

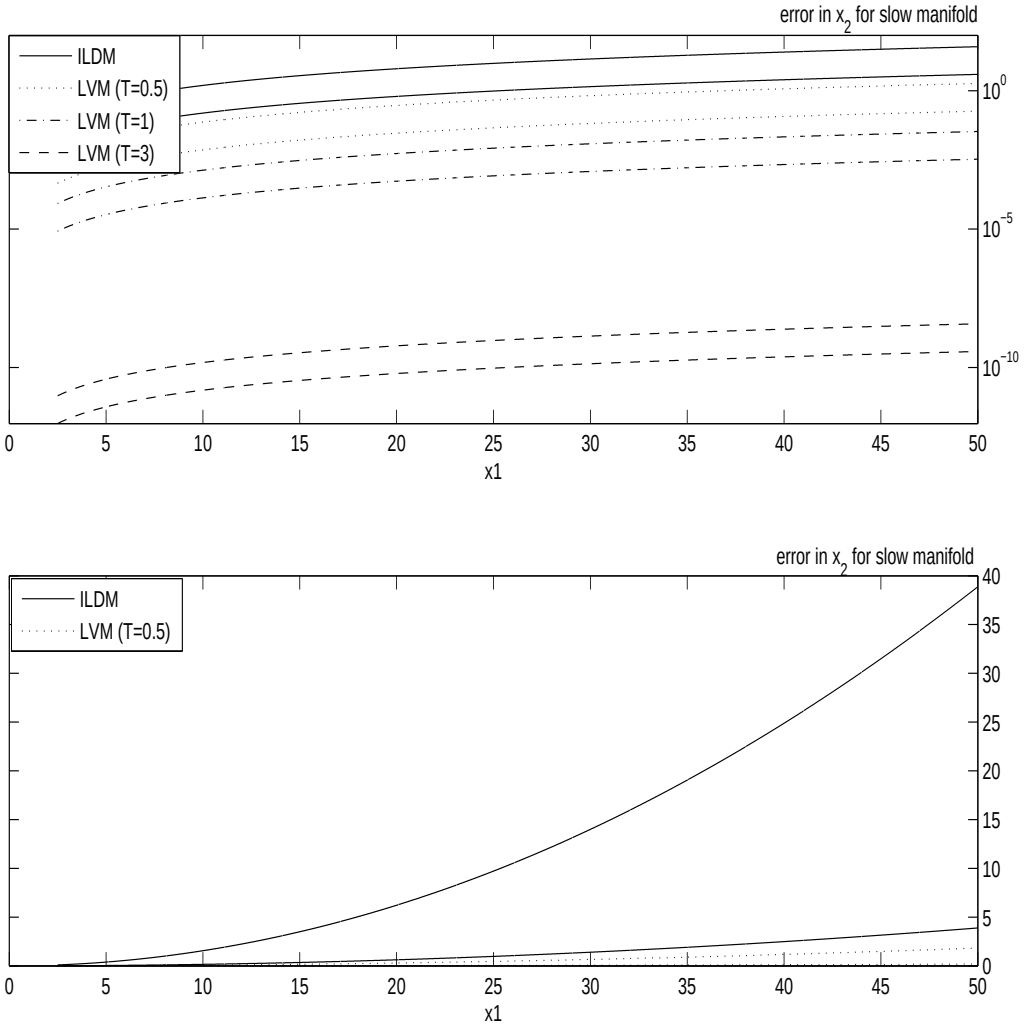

Figure 3.5: Comparison of errors in determining slow manifold from orthogonality conditions using eigenvectors (ILDM method) and using Lyapunov vectors.

3.7 Slow Manifold Determination in Powered Descent Dynamics

In a controlled system two-timescale behavior may be introduced by a high gain feedback law. Consider the vertical plane dynamics of a powered, lunar lander

$$\begin{aligned} \dot{x} &= u, \\ \dot{h} &= v, \\ \dot{u} &= \tau_x, \\ \dot{v} &= -g + \tau_h, \end{aligned} \tag{3.34}$$

where x and h are the horizontal and vertical position variables, u and v are horizontal and vertical velocity variables, g is the gravitational acceleration and τ_x and τ_h are the horizontal and vertical components of the thrust, normalized by the mass of the vehicle. All the variables are defined in some consistent set of units which we will not specify since the information is not relevant here. To track the reference velocity profiles u_{ref} and v_{ref}, given as functions of x and h, we choose the thrust components such that the error dynamics are

$$\begin{aligned} \dot{u} - \dot{u}_{ref} = &\quad \lambda_1(u - u_{ref}), \\ \dot{v} - \dot{v}_{ref} = &\quad \lambda_2(v - v_{ref}), \end{aligned} \tag{3.35}$$

where λ_1 and λ_2 are specified gains. Specifying λ_1 and λ_2 to be sufficiently large negative numbers ensures the fast convergence of the tracking errors to zero.

The reference velocity profiles are two constraints on the four dimensional state and define a two dimensional surface in the state space. Trajectories beginning off this surface approach it quickly and then follow it at the slower rate at which trajectories on the surface evolve. Thus there is a two-timescale behavior and the reference trajectory surface is the slow manifold.

Let the reference velocity profiles be $u_{ref} = -\alpha_1 x^2$ and $v_{ref} = -\alpha_2 h^2$. In order to achieve the error dynamics in Eq.(3.35), the thrust laws are $\tau_x = \lambda_1(\alpha_1 x^2 + u) - 2\alpha_1 xu$ and $\tau_h = \lambda_2(\alpha_1 h^2 + v) - 2\alpha_2 hv$. The resulting closed-loop dynamics are

$$\begin{aligned} \dot{x} = &\quad u, \\ \dot{h} = &\quad v, \\ \dot{u} = &\quad \lambda_1(\alpha_1 x^2 + u) - 2\alpha_1 xu, \\ \dot{v} = &\quad \lambda_2(\alpha_2 h^2 + v) - 2\alpha_2 hv, \end{aligned} \tag{3.36}$$

We chose $\alpha_1 = 0.02$, $\alpha_2 = 0.04$, $\lambda_1 = -10$ and $\lambda_2 = -11$ to achieve two-timescale behavior. The slow manifold can then be expressed as $\mathcal{S} = \{(x, h, u, v) \in \mathcal{X} : \alpha_1 x^2 + u =$

$0,\ \alpha_2 h^2 + v = 0\}$. Figure (3.6) shows the projections of some representative trajectories onto the $x - u$ and $h - v$ planes.

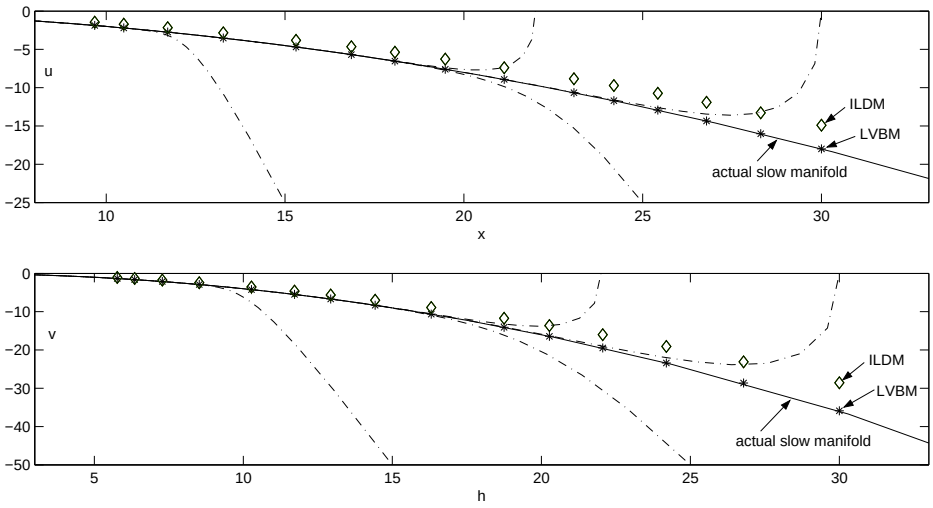

Figure 3.6: Planar slices of the state portrait for nonlinear system, Eq. (3.34), showing actual slow manifold and approximate slow manifold points determined from orthogonality conditions using eigenvectors (ILDM method) and using Lyapunov vectors (LVM).

Now we will demonstrate, using Lyapunov exponents and vectors, the diagnosis of two-timescales and the determination of the slow manifold. The bounded state space region to be analyzed is chosen to be $\mathcal{X} = \{(x, h, u, v) \in \mathcal{R}^4\ s.t.\ 2 \leq x \leq 40,\ 2 \leq h \leq 40,\ -32 \leq u \leq -1\ and -64 \leq v \leq -2\}$, a region containing the relevant portion of the reference trajectory and the range of expected state perturbations. The characteristic time T_c is 6 seconds. By calculating the Lyapunov exponents at several points in $\mathcal{X}$ for various averaging times, we diagnose that $\mathcal{X}$ is a two-timescale set with $\mu^f = 11$, $\mu^s = 3$, $T_{min} = 0.3$, $n^{fc} = 2$, $n^s = 2$, and $n^{fe} = 0$. An averaging time of 1 second is sufficient for accurate computation of the Lyapunov vectors, since the gap is $\Delta\mu = 8$. Figure (3.7) shows the forward and backward Lyapunov exponents with 1 second averaging time for points on the slow manifold $\mathcal{S}$.

Because $n^{fc} = 2$, $n^s = 2$, and $n^{fe} = 0$, the slow manifold, if present, is two-dimensional

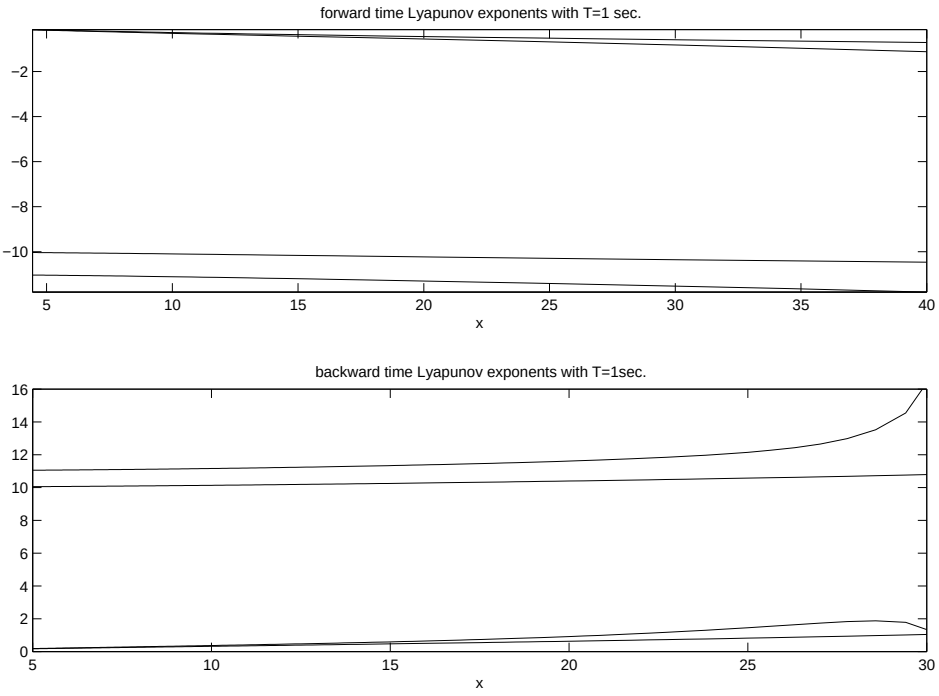

Figure 3.7: Forward and backward Lyapunov exponents versus x for T=1 sec. in slow manifold determination in powered descent dynamics example

and attracting. The slow subspace $E^s(T,\vec{x}) = L^-_{n^{fc}}(T,\vec{x}) = span\{l_3^-(T,\vec{x}), l_4^-(T,\vec{x})\}$ and using Proposition (3.5.2), we have $[E^s(T,\vec{x})]^\perp = span\{l_1^-(T,\vec{x}), l_2^-(T,\vec{x})\}$, where $\vec{x} = (x,h,y,v)^T$. For each value of (x,h) consistent with $\mathcal{X}$, the corresponding u and v values for the point on the slow manifold are obtained by solving the following algebraic equations

$$\begin{aligned} < f(\vec{x}), l_1^-(T,\vec{x}) > &= 0, \\ < f(\vec{x}), l_2^-(T,\vec{x}) > &= 0. \end{aligned} \tag{3.37}$$

Figure (3.6) shows the actual slow manifold, the slow manifold computed using the Lyapunov vectors with 1 second averaging time, and the slow manifold computed by the ILDM method, in both the $x-u$ plane ($h=v=0$) and $h-v$ plane ($x=u=0$). The Lyapunov vector method identifies the points on the slow manifold more accurately than the ILDM method.

3.8 Slow Manifold Determination in Van der Pol Oscillator Dynamics

In this section the widely known Van der Pol equations are examined and the orthogonality conditions using the eigenvectors and Lyapunov vectors are used in order to compute the slow manifold. Consider the Van der Pol equation given in the singularly perturbed form

$$\begin{aligned} \dot{x}_1 &= x_2, \\ \epsilon \dot{x}_2 &= -x_1 + x_2 - \tfrac{1}{3}x_2^3. \end{aligned} \tag{3.38}$$

where $\epsilon = 0.1$. The dynamics in Eq. (3.38) have an unstable equilibrium point at the origin and -it is known that- a stable limit cycle [49]. The trajectories starting from different initial conditions are shown in Fig. (3.8).

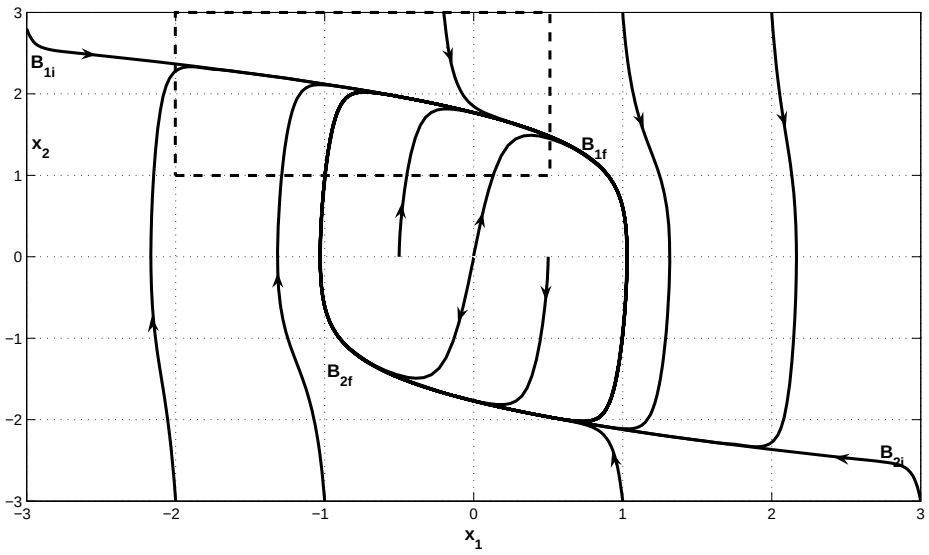

Figure 3.8: Phase portrait of the Van der Pol oscillator for $\epsilon = 0.1$.

Depending on the initial condition, all trajectories are attracted to a branch of the slow manifold, either to $B_{1i} - B_{1f}$ branch or to $B_{2i} - B_{2f}$ branch. Then, the trajectory slides along the slow manifold and is attracted to the other branch after a certain point. For details of the dynamics within the context of the singular perturbation theory see [49]. Our aim is to concentrate on the rectangular region in Fig. (3.8) and compute the part of

the slow manifold in that region. The compact $\mathcal{X}$ region is $\mathcal{X} = \{(x_1, x_2) \in \mathcal{R}^2 \ : \ -2 \leq x_1 \leq 0.5 \ and \ 1 \leq x_2 \leq 3\}$.

The methodology for diagnosing a two-timescale set is applied to the region $\mathcal{X}$. Figure (3.9) shows the forward and backward finite time Lyapunov exponents computed at several points along a trajectory for an averaging time $T = 0.2$ versus the x_1 components of the points.

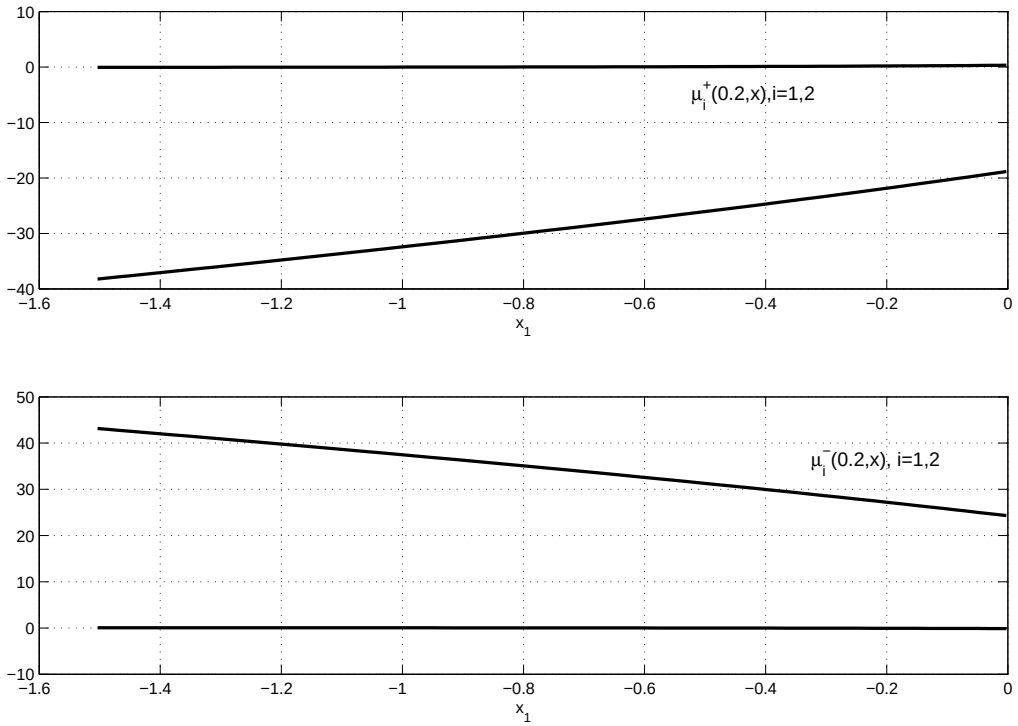

Figure 3.9: Forward and backward Lyapunov exponents for the Van der Pol dynamics versus x_1 for $T = 0.2$.

For the finite time Lyapunov exponents with the averaging time $T = 0.2$ there exists a gap of around 20. At point $[-1, 2.1]$ the finite time forward and backward Lyapunov exponents and the angles between the finite time Lyapunov vectors and the horizontal axis are illustrated in Fig. (3.10). From Fig. (3.10) the gap exists for all averaging times $T \in (0, 0.2]$ and the Lyapunov vectors converge. This convergence behavior is representative of that at all points in $\mathcal{X}$. Thus, the closed set $\mathcal{X}$ is a two-timescale set

with a uniform spectral gap $\Delta\mu = 18$, $\mu^f = 19$, $\mu^s = 1$, $n^{fc} = 1$ and $n^s = 1$. Although T_c is about 0.8, an averaging time of 0.2 is appropriate for the convergence of the directions. T_{min} can be taken zero in this case.

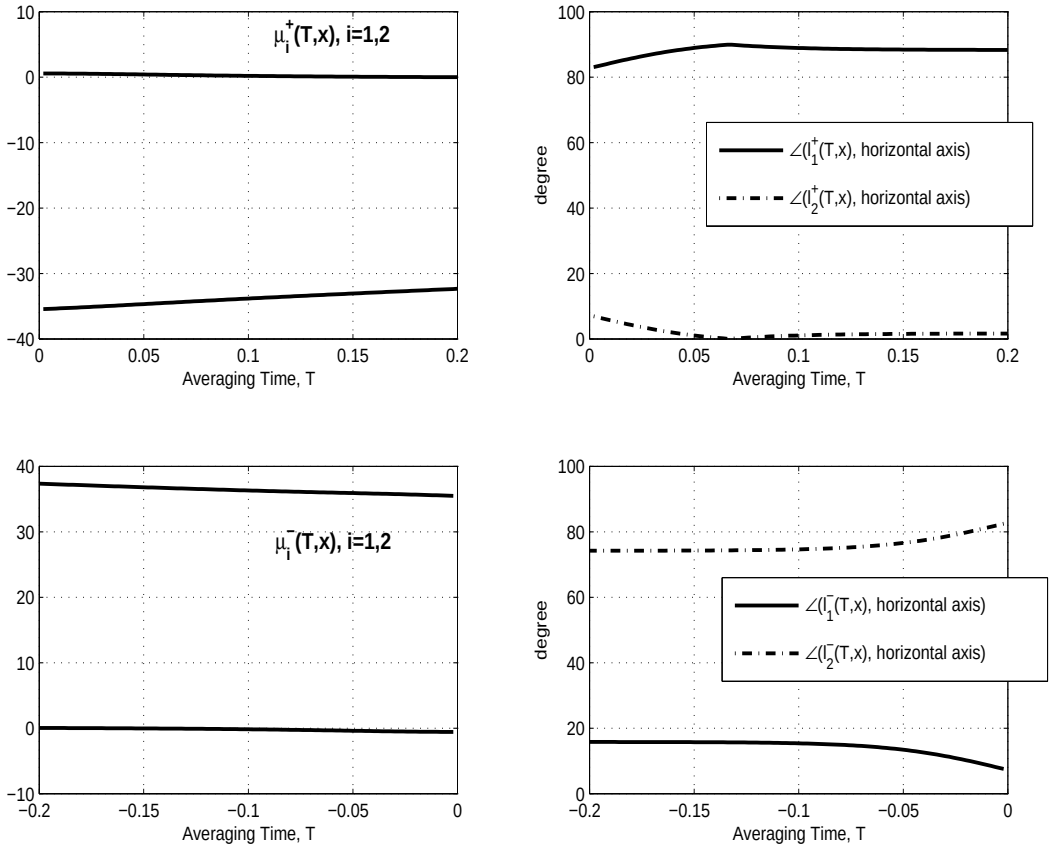

Figure 3.10: Forward and backward Lyapunov exponents for the Van der Pol dynamics versus the averaging time at point $(-1; 2.1)$.

Because $n^{fc} = 1$, $n^s = 1$, and $n^{fe} = 0$, the slow manifold, if exists, is one-dimensional and attracting. The slow subspace is spanned by $l_2^-(T, x)$. Using Proposition (3.5.2), $[E^s(T, x)]^\perp = span\{l_1^-(T, x)\}$. For each value of x_1 consistent with $\mathcal{X}$, the corresponding values for the point on the slow manifold are obtained by solving the following algebraic equation

$$\langle f(x), l_1^-(T, x)\rangle = 0. \tag{3.39}$$

The slow manifold is computed by solving the following equation which is the orthogonality condition of the ILDM method

$$\langle f(x), v_e(x) \rangle = 0, \tag{3.40}$$

where $v_e(x)$ is the eigenvector of $\frac{\partial f(x)}{\partial x}$ at the point x corresponding to the eigenvalue of $\frac{\partial f(x)}{\partial x}$ with smaller absolute value.

Figure (3.11) shows the slow manifold computed using the Lyapunov vectors with $T = 0.2$, the slow manifold computed by the ILDM method and some representative trajectories in region $\mathcal{X}$. The Lyapunov vector method identifies the points on the slow manifold more accurately than the ILDM method. The accuracy of the computation using the Lyapunov vectors can be further improved by increasing the averaging time. Note that an averaging time $T = 0.2$ is used in the computation of the slow manifold although $T_c = 0.8$.

3.9 Slow Manifold Determination in a 3 Species Kinetics Problem

In this section, we will demonstrate the slow manifold determination in a 3 species kinetics problem. The same problem is used in [50]. The dynamics under consideration is given as

$$\begin{bmatrix} \dot{x}_1 \\ \dot{x}_2 \\ \dot{x}_3 \end{bmatrix} = \frac{1}{\epsilon} \begin{bmatrix} -5x_1 - x_1x_2 + \epsilon x_2x_3 + 5x_2^2 + x_3 - \epsilon x_1 \\ 10x_1 - x_1x_2 - \epsilon x_2x_3 - 10x_2^2 + x_3 + \epsilon x_1 \\ x_1x_2 - \epsilon x_2x_3 - x_3 + \epsilon x_1 \end{bmatrix}, \tag{3.41}$$

where $\epsilon = 0.01$. For this system, the compact region $\mathcal{X} = \{x_1, x_2, x_3 \in \mathcal{R}^3 \ : \ 0 \leq x_1,\ x_2,\ x_3 \leq 1\}$ is chosen. The finite time Lyapunov exponents at the point $(0.6, 0.8, 0.5)$ are shown in Fig. (3.12). It can be seen in Fig. (3.12) that there are spectral gaps of around 1800 and 200 between $\mu_1^+(T,x)$ and $\mu_2^+(T,x)$ and between $\mu_2^+(T,x)$ and $\mu_3^+(T,x)$ respectively. Because of the spectral gap between $\mu_1^+(T,x)$ and $\mu_2^+(T,x)$, there should be a 2 dimensional manifold toward which all the trajectories off that manifold should

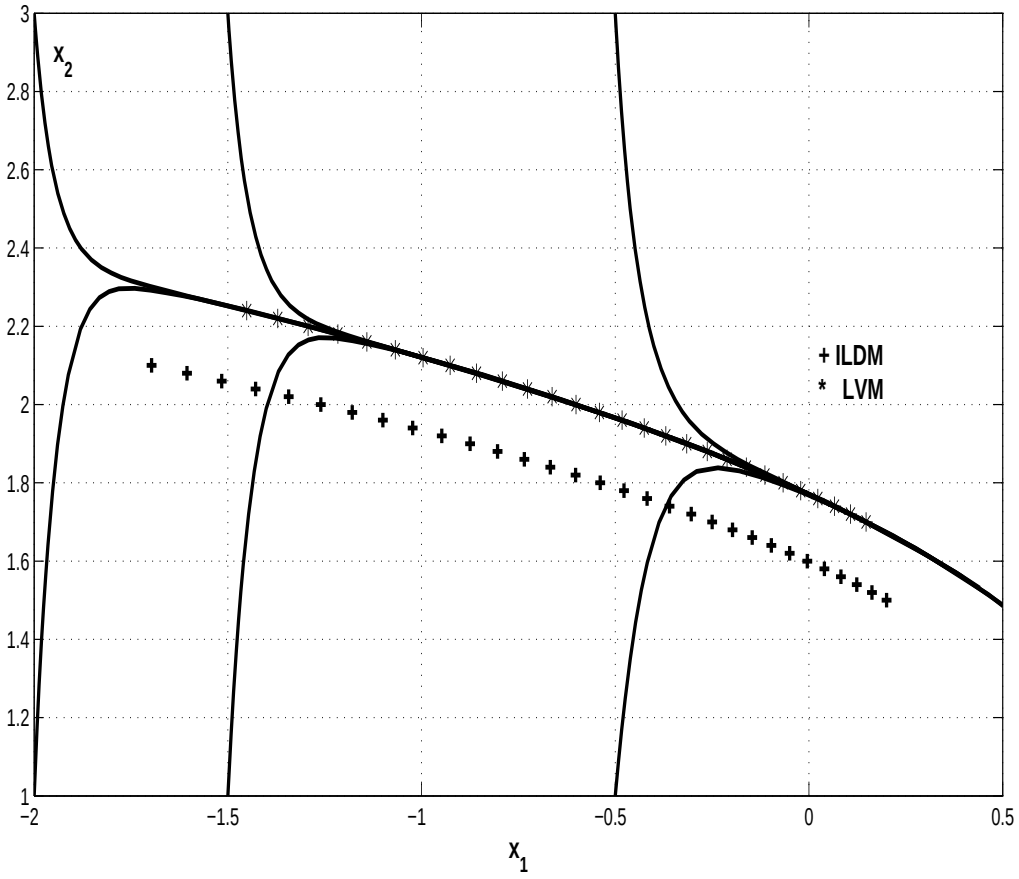

Figure 3.11: The slow manifold computed using the orthogonality conditions with the Lyapunov vectors and the eigenvectors of the Jacobian matrix.

converge. Besides this 2 dimensional manifold, due to the spectral gap between $\mu_2^+(T,x)$ and $\mu_3^+(T,x)$, there should be a 1 dimensional submanifold of the 2 dimensional manifold to which all the trajectories eventually converge.

The 2 dimensional manifold can be computed by using $n^{fc} = 1$ and $n^s = 2$. In this case, the partial equilibrium conditions become

$$\langle f(x), l_1^-(T,x)\rangle = 0. \tag{3.42}$$

On the other hand, the 1 dimensional manifold can be computed by using $n^{fc} = 2$ and $n^s = 1$. In this case, the constraints to be satisfied at the points on the 1 dimensional

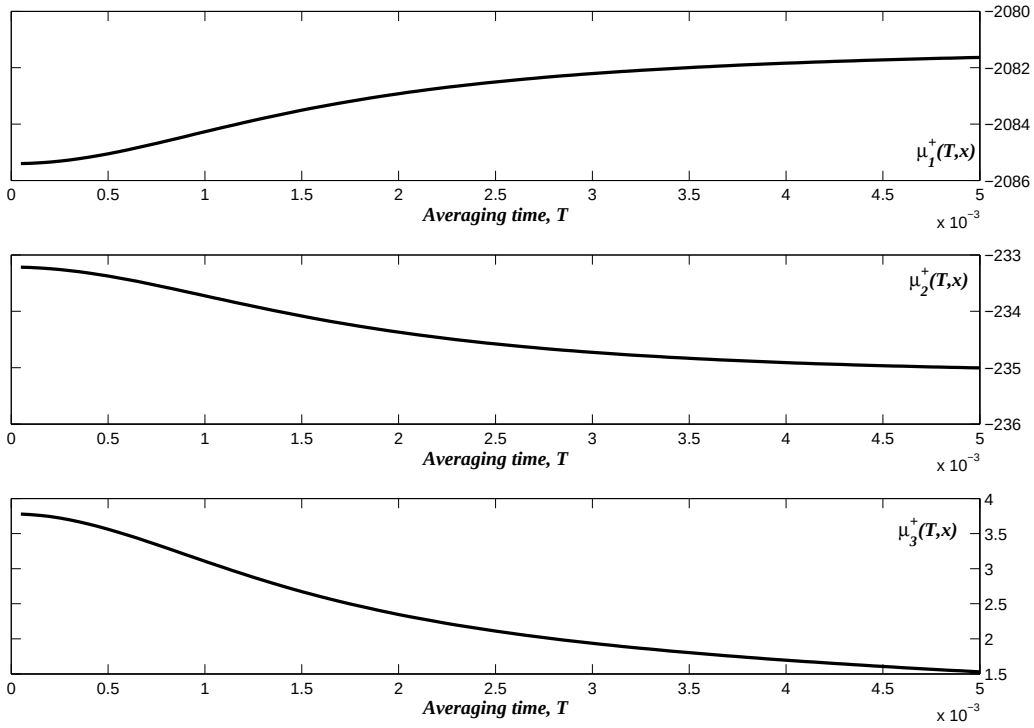

Figure 3.12: The finite time Lyapunov exponents at the point $(0.6, 0.8, 0.5)$ for the 3 species kinetics problem.

manifold are

$$\begin{aligned} \langle f(x), l_1^-(T,x)\rangle &= 0, \\ \langle f(x), l_2^-(T,x)\rangle &= 0. \end{aligned} \tag{3.43}$$

These two sets of constraints are solved separately. The dots in Fig. (3.13) show the 2 dimensional slow manifold computed by using Eq. (3.42).The stars in Fig. (3.13) show the 1 dimensional slow manifold computed by using Eq. (3.43). Some trajectories of the dynamics in Eq. (3.41) are also shown in Fig. (3.13). As we expect all the trajectories quickly get close to a 2 dimensional manifold and then all the trajectories converge to a 1 dimensional manifold, which is a submanifold of the 2 dimensional manifold. Figure (3.14), which is another view of Fig. (3.13), clearly shows that the trajectories quickly get close to the 2 dimensional manifold computed by the Lyapunov vectors.

This example demonstrates that the methodology for locating the slow manifold can

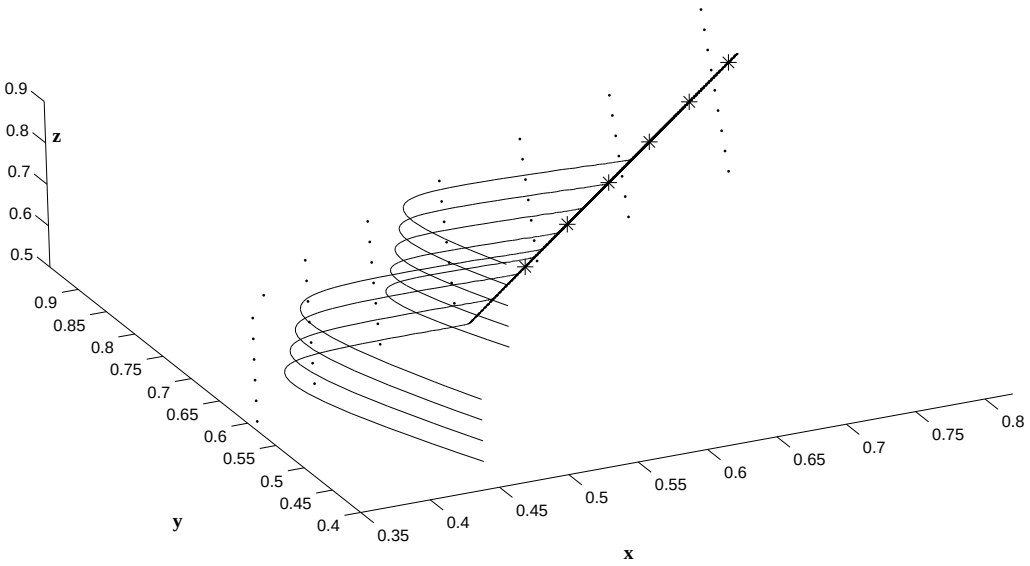

Figure 3.13: Phase portrait, 1 dimensional and 2 dimensional slow manifolds computed by using the constraints in Eqs. (3.42) and (3.43).

be used in the existence of multiple spectral gaps. The procedure is a repetition of the method explained for a single spectral gap. By adjusting the constants n^{fc}, n^{s}, and n^{fe}, the slow manifolds of different dimensions can be computed. Note that the accuracy of the slow manifold computed is dependent on the associated spectral gap.

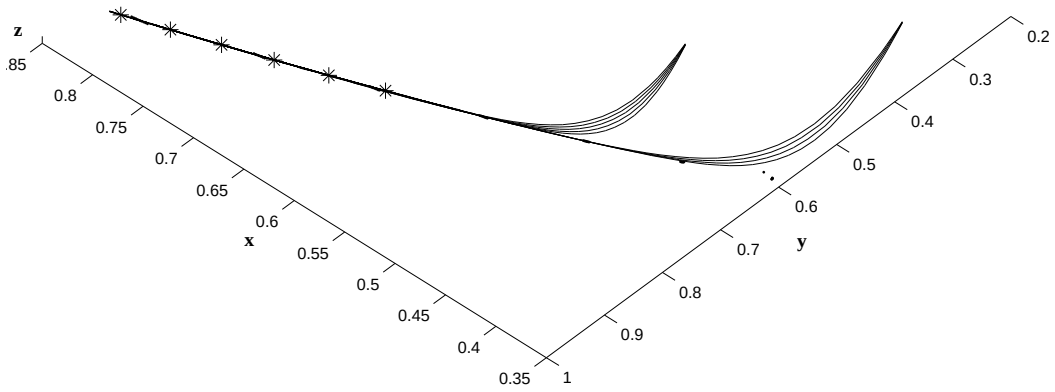

Figure 3.14: Convergence of the trajectories of 3 species kinetics problem to the 2 dimensional manifold computed by using the finite time Lyapunov exponents.

Chapter 4

Lyapunov Vector Dichotomic Basis Method for Solving Hyper-Sensitive Optimal Control Problems

4.1 Introduction to the problem and literature

In general the methods for solving optimal control problems are classified as direct methods and indirect methods. Direct methods parametrize the control and/or state and cast the optimal control problem as a nonlinear programming problem with dynamical and boundary constraints. Indirect methods are based on the first-order optimality conditions and solve the associated Hamiltonian boundary-value problem (HBVP).

HBVPs are hard to solve because of the ill-conditioning due to the sensitive dependence on the unknown initial conditions. Hamiltonian systems have the volume preserving feature, i.e., if a bounded, open set of initial conditions are propagated according to the Hamiltonian vector field, the set of the propagated points occupy the same volume as the initial set. If the set contracts in some directions, it expands in some other directions. This means there exists an equal number of stable and unstable directions in the Hamiltonian vector field. An error in the unknown initial conditions grows exponentially in certain directions with the time span of interest.

An optimal control problem and its corresponding HBVP are called completely hyper-

sensitive, if the time interval of interest is very long relative to the minimum rate of contraction and expansion of the Hamiltonian system in the neighborhood of the optimal solutions to the HBVP [4, 5]. If the expansion and the contraction are fast only in some directions, it is called partially hyper-sensitive. Achieving a specified accuracy on the terminal boundary conditions requires the initial conditions in the fast expanding directions to be very accurate or even to exceed the available precision. The indirect shooting method can be modified using multiple shooting nodes, denser in the boundary-layers, to handle the hyper-sensitivity. Although multiple shooting method may be capable of producing solutions with the required accuracy, it does not provide any information regarding the structure of the solution on the Hamiltonian state space.

The solution of a hyper-sensitive HBVP is composed of a short initial boundary-layer segment, a long intermediate segment dominated by the slow behavior and a short terminal boundary-layer segment. Besides the dynamics themselves, the intermediate segment is determined primarily by the cost functional, whereas the boundary-layers connect the intermediate segment to the boundary conditions. The initial boundary-layer trajectory approaches the intermediate segment in forward time and the terminal boundary layer approaches the intermediate segment in backward time. For the completely hyper-sensitive HBVP, the slow segment is the equilibrium solution. The composite solution to the partially hypersensitive problems can be constructed by the analytical singular perturbation method in the special case, where the two-timescale Hamiltonian dynamics are given in the standard singularly perturbed form [34]. It decomposes the system into fast and slow subsystems and solves the reduced-order problems. The solution to the HBVP is then constructed by matching the asymptotic expansions of the solutions for the boundary-layer segments and the intermediate segment [2, 38]. Unfortunately, a systematic procedure for

transforming a two-timescale Hamiltonian system in general form to standard singularly perturbed form is not available. This restricts the applicability of the singular perturbation method.

For completely hyper-sensitive optimal control problems in general form, an indirect solution method based on the underlying geometric structure of the trajectories of the Hamiltonian system in the state-costate space has been introduced [4, 5]. The method uses a dichotomic transformation to decouple the contracting and expanding behavior. The solution to the HBVP is constructed by forward integration of the contracting part of the dynamics and backward integration of the expanding part of the dynamics. The use of dichotomic transformations for the solution of linear boundary-value problems is well known in the numerical analysis literature [23]. Chow [51] used dichotomic transformations for nonlinear two-timescale HBVPs in standard form with linear boundary layer dynamics. Rao and Mease [4, 5] used the geometric characterization of two-timescale systems by Fenichel [33] and the stable and unstable sub-bundles of Sacker and Sell [52] to extend the use of dichotomic transformations to nonlinear HBVPs.

In [4, 5] the basis vectors to construct approximate dichotomic transformations are local eigenvectors of the Jacobian of the Hamiltonian vector field. It is well known that the eigenvectors do not provide the correct structure of the linear time-varying system which results when the nonlinear Hamiltonian system is linearized around a reference trajectory. Thus, an iterative algorithm was used to approximate the initial and terminal boundary-layers. In [11, 12] it is shown that Lyapunov vectors give accurate information on the geometry of the underlying linearized time-varying systems of the nonlinear systems. In this work, we propose to use appropriate Lyapunov vectors to construct the dichotomic basis, and demonstrate that the finite averaging time Lyapunov vectors can be used to

approximate the Lyapunov vectors for this purpose.

4.2 Hamiltonian Boundary Value Problem

Consider the following optimal control problem of finding a piecewise continuous control $u(t) \in \mathcal{R}^m$ on $[0, t_f]$ that minimizes the scalar cost

$$J = \int_0^{t_f} L(s,u)dt \tag{4.1}$$

subject to system dynamics

$$\dot{s} = f(s,u) \tag{4.2}$$

and boundary conditions

$$\begin{aligned} s(0) &= s_0 \\ s(t_f) &= s_f \end{aligned} \tag{4.3}$$

where $s(t) \in \mathcal{R}^n$ is the state.

The first-order necessary optimality conditions lead to a HBVP which is composed of the Hamiltonian differential equations

$$\begin{aligned} \dot{s} &= H_\lambda^{*T} \\ \dot{\lambda} &= -H_s^{*T} \end{aligned} \tag{4.4}$$

with the boundary conditions (4.3), where $\lambda(t) \in \mathcal{R}^n$ is the costate,

$$H^*(s,\lambda) = L(s,u^*(s,\lambda)) + \lambda^T f(s,u^*(s,\lambda)) \tag{4.5}$$

is the Hamiltonian evaluated for the optimal control

$$u^*(s,\lambda) = \arg\min_u H(s,\lambda,u), \tag{4.6}$$

and H_λ and H_s are partial derivatives with respect to the subscripted variable. We assume that H is a continuously differentiable function of s and λ.

The vector field of Eq.(4.4) is called Hamiltonian vector field. Hamiltonian vector fields are divergence-free, i.e.,

$$div \begin{pmatrix} H_\lambda^T \\ \\ -H_s^T \end{pmatrix} = \frac{\partial}{\partial s}\frac{\partial H}{\partial \lambda} - \frac{\partial}{\partial \lambda}\frac{\partial H}{\partial s} = 0. \tag{4.7}$$

By Liouville's theorem [53], the Hamiltonian flow is volume-preserving, and for every direction along which the flow is contracting, there exists a corresponding direction along which the flow is expanding at the same rate as the contracting behavior. If there is a full set of boundary conditions at the initial or final time, the the vector field can be integrated and the solution trajectory can be obtained. However, for the two-point boundary value problems, with some boundary conditions given at the initial time and some at the final time, the error in the solution will grow as a consequence of the error in the unknown boundary conditions because of the expanding directions in the Hamiltonian vector field.

The s-space and the (s, λ)-space are called the state space and the phase space, respectively. Our attention is on the HBVP, its solution, and the structure of this solution trajectory and its neighbors in the phase space.

4.3 Supporting Theory and Terminology

In order to simplify the notation, $x = (s, \lambda)$, and

$$\dot{x} = \begin{pmatrix} \dot{s} \\ \dot{\lambda} \end{pmatrix} = f(x) = (H_\lambda(x), -H_s(x)) \tag{4.8}$$

are sometimes used. $\mathcal{P}$ represents the Euclidean phase space $\mathcal{R}^{2n}$. The tangent space at a point x of the phase space $\mathcal{P}$ is the space of the tangent vectors, $(\delta s, \delta\lambda)$, of all possible continuously differentiable trajectories through x. The tangent space at $x \in \mathcal{P}$ is a linear vector space isomorphic to $\mathcal{R}^{2n}$ and is denoted by $T_x\mathcal{P}$. The tangent bundle is $T\mathcal{P} = \cup_{x\in\mathcal{P}} \mathcal{T}_x\mathcal{P}$. A point in the tangent bundle is denoted by (x, v) where $v = (\delta s, \delta\lambda)$

is the $2n$-dimensional vector in the tangent space with base point x, i.e. $v \in T_x\mathcal{P}$, and satisfies the following differential equation

$$\dot{v} = \frac{\partial f}{\partial x} v. \tag{4.9}$$

The theory of Sacker and Sell [52] can be used to determine the contracting and expanding directions of the Hamiltonian system by considering the linearized dynamics with respect to a solution trajectory of Eq.(4.4). The Hamiltonian vector field $\dot{x} = f(x)$ on the phase space induces a linear Hamiltonian flow on the tangent bundle. An initial point (x, v) is mapped in time t to the point $(\phi(t, x), \Phi(t, x)v)$, where $v \in T_x\mathcal{P}$ and $\Phi(t, x)v \in T_{\phi(t,x)}\mathcal{P}$, and $\phi(t, x)$ and $\Phi(t, x)$ are the solutions of the following initial value problems

$$\dot{\phi} = f(\phi), \qquad \phi(0, x) = x, \tag{4.10}$$

$$\dot{\Phi} = \frac{\partial f}{\partial x}(\phi)\Phi, \qquad \Phi(0, x) = I, \tag{4.11}$$

where I is $2n \times 2n$ identity matrix.

Definition 4.3.1 *Let $\mathcal{Y} \subset \mathcal{P}$ be a smooth, compact, connected submanifold of $\mathcal{P}$, and let $\mathcal{Y}$ be invariant with respect to the Hamiltonian flow $\dot{x} = f(x)$. Then, the induced linear Hamiltonian flow on the tangent bundle $T\mathcal{Y}$ admits an exponential dichotomy, if there exist a projector on $T\mathcal{Y}$, a mapping $\hat{\Pi} : T\mathcal{Y} \to \mathcal{T}\mathcal{Y}$ such that (i) $\hat{\Pi}$ is continuous, and (ii) for each $x \in \mathcal{Y}$, there is a linear projection $\Pi(x)$ in $T_x\mathcal{Y}$ such that $\hat{\Pi}(x, v) = (x, \Pi(x)v)$ for all $(x, v) \in T\mathcal{Y}$, where $\Pi(x)$ has rank n on $\mathcal{Y}$, and positive constants K and α such that*

$$\begin{aligned} \|\Phi(t, x)\Pi(x)\Phi^{-1}(\tau, x)\| &\leq Ke^{-\alpha(t-\tau)}, \quad t \geq \tau \\ \|\Phi(t, x)(I - \Pi(x))\Phi^{-1}(\tau, x)\| &\leq Ke^{-\alpha(t-\tau)}, \quad t \leq \tau \end{aligned} \tag{4.12}$$

for all $x \in \mathcal{Y}$. The range and null space of a projector on $T\mathcal{Y}$ are defined as

$$\begin{aligned} range(\hat{\Pi}) &= \mathcal{R} = \{(x, v) \in T\mathcal{Y} : \ \Pi(x)v = v\} \\ nullspace(\hat{\Pi}) &= \mathcal{N} = \{(x, v) \in T\mathcal{Y} : \ \Pi(x)v = 0\} \end{aligned} \tag{4.13}$$

and are complementary sub-bundles of $T\mathcal{Y}$*, i.e.,* $\mathcal{R}(x) \cap \mathcal{N}(x) = \{0\}$ *and* $T_x\mathcal{Y} = \mathcal{R}(x) \bigoplus \mathcal{N}(x)$*, where* $\mathcal{R}(x)$ *and* $\mathcal{N}(x)$ *denote fibers of the sub-bundles at* $x \in \mathcal{Y}$*.*

If the induced linear Hamiltonian flow on the tangent bundle $T\mathcal{Y}$ admits an exponential dichotomy with the projector $\hat{\Pi}$, then $\hat{\Pi}$ allows the splitting of $T\mathcal{Y}$ into invariant, complementary stable and unstable bundles

$$\begin{aligned} \mathcal{R} = range(\hat{\Pi}) = \mathcal{V}_s = \{(x,v) \in T\mathcal{Y} : \ \|\Phi(t,x)v\| \to 0 \ \ as \ \ t \to +\infty\} \\ \mathcal{N} = nullspace(\hat{\Pi}) = \mathcal{V}_u = \{(x,v) \in T\mathcal{Y} : \ \|\Phi(t,x)v\| \to 0 \ \ as \ \ t \to -\infty\} \end{aligned} \tag{4.14}$$

Consider a linear coordinate change $(x,v) \mapsto (x,w_f)$ on $T\mathcal{Y}$ with $v = D_f(x)w_f$, where w_f is the new coordinate vector and D_f is a nonsingular and continuously differentiable $2n \times 2n$ matrix valued function of x on $\mathcal{Y}$. The columns of $D_f(x)$ are basis vectors for $T_x\mathcal{Y}$ for each $x \in \mathcal{Y}$. In terms of w_f, the variational equation (4.9) becomes

$$\dot{w_f} = [D_f^{-1} J D_f - D_f^{-1}\dot{D}_f] = \Lambda(x) w_f, \tag{4.15}$$

where $J = \partial f/\partial x$ is the local Jacobian matrix, $\dot{D}_f$ is obtained by taking the Lie derivative, in the f direction, of each element of D_f, and Λ is used to denote the transformed system matrix more concisely.

Definition 4.3.2 *Concerning the exponential dichotomy for the linear flow on* $T\mathcal{Y}$*, a basis* D_f *is a dichotomic basis, if it satisfies the following two requirements.*

1. *The corresponding system matrix* Λ *is block-triangular of the form*

$$\Lambda = \begin{pmatrix} \Lambda_s(x) & \Lambda_{su}(x) \\ 0 & \Lambda_u(x) \end{pmatrix} \tag{4.16}$$

   for all $x \in \mathcal{Y}$*, and the matrices* Λ_s *and* Λ_u *are both* $(n \times n)$ *dimensional.*

2. *The transition matrices* $\Phi_s(t,x)$ *and* $\Phi_u(t,x)$ *corresponding to* Λ_s *and* Λ_u*, defined such that* $\Phi_s(0,x) = I$ *and* $\Phi_u(0,x) = I$ *satisfy the inequalities*

$$\begin{aligned} \|\Phi_s(t,x)\Phi_s^{-1}(\tau,x)\| \le K_1 \|D_f(\phi(\tau,x)\| \|D_f^{-1}(\phi(t,x))\| e^{-\alpha(t-\tau)}, \quad t \ge \tau \\ \|\Phi_u(t,x)\Phi_u^{-1}(\tau,x)\| \le K_1 \|D_f(\phi(\tau,x)\| \|D_f^{-1}(\phi(t,x))\| e^{-\alpha(t-\tau)}, \quad t \le \tau \end{aligned} \tag{4.17}$$

where α and K_1 are positive constants.

The subscripts "s" and "u" indicate the stable and unstable nature of the two subsystems.

A dichotomic basis can be split in the form

$$D_f(x) = [D_{f_s}(x)\ D_{f_u}(x)], \tag{4.18}$$

where

$$\begin{aligned} D_{f_s}(x) &= [d_1(x)\ ...\ d_n(x)] \\ D_{f_u}(x) &= [d_{n+1}(x)\ ...\ d_{2n}(x)]. \end{aligned} \tag{4.19}$$

Correspondingly, the new coordinate vector splits as

$$w_f = \begin{pmatrix} w_{f_s} \\ w_{f_u} \end{pmatrix}. \tag{4.20}$$

A point in the stable sub-bundle $\mathcal{V}_s$ has the form $(x, (w_{f_s}, 0))$. The fiber $\mathcal{V}_s(x)$ of the stable sub-bundle is given by the column span of $D_{f_s}(x)$. Note that the stable sub-bundle is invariant under the dynamics, since an initial point of the form $(x, (w_{f_s}(0), 0))$ maps to a point $(\phi(t,x), (w_{f_s}(t), 0)) = (\phi(t,x), (\Phi_s(t)w_{f_s}(0), 0))$ and remains in the stable sub-bundle. In addition, it could be required that a dichotomic basis yield $\Lambda_{su} = 0$. Then $\mathcal{V}_u(x)$ would be spanned by $D_{f_u}(x)$. But this property is not needed for our purposes.

The Hamiltonian vector field f assigns to each phase point $x = (s, \lambda)$ a vector $f(x) = (H_\lambda(s,\lambda), -H_s(s,\lambda))$ in the tangent space at that point. At each phase point, this particular tangent vector can be expressed in the dichotomic basis as

$$f(x) = \begin{pmatrix} H_\lambda^T(s,\lambda) \\ -H_s^T(s,\lambda) \end{pmatrix} = D_{f_s}(s,\lambda)w_{f_s} + D_{f_u}(s,\lambda)w_{f_u}, \tag{4.21}$$

where the tangent vector coordinates w_{f_s} and w_{f_u} are determined by

$$\begin{aligned} w_{f_s} &= h_{f_s}(s,\lambda) = D_{f_s}^\dagger(s,\lambda)f(s,\lambda), \\ w_{f_u} &= h_{f_u}(s,\lambda) = D_{f_u}^\dagger(s,\lambda)f(s,\lambda), \end{aligned} \tag{4.22}$$

where $D_{f_s}^{\dagger}(x) \in \mathcal{R}^{n\times 2n}$ and $D_{f_u}^{\dagger}(x) \in \mathcal{R}^{n\times 2n}$ and are the first and second, respectively, n rows of $D_f{}^{-1}$

$$D_f{}^{-1}(x) = \begin{pmatrix} D_{f_s}^{\dagger}(x) \\ D_{f_u}^{\dagger}(x) \end{pmatrix}. \tag{4.23}$$

An alternative to integrating Eq.(4.4) to compute the extremal for a given initial condition (s_0, λ_0) is to integrate the system

$$\begin{pmatrix} \dot{s} \\ \dot{\lambda} \end{pmatrix} = D_{f_s}(s,\lambda) w_{f_s} + D_{f_u}(s,\lambda) w_{f_u}$$
$$\begin{pmatrix} \dot{w}_{f_s} \\ \dot{w}_{f_u} \end{pmatrix} = \begin{pmatrix} \Lambda_s(s,\lambda) & \Lambda_{su}(s,\lambda) \\ 0 & \Lambda_u(s,\lambda) \end{pmatrix} \begin{pmatrix} w_{f_s} \\ w_{f_u} \end{pmatrix} \tag{4.24}$$

with the initial conditions

$$s(0) = s_0, \quad \lambda(0) = \lambda_0,$$
$$w_{f_s}(0) = h_{f_s}(s_0,\lambda_0), \quad w_{f_u}(0) = h_{f_u}(s_0,\lambda_0). \tag{4.25}$$

This alternative makes clear that a property of a dichotomic basis is for a given initial condition on the state, $s(0) = s_0$, the unstable component of the Hamiltonian vector field can be suppressed at $t = 0$ by choosing $\lambda(0) = \lambda_0$ such that $h_{f_u}(s_0, \lambda_0) = 0$; and that the unstable component will remain suppressed, due to the lack of coupling from w_{f_s} to w_{f_u}. In other words, we choose λ_0 such that we are at a point in the phase space on the $s = s_0$ hyper-plane where the Hamiltonian vector field lies in the fiber $\mathcal{V}_s(s_0, \lambda_0)$ of the stable sub-bundle.

Another dichotomic transformation can be obtained by changing the order of the blocks in the transformation, $D_f(x)$, which span the fibers $\mathcal{V}_s(x)$ and $\mathcal{V}_u(x)$ of the stable and unstable sub-bundles, respectively, as

$$D_b(x) = \begin{pmatrix} D_{b_u}(x) & D_{b_s}(x) \end{pmatrix}. \tag{4.26}$$

The dichotomic transformation, $D_b(x)$, brings the linearized system matrix into the form

$$\Lambda = \begin{pmatrix} \Lambda_u(x) & \Lambda_{us}(x) \\ 0 & \Lambda_s(x) \end{pmatrix} \tag{4.27}$$

for all $x \in \mathcal{Y}$. The transition matrices $\Phi_u(t,x)$ and $\Phi_s(t,x)$ corresponding Λ_u and Λ_s satisfy the second property in Definition (4.3.2).

For backward integration, Λ_s subsystem is unstable and Λ_u subsystem is stable. For a given final condition (s_f, λ_f), the differential equations

$$\begin{aligned} \begin{pmatrix} \dot{s} \\ \dot{\lambda} \end{pmatrix} &= D_{b_s}(s,\lambda) w_{b_s} + D_{b_u}(s,\lambda) w_{b_u} \\ \begin{pmatrix} \dot{w}_{b_u} \\ \dot{w}_{b_s} \end{pmatrix} &= \begin{pmatrix} \Lambda_u(s,\lambda) & \Lambda_{us}(s,\lambda) \\ 0 & \Lambda_s(s,\lambda) \end{pmatrix} \begin{pmatrix} w_{b_u} \\ w_{b_s} \end{pmatrix} \end{aligned} \tag{4.28}$$

with the final conditions

$$\begin{aligned} s(t_f) = s_f, \quad \lambda(t_f) = \lambda_f, \\ w_{b_s}(t_f) = h_{b_s}(s_f, \lambda_f), \quad w_{b_u}(t_f) = h_{b_u}(s_f, \lambda_f). \end{aligned} \tag{4.29}$$

can equivalently be integrated instead of integrating Eq.(4.4), where $v = D_b(x) w_b = D_b(x) \begin{pmatrix} w_{b_u} \\ w_{b_s} \end{pmatrix}$, $h_{b_s} = D_{b_s}^{\dagger}(x) f(x)$, $h_{b_u} = D_{b_u}^{\dagger}(x) f(x)$, and $D_b{}^{-1}(x) = \begin{pmatrix} D_{b_u}^{\dagger} \\ D_{b_s}^{\dagger} \end{pmatrix}$. For a given final condition on the state, $s(t_f) = s_f$, the stable component, which is unstable under backward propagation, of the Hamiltonian vector field can be suppressed at $t = t_f$ by choosing $\lambda(t_t) = \lambda_f$ such that $h_{b_s}(s_f, \lambda_f) = 0$; and the stable components will remain suppressed under backward propagation, because w_{b_s} is decoupled from w_{b_u}. In other words, λ_f is chosen such that the Hamiltonian vector field, $f(x)$, lies in the fiber $\mathcal{V}_u(s_f, \lambda_f)$ of the unstable sub-bundle, at the final point on the $s = s_f$ hyper-plane.

4.4 Geometric Structure of the Solution to Hyper-Sensitive Hamiltonian Boundary-Value Problem

In the phase space, the solution trajectories to a hyper–sensitive HBVP lie in a normally hyperbolic slow invariant manifold and its transverse fast-stable and fast-unstable manifolds. Outside the initial and terminal boundary-layers, the solution is well approximated by a trajectory in the slow manifold, called the reduced-order trajectory. The complete solution trajectory begins slightly off the fast-stable manifold of the reduced-order trajectory

and follows it quickly towards the slow manifold. The trajectory then progresses slowly along the reduced-order trajectory. Near the final time, the trajectory quickly follows the fast-unstable manifold of the reduced-order trajectory to the final condition slightly off the fast-unstable manifold. For the fixed boundary conditions on the state, as the final time increases, the initial and terminal boundary-layer segments of the trajectory lie closer and closer to the fast-stable and fast-unstable manifolds of the reduced-order trajectory, respectively. In the degenerate case of a completely hyper-sensitive HBVP the reduced-order trajectory is a saddle-type equilibrium point. The fast-stable and fast-unstable manifolds become n-dimensional stable and unstable manifolds of the saddle point. The stable and unstable eigenspaces of the linearized Hamiltonian system at the saddle point are n-dimensional hyperplanes tangent to the stable and unstable manifolds.

The stable manifold, $\mathcal{M}_s$, is invariant with respect to the Hamiltonian flow, i.e. a trajectory that begins on the stable manifold will remain on the stable manifold as time progresses. An equivalent requirement for invariance is that $f(x) \in T_x\mathcal{M}_s$ for all $x \in \mathcal{M}_s$, which means that the trajectory through x is tangent to $\mathcal{M}_s$ and will thus stay on $\mathcal{M}_s$. For all $x \in \mathcal{M}_s$, $T_x\mathcal{M}_s$ and $\mathcal{V}_s(x)$ are the same subspace of $T_x\mathcal{Y}$. Thus, $f(x) \in \mathcal{V}_s(x)$ for all $x \in \mathcal{M}_s$. Representing $f(x)$ in a dichotomic basis as in Eq. (4.21), points $x \in \mathcal{M}_s$ are identified as those for which the unstable component of the Hamiltonian vector field is zero, i.e., $w_{f_u} = h_{f_u}(s, \lambda) = 0$. This can be viewed as a partial-equilibrium condition, partial in the sense that the vector field f needs only be zero in certain directions. It is clear from the block triangular form of the variational equations in Eq.(4.24) that if the unstable component is zero at some initial point, it will remain zero along the subsequent trajectory.

Similarly, the unstable manifold, $\mathcal{M}_u$, is invariant with respect to the Hamiltonian

flow. Therefore, $f(x) \in T_x\mathcal{M}_u$ and the subspaces $T_x\mathcal{M}_u$ and $\mathcal{V}_u(x)$ of $T_x\mathcal{Y}$ coincide for all $x \in \mathcal{M}_u$. Representing $f(x)$ in a dichotomic basis as $f(x) = D_{b_s}(x)w_{b_s} + D_{b_u}(x)w_{b_u}$, points $x \in \mathcal{M}_u$ are identified as those for which the stable component of the Hamiltonian vector field is zero, i.e., $w_{b_s} = h_{b_s}(s, \lambda) = 0$. It is clear from the block triangular form of the variational equations in Eq. (4.28) that if the stable component is zero at some final point, it will remain zero under backward propagation.

4.5 Solution of Completely Hyper-Sensitive HBVPs and Dichotomic Basis Method

Based on the geometric structure of the phase space around the solution of the hyper-sensitive HBVPs an approximate composite solution can be given for sufficiently large final times as

$$\hat{x} = \begin{cases} x_s(t), & 0 \leq t \leq t_{ibl} \\ x_{eq}(t), & t_{ibl} < t < t_{fbl} \\ x_u(t), & t_{fbl} \leq t \leq t_f \end{cases} \tag{4.30}$$

where x_s is the solution to Eq. (4.4) with the initial condition $x_s(0) = (s_0, \lambda_0)$ and λ_0 is chosen such that $x_s(0) = (s_0, \lambda_0) \in \mathcal{V}_s(x_{eq})$; x_u is the solution to Eq. (4.4) with final condition $x_u(t_f) = (s_f, \lambda_f)$ and λ_f chosen such that $x_u(t_f) = (s_f, \lambda_f) \in \mathcal{V}_u(x_{eq})$; and x_{eq} is the equilibrium solution. The final time is t_f, the duration of the initial boundary-layer is t_{ibl}, and the duration of the final boundary-layer is $t_f - t_{fbl}$.

The composite solution can be continuous by introducing bridging segments. Discontinuities within a specified tolerance can also be allowed at the junctions.

4.5.1 Dichotomic Basis Method

In this section a method based on a given dichotomic basis to compute the initial and terminal boundary-layer segments of the composite solution to the completely hyper-sensitive

HBVPs is explained.

Assume that a dichotomic basis $D_f(x)$, that decomposes the Hamiltonian vector field and the associated linearized vector field as in Eq. (4.24), is given. The stable manifold is composed of phase points for which the unstable component of the vector field is zero. Thus, $\lambda(0) = \lambda_0$ can be determined such that

$$w_{f_u}(0) = h_{f_u}(s_0, \lambda_0) = 0 \tag{4.31}$$

is satisfied for the initial state s_0. The initial boundary-layer solution is then computed by integrating Eq. (4.24) to ensure that the trajectory remains on the stable manifold. The integration is continued until the trajectory is close enough to the equilibrium, such that $\|x(t_{ibl}) - x_{eq}\| \leq \epsilon$ for a specified tolerance ϵ, to connect it to the equilibrium solution.

In order to compute the terminal boundary-layer segment, suppose that another dichotomic basis, $D_b(x)$, that decomposes the Hamiltonian vector field and the associated linearized vector field as in Eq.(4.28), is known. The unstable manifold is composed of phase points for which the stable component of the vector field is zero. Thus, $\lambda(t_f) = \lambda_f$ can be determined such that

$$w_{b_s}(0) = h_{b_s}(s_f, \lambda_f) = 0 \tag{4.32}$$

is satisfied for the final state s_f. The terminal boundary-layer solution is then computed by integrating Eqs.(4.28) to ensure that the trajectory remains on the stable manifold.

4.6 Lyapunov Vectors as Dichotomic Basis Vectors

The linearized Hamiltonian system in Eq. (4.9) has an equal number of expanding and decaying directions. Assuming that there is no zero Lyapunov exponent, there exist n forward and backward Lyapunov exponents smaller than zero, namely $\mu_i^+(x) < 0,\ i =$

$1, ..., n$ and $\mu_i^-(x) < 0,\ i = n+1, ..., 2n$, n forward and backward Lyapunov exponents greater than zero, namely $\mu_i^+(x) > 0,\ i = n+1, ..., 2n$ and $\mu_i^-(x) > 0,\ i = 1, ..., n$, for all $x \in \mathcal{Y}$. The subspaces $\mathcal{V}_s(x)$ and $\mathcal{V}_u(x)$ in Eq.(4.14) can be written in terms of the subspaces $L_i^+(x)$, and $L_i^-(x)$ as

$$\begin{aligned} \mathcal{V}_s(x) &= L_n^+(x) \\ \mathcal{V}_u(x) &= L_{n+1}^-(x). \end{aligned} \tag{4.33}$$

Using this characterization of $\mathcal{V}_s(x)$ and $\mathcal{V}_u(x)$, it can be shown that there exist $C > 0$ and $\mu^{su} > 0$ such that

$$\begin{aligned} v \in \mathcal{V}_s(x) \quad &\Rightarrow \quad \|\Phi(t,x)v\| \leq Ce^{-\mu^{su}t}\|v\|, \qquad t > 0,\ \forall x \in \mathcal{Y} \\ v \in \mathcal{V}_u(x) \quad &\Rightarrow \quad \|\Phi(t,x)v\| \leq Ce^{\mu^{su}t}\|v\|, \qquad t < 0,\ \forall x \in \mathcal{Y}. \end{aligned} \tag{4.34}$$

As a corollary of Theorem (2.2.6), only the Lyapunov vector corresponding to the smallest Lyapunov exponent is invariant under linear flow. It does not preserve the mutual orthogonality between the Lyapunov vectors corresponding to different Lyapunov exponents. Differential equations that govern the propagation of the Lyapunov vectors l_i^+ and l_i^- can be derived by performing a continuous Gram-Schmidt re-orthonormalization starting with the Lyapunov vector corresponding to the smallest exponent, namely l_1^+ and l_n^-, as the Lyapunov vectors are propagated using the linear flow. The differential equations, that can be utilized to propagate any of the Lyapunov vectors from $\phi(0,x)$ to other points, $\phi(t,x)$, along the trajectory and preserve the orthonormality and invariance properties, are [54]

$$\begin{aligned} \dot{l}_i^+(x) = J(x)l_i^+(x) - \quad & (l_i^+(x)^T J(x) l_i^+(x)) l_i^+(x) \\ & - \textstyle\sum_{j=1}^{i-1} (l_i^+(x)^T J(x) l_j^+(x) + l_j^+(x)^T J(x) l_i^+(x)) l_j^+(x) \\ \dot{l}_i^-(x) = J(x)l_i^-(x) - \quad & (l_i^-(x)^T J(x) l_i^-(x)) l_i^-(x) \\ & - \textstyle\sum_{j=i+1}^{2n} (l_i^-(x)^T J(x) l_j^-(x) + l_j^+(x)^T J(x) l_i^-(x)) l_j^-(x) \end{aligned} \tag{4.35}$$

We are now in a position to show that the basis of appropriate L^+ subspaces can be used to construct a dichotomic basis defined in Definition (4.3.2).

Proposition 4.6.1 *Let $D_f \in \mathcal{R}^{2n\times 2n}$ be a matrix whose columns can be partitioned as $D_f(x) = [l_1^+(x)...l_{2n}^+(x)]$, where $l_i^+(x),\ i = 1, ..., 2n$ are the Lyapunov vectors. Then, the columns of D_f form a dichotomic basis as defined in Definition (4.3.2), i.e., D_f satisfies the properties in Definition (4.3.2).*

Proof: As given in Eq.(4.33), $\mathcal{V}_s(x) = L_n^+(x)$. We know that $L_n^+(x)$ is spanned by $l_1^+(x), ..., l_n^+(x)$. Thus $D_{f_s}(x)$ can be chosen as $[l_1^+(x)...l_n^+(x)]$. In this case $D_{f_u}(x) = [l_{n+1}^+(x)...l_{2n}^+(x)]$. Note that the columns of $D_{f_u}(x)$ do not span $\mathcal{V}_u(x)$ and this is not required to get the block-triangular form in Eq.(4.16).

Using the first differential equation for $\dot{l}_i^+(x)$ in Eq.(4.35) $\dot{D}$ can be written as

$$\dot{D}_f(x) = [\dot{l}_1^+(x)\ \ldots\ \dot{l}_{2n}^+(x)] = J(x)D_f(x) - D_f(x)R(x), \tag{4.36}$$

where R is upper-triangular and can be written as

$$R(x) = \begin{cases} l_i^+(x)^T J(x) l_j^+(x) + l_j^+(x)^T J(x) l_i^+(x), & if\ i < j \\ l_i^+(x)^T J(x) l_j^+(x) & ,\ if\ i = j \\ 0 & ,\ if\ i > j \end{cases} \tag{4.37}$$

Substituting $\dot{D}_f$ in Eq.(4.15)

$$\begin{aligned} \dot{w} &= [{D_f}^{-1}(x)J(x)D_f(x) - {D_f}^{-1}(x)\dot{D}_f(x)]w \\ &= [{D_f}^{-1}(x)J(x)D_f(x) - {D_f}^{-1}(x)J(x)D_f(x) + {D_f}^{-1}(x)D_f(x)R(x)]w \\ &= R(x)w, \end{aligned} \tag{4.38}$$

the block-triangular form in Eq.(4.16) is obtained since $R(x)$ is an upper-triangular matrix.

It is known [20] that Lyapunov transformations, T, such that T, T^{-1}, and $\dot{T}$ are bounded, do not change the Lyapunov exponents. All Lyapunov vectors have, by definition, unit length; thus D_f is bounded. If $J(x)$ is bounded then $\dot{D}_f$ is bounded. Since D_f is an orthogonal matrix, ${D_f}^{-1} = {D_f}^T$. Therefore, ${D_f}^{-1}$ is bounded. Since D_f is a Lyapunov transformation, $\dot{v} = Jv$ and $\dot{w} = Rw$ have the same Lyapunov exponents.

The Lyaponuv vector $l_i^+(x)$ is represented by $(0, ..., 0, 1, 0, ..., 0)^T$, where i-th entry is 1, in w-coordinates. So, the Lyapunov exponents of the subsystem, Λ_s, are the smallest n Lyapunov exponents, $\mu_1^+, ..., \mu_n^+$, of the original system and the Lyapunov exponents of the subsystem, Λ_u are the other n Lyapunov exponents, $\mu_{n+1}^+, ..., \mu_{2n}^+$, of the original system. The bounds in the second property of Definition (4.3.2) are obtained by using the first inequality in Eq.(4.34). □

Another dichotomic transformation that is used for computing the terminal boundary can be constructed by using the appropriate backward Lyapunov vectors.

Proposition 4.6.2 *Let $D_b \in \mathcal{R}^{2n\times 2n}$ be a matrix whose columns can be partitioned as $D_b(x) = [l_{2n}^-(x)...l_1^-(x)]$, where $l_i^-(x),\ i = 1, ..., 2n$ are the backward Lyapunov vectors. Then, the columns of D_b form a dichotomic basis as defined in Definition (4.3.2), i.e., D_b satisfies the properties in Definition (4.3.2) with the stable subsystem Λ_s is decoupled from the unstable subsystem Λ_u as in Eq. (4.28).*

The proof of Proposition (4.6.2) is based on the invariance of the subspaces $L_i^-(x),\ i = 1, ..., 2n$ and particularly of the subspace $L_{n+1}^-(x)$ and uses the second equation in Eq.(4.35).

Propositions (4.6.1) and (4.6.2) show that appropriate Lyapunov vectors form sets of dichotomic basis vectors which can be utilized in the dichotomic basis method for solving completely hyper-sensitive HBVPs. No practical method to determine Lyapunov exponents and vectors emerges from the analysis because existing theory considers asymptotic behavior using infinite time limits on an invariant subset of the phase space. On the other hand, most optimal control problems are posed for a finite time interval and on a compact subset that is not necessarily invariant. When the subset is not invariant, the timescales and the associated geometric structure characteristics of the flow on the subset must be computable on finite-time trajectory segments. In the next section, a method for extract-

ing the timescale information and its associated tangent space structure on a compact non-invariant subset is presented.

4.7 Finite Time Lyapunov Vectors as Approximate Dichotomic Basis Vectors

We define the finite averaging time approximations of the stable and unstable subspaces by $\mathcal{V}_s(T,x) = L_n^+(T,x)$ and $\mathcal{V}_u(T,x) = L_{n+1}^-(T,x)$, respectively. The accuracy with which $\mathcal{V}_s(T,x)$ and $\mathcal{V}_u(T,x)$ approximate the stable and unstable subspaces depends on the size of the gap relative to the available averaging time. Due to the volume-preserving feature of the Hamiltonian systems, n of the forward and backward finite time Lyapunov exponents are positive and n of them are negative and they are symmetric around zero. Thus, for completely hyper-sensitive HBVPs bounds denoted by positive real numbers μ^f and μ^b for the forward and backward finite time Lyapunov exponents exist such that

$$\begin{aligned} &For\ each\ x \in \mathcal{X},\ \mu_n^+(T,x) \leq -\mu^f\ and\ \mu^f \leq \mu_{n+1}^+(T,x)\ for\ all\ T \in (T_{min}, \bar{t}(x)] \\ &For\ each\ x \in \mathcal{X},\ \mu_n^-(T,x) \geq \mu^b\ and\ \mu_{n+1}^-(T,x) \leq -\mu^b\ for\ all\ T \in [\underline{t}(x), -T_{min}). \end{aligned} \tag{4.39}$$

Let $\Delta\mu$ be a positive real number such that $\Delta\mu = 2min\{\mu^f, \mu^b\}$. Regardless of how large this gap is, the subspaces $L_n^+(T,x)$ and $L_{n+1}^-(T,x)$ will converge to $L_n^+(x)$ and $L_{n+1}^-(x)$, respectively, as $T \to \infty$. However, we require this gap to be large enough so that the finite time subspaces approximate the infinite time subspaces with sufficient accuracy. In analysis the condition we are looking for is

$$\frac{(\Delta\mu)^{-1}}{T_c - T_{min}} = \frac{(2min\{\mu^f, \mu^b\})^{-1}}{T_c - T_{min}} \ll 1. \tag{4.40}$$

The conditions in Eq. (4.39) are illustrated in Fig. (4.1) for only one averaging time T, but this structure is required for all specified values of T and x.

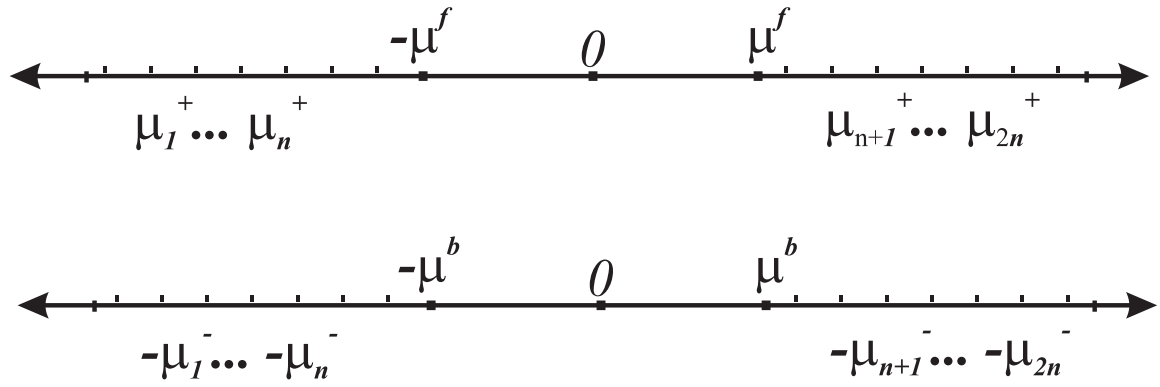

Figure 4.1: Spectra of forward and backward Lyapunov exponents illustrating the spectral gap.

Now, let the $\hat{D}_f(T,x) \in \mathcal{R}^{2n\times 2n}$ be the matrix whose columns are partitioned as

$$\hat{D}_f(T,x) = [l_1^+(T,x) \ ... \ l_{2n}^+(T,x)]. \tag{4.41}$$

Since the columns of $\hat{D}_f(T,x)$ do not form a dichotomic basis $\hat{\Lambda}(x)$, defined as

$$\hat{\Lambda}(x) = \hat{D}_f(T,x)^{-1}J(x)\hat{D}_f(T,x) - \hat{D}_f(T,x)^{-1}\dot{\hat{D}}_f(T,x), \tag{4.42}$$

will not be in block-triangular form. However, when the conditions in Eqs. (4.39) and (4.40) are satisfied, the subspace spanned by the columns $L_n^+(T,x)$ will approach its infinite time limit, the span of the column vectors of $L_n^+(x)$, at the rate of $1/(e^{\Delta\mu T} - e^{-\Delta\mu T})$. Therefore, when the available averaging time is long enough, the finite time Lyapunov vectors can be used to construct a transformation to approximately decouple the stable and unstable modes in $\hat{D}_f(T,x)^{-1}J(x)\hat{D}_f(T,x) - \hat{D}_f(T,x)^{-1}\dot{\hat{D}}_f(T,x)$. There are two differences between $\Lambda(x)$ and $\hat{\Lambda}(x)$:

- $(2,1)$-block of $\hat{\Lambda}(x)$ is not zero, i.e. the stable and unstable modes in $\hat{\Lambda}(x)$ are not decoupled. However, because of the exponentially fast convergence of $L_n^+(T,x)$, the elements of $(2,1)$-block of $\hat{\Lambda}(x)$ decays exponentially.

- Note from Eqs. (4.37) and (4.38) that $\Lambda(x)$ is not only upper block diagonal but also upper triangular. This can be interpreted as follows: The change in w_{i+1} is

independent of w_i for any $i = 1, ..., 2n-1$ where $w = (w_1, ..., w_{2n})^T$. When the approximate dichotomic basis used the change in $\hat{w}_{n+1}, ..., ...\hat{w}_{2n}$ is weakly dependent on $\hat{w}_1, ..., ...\hat{w}_n$ due to the first property. However, the dependence of the change of $\hat{w}_{i+1}$ on $\hat{w}_i$ for $i = 1, ..., n-1$ and the dependence of the change of $\hat{w}_{j+1}$ on $\hat{w}_j$ for $j = n+1, ..., 2n-1$ may not be weak, because only the span of the column vectors of $L_n^+(T, x)$ convergence at the rate $e^{-\Delta\mu T}$. The individual column vectors of $L_n^+(T, x)$ converge at a slower rate, if they do.

A set of linearly independent vectors that approximately decouple the linearized dynamics is called "approximate dichotomic basis" in [5, 4]. We propose to use the finite time Lyapunov vectors as an approximate dichotomic basis. Similarly, the transformation $\hat{D}_b(T, x) = [l_{2n}^-(T, x) \ ... \ l_1^-(T, x)]$ is another approximate dichotomic transformation that brings the original linearized dynamics into an approximately decoupled form in which the dependence of the rate of change of the stable components on the unstable components is weak.

4.8 Approximate Dichotomic Basis Method

In this section, the use of an approximate dichotomic basis is justified and the advantages of using the finite time Lyapunov vectors, instead of the eigenvectors of $J(x)$, as the approximate dichotomic basis are explained.

In order to compute the initial boundary layer of the composite solution to the completely hyper-sensitive HBVP, let $\hat{D}_f(x) = [\hat{D}_{f_s}(x)\hat{D}_{f_u}(x)]$ be an approximate dichotomic basis, constructed from the finite time Lyapunov vectors, on $\mathcal{X}$ where $\hat{D}_{f_s}(x) \in \mathcal{R}^{2n\times n}$ and $\hat{D}_{f_u}(x) \in \mathcal{R}^{2n\times n}$. Furthermore, let $\hat{D}_f^{-1}(x)$ be written in terms of two matrices

$\hat{D}^{\dagger}_{f_s}(x) \in \mathcal{R}^{n\times 2n}$ and $\hat{D}^{\dagger}_{f_u}(x) \in \mathcal{R}^{n\times 2n}$ such that

$$\hat{D}_f^{-1}(x) = \begin{pmatrix} \hat{D}^{\dagger}_{f_s}(x) \\ \hat{D}^{\dagger}_{f_u}(x) \end{pmatrix} \tag{4.43}$$

and let $\hat{w}_f$ represent the co-ordinate vector for the basis $\hat{D}_f$ with n-dimensional components $\hat{w}_{f_s}$ and $\hat{w}_{f_u}$

$$\hat{w}_f = \begin{pmatrix} \hat{w}_{f_s} \\ \hat{w}_{f_u} \end{pmatrix}. \tag{4.44}$$

In terms of $\hat{D}_f(x)$, the differential equations for x and $\hat{w}_f$ are

$$\begin{pmatrix} \dot{x} \\ \dot{\hat{w}}_{f_s} \\ \dot{\hat{w}}_{f_u} \end{pmatrix} = \begin{pmatrix} \hat{D}_{f_s}(x) & \hat{D}_{f_u}(x) \\ \hat{\Lambda}_s(x) & \hat{\Lambda}_{su}(x) \\ \hat{\Lambda}_{us}(x) & \hat{\Lambda}_u(x) \end{pmatrix} \begin{pmatrix} \hat{w}_{f_s} \\ \hat{w}_{f_u} \end{pmatrix}, \tag{4.45}$$

where

$$\hat{\Lambda} = \begin{pmatrix} \hat{\Lambda}_s(s) & \hat{\Lambda}_{su}(x) \\ \hat{\Lambda}_{us}(x) & \hat{\Lambda}_u(x) \end{pmatrix} = \hat{D}_f^{-1} J \hat{D}_f - \hat{D}_f^{-1}\dot{\hat{D}}_f. \tag{4.46}$$

Let $\Gamma_s(t,x)$ and $\Gamma_u(t,x)$ be the transition matrices corresponding to $\hat{\Lambda}_s$ and $\hat{\Lambda}_u$, respectively. Because the columns of $\hat{D}_f(x)$ form only an approximate dichotomic basis, in general, the transition matrices $\Gamma_s(t,x)$ and $\Gamma_u(t,x)$ have both contracting and expanding behavior along trajectory segments in $\mathcal{X}$ and $\hat{\Lambda}_{us}(x) \neq 0$ for $p \in \mathcal{X}$. In terms of the dichotomic and non-dichotomic bases, the vector $f(x)$ can be written as

$$f(x) = D_{f_s}(x) w_s + D_{f_u}(x) w_u = \hat{D}_{f_s}(x)\hat{w}_{f_s} + \hat{D}_{f_u}(x)\hat{w}_{f_u}. \tag{4.47}$$

Suppose we attempt to place the initial point x_0 on the stable manifold by choosing $\lambda(0)$ so that $\hat{w}_{f_u}(0) = 0$. Because the basis is non-dichotomic, the calculated initial point will not be on the stable manifold. The size of the unstable component w_u is a measure of the error. The unstable components of $f(x)$ at the beginning and end of the initial boundary layer are

$$w_u(0) = D^{\dagger}_{f_u}(x_0)\hat{D}_{f_s}(x_0)\hat{w}_{f_s}(0) \tag{4.48}$$

and

$$w_u(t_{ibl}) = \Phi_u(t_{ibl}, x_0) D_{f_u}^{\dagger}(x_0) \hat{D}_{f_s}(x_0) \hat{w}_{f_s}(0) \tag{4.49}$$

In terms of the Lyapunov vectors and finite time Lyapunov vectors $D_{f_s}^{\dagger}(x)$, $D_{f_u}^{\dagger}(x)$, $\hat{D}_{f_s}^{\dagger}(T,x)$, and $\hat{D}_{f_u}^{\dagger}(T,x)$ are written as

$$\begin{aligned} D_{f_s}^{\dagger}(x) &= \begin{pmatrix} l_1^+(x)^T \\ \vdots \\ l_n^+(x)^T \end{pmatrix}, \qquad D_{f_u}^{\dagger}(x) = \begin{pmatrix} l_{n+1}^+(x)^T \\ \vdots \\ l_{2n}^+(x)^T \end{pmatrix} \\ \hat{D}_{f_s}^{\dagger}(T,x) &= \begin{pmatrix} l_1^+(T,x)^T \\ \vdots \\ l_n^+(T,x)^T \end{pmatrix}, \qquad \hat{D}_{f_u}^{\dagger}(T,x) = \begin{pmatrix} l_{n+1}^+(T,x)^T \\ \vdots \\ l_{2n}^+(T,x)^T \end{pmatrix} \end{aligned} \tag{4.50}$$

by the mutual orthogonality of the Lyapunov vectors. Note that $\hat{D}_f(T,x)$ is the approximate dichotomic basis composed of the finite time Lyapunov vectors with an averaging time T.

$D_{f_u}^{\dagger}(x_0)\hat{D}_{f_s}(T,x_0) \in \mathcal{R}^{n\times n}$ and can be written as

$$[D_{f_u}^{\dagger}(x_0)\hat{D}_{f_s}(T,x_0)]_{ij} = l_{i+n}^+(x_0)^T l_j^+(T,x_0). \tag{4.51}$$

Any finite time Lyapunov vector can be written in terms of the infinite time Lyapunov vectors because they form a basis for $\mathcal{R}^{n\times n}$

$$l_j^+(T,x_0) = \sum_{k=1}^{n} c_k l_k^+(x_0). \tag{4.52}$$

By the convergence of the subspaces spanned by the Lyapunov vectors, $|c_k| \leq |a_k|/(e^{\Delta\mu T} - e^{-\Delta\mu T})$, $for\ k = n{+}1, ..., 2n$ where $|a_k| \leq 1$ due to the unit length property of the Lyapunov vectors. Thus, each entry of $D_{f_u}^{\dagger}(x_0)\hat{D}_{f_s}(T,x_0)$ is bounded by $a_{ij}/(e^{\Delta\mu T} - e^{-\Delta\mu T})$ where $|a_{ij}| \leq 1$.

The norm of $w_{f_u}(t_{ibl})$ can be bounded by

$$\|w_{f_u}(t_{ibl})\| \leq \|\Phi_u(t_{ibl}, x_0)\| \|D_{f_u}^{\dagger}(x_0)\hat{D}_{f_s}(T,x_0)\| \|\hat{w}_{f_s}(0)\|, \tag{4.53}$$

where $\|\Gamma_u(t_{ibl}, x_0)\|$ and $\|D_{f_u}^{\dagger}(x_0)\hat{D}_{f_s}(T, x_0)\|$ denote the matrix norms induced by the vector norm. Note that $\|D_{f_u}^{\dagger}(x_0)\hat{D}_{f_s}(T, x_0)\|$ determines the size of w_u and is a measure of how well the basis $\hat{D}_f$ approximates the dichotomic basis D_f at point x_0, because $\|D_{f_u}^{\dagger}(x_0)D_{f_s}(T, x_0)\| = 0$. In general $\|\Gamma_u(t, x_0)\|$ is exponentially increasing with t; thus, the size of t_{ibl} relative to the rate of growth determines how small $\|D_{f_u}^{\dagger}(x_0)\hat{D}_{f_s}(T, x_0)\|$ must be to achieve a prescribed level of accuracy. The key benefit of the composite approximation approach is that error growth, an inherent feature of numerically integrating a Hamiltonian system, is only taking place over the time interval t_{ibl} , which is much smaller than t_f. The factor $\|D_{f_u}^{\dagger}(x_0)\hat{D}_{f_s}(T, x_0)\|$ provides additional attenuation of the growing component of the solution since it is bounded by

$$\|D_{f_u}^{\dagger}(x_0)\hat{D}_{f_s}(T, x_0)\| \leq n|a_{max}|/(e^{\Delta\mu T} - e^{-\Delta\mu T}), \tag{4.54}$$

where $|a_{max}| = \max_{i,j} |a_{ij}| \leq 1$, using the definition of the Frobenius norm,

$$\|D_{f_u}^{\dagger}(x_0)\hat{D}_{f_s}(T, x_0)\|_F \leq n|a_{max}|/(e^{\Delta\mu T} - e^{-\Delta\mu T}), \tag{4.55}$$

and the relation $\|A\| \leq \|A\|_F$ for any matrix A [55].

Another way to attenuate the error growth is re-initialization of the propagation along the trajectory. Let $[0, t_{ibl}]$ be subdivided into intervals $[t_{k-1}, t_k]$, $k = 1, ..., r$, where $t_0 = 0$ and $t_r = t_{ibl}$. By using $\hat{D}_{f_u}^{\dagger}(T, x(t_{k-1}))f(x(t_{k-1})) = \hat{w}_{f_u}(t_{k-1}) = 0$, $k = 1, ..., r$, the new co-state corresponding to the current state can be found. This changes the costate such that $(x(t_{k-1}, \lambda(t_{k-1}))$ is closer to the stable manifold. The trajectory may be discontinuous in λ. Re-initialization of the propagation requires re-calculation of the Lyapunov vectors and solving the algebraic equation $\hat{D}_{f_u}^{\dagger}(T, x(t_{k-1}))f(x(t_{k-1})) = \hat{w}_{f_u}(t_{k-1}) = 0$. However, it decreases the error accumulation and increases the accuracy of the method. Note that by estimating $\|\Phi_u(t_k - t_{k-1}, x(t_{k-1}))\|$ by the maximum singular value of $\Phi(t_k - t_{k-1}, x(t_{k-1}))$,

$\overline{\sigma}$, $e^{(\overline{\sigma}-\Delta\mu)(t_k-t_{k-1})} \leq \epsilon$ can be used as a measure of the accuracy level for some desired ϵ.

An analogous procedure can be used to compute the terminal boundary layer by backward integrating from the final conditions and using the approximate dichotomic transformation $\hat{D}_b(x) = [l_{2n}^-(T,x)\ ...l_1^-(T,x)]$, which can be decomposed as $\hat{D}_b(x) = [\hat{D}_{b_u}(x)\hat{D}_{b_s}(x)]$, where $\hat{D}_{b_u} = [l_{2n}^-(T,x)\ ...l_{n+1}^-(T,x)]$ and $\hat{D}_{b_s} = [l_n^-(T,x)\ ...l_1^-(T,x)]$. In backward propagation $\hat{w}_{b_s}$ is unstable. It is suppressed by choosing $\lambda(t_f)$ so that $\hat{w}_{b_s}(t_f) = 0$. Since the basis is approximately dichotomic, the computed final point will not be on the unstable manifold. The size of the stable component $\hat{w}_{b_s}$ is a measure of the error growth under backward propagation. When calculating the terminal boundary layer, the method aims to control the magnitude of $\hat{w}_{b_s}$.

4.9 Iterative Procedure for Increasing the Accuracy of the Approximate Dichotomic Basis Method

Rao and Mease [4, 5] developed an iterative procedure which starts with an approximate dichotomic basis and determines the initial boundary-layer segment, x_s, of the composite solution by forward integrating

$$\begin{pmatrix} \dot{x} \\ \dot{\hat{w}}_{f_s} \end{pmatrix} = \begin{pmatrix} \hat{D}_{f_s}(x) & \hat{D}_{f_u}(x) \\ \Lambda_s & \Lambda_{su} \end{pmatrix} \begin{pmatrix} \hat{w}_{f_s} \\ \hat{w}_{f_u} \end{pmatrix} \tag{4.56}$$

using $\hat{w}_{f_u}(\cdot)$ as input and by backward integrating

$$\begin{pmatrix} \dot{x} \\ \dot{\hat{w}}_{f_u} \end{pmatrix} = \begin{pmatrix} \hat{D}_{f_s}(x) & \hat{D}_{f_u}(x) \\ \Lambda_{us} & \Lambda_u \end{pmatrix} \begin{pmatrix} \hat{w}_{f_s} \\ \hat{w}_{f_u} \end{pmatrix} \tag{4.57}$$

using $\hat{w}_{f_s}(\cdot)$ as the input. However, since neither $\hat{w}_{f_s}$ nor $\hat{w}_{f_u}$ along x_s is known a priori, this procedure is repeated until the solution converges within a specified tolerance. The local eigenvectors of $J(x)$ are used to construct the approximate dichotomic basis. Since the local eigenvectors of $J(x)$ do not provide the correct stable and unstable directions, they

used the iterative procedure inspired by the Computational Singular Perturbations (CSP) Method [10] which starts with the local eigenvectors of $J(x)$ and uses successive corrections to the eigenvectors to get the stable and unstable directions. The alternative basis vectors, the finite time Lyapunov vectors, proposed in this paper are better approximations of the correct stable and unstable directions. [11, 12] Our experience shows that the boundary-layers x_s and x_u can be determined without using the iterative procedure developed by Rao and Mease, when the finite time Lyapunov vectors are used and the conditions in Eqs. (4.39) and (4.40) are satisfied.

4.10 Example: Nonlinear Spring-Mass System

In this section, we will illustrate the approximate dichotomic basis method on an optimal control problem and compare the results with the exact solution obtained by using a multi-purpose optimization software "GESOP" [56]. The system considered is a nonlinear spring-mass system whose schematic is shown in Fig. (4.2). The displacement x of the

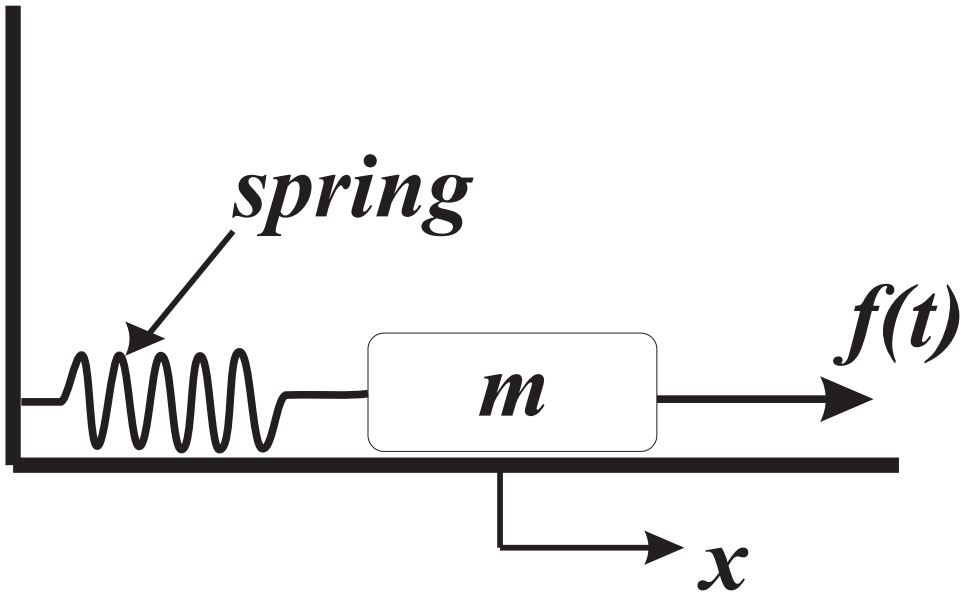

Figure 4.2: Schematic of the nonlinear spring-mass system.

mass is measured from the rest position of the spring, $x = 0$. The spring force is a nonlinear

function of x

$$f_s(x) = -k_1 x - k_2 x^3. \tag{4.58}$$

The control that acts on the mass is an external force and is denoted by $f(t)$. The equation of motion of the mass is

$$m\ddot{x} - f_s(x) = f(t). \tag{4.59}$$

By using the state variables $x_1 = x$ and $x_2 = \dot{x}$, Eq. (4.59) can be written as

$$\begin{bmatrix} \dot{x}_1 \\ \dot{x}_2 \end{bmatrix} = \begin{bmatrix} x_2 \\ -\frac{k_1 x_1 + k_2 x_1^3}{m} + u \end{bmatrix} \tag{4.60}$$

where $u = f(t)/m$.

Optimal Control Problem: The optimal control problem is to minimize the cost functional

$$J = \frac{1}{2} \int_0^{t_f} \left(q_1 x_1^2 + q_2 x_2^2 + r u^2 \right) dt, \tag{4.61}$$

where q_1, q_2, and q_3 are positive constants, subject to the dynamic constraint in Eq. (4.59) and the boundary constraints

$$\begin{array}{ll} x_1(0) = x_{1i}, & x_1(t_f) = x_{1f}, \\ x_2(0) = x_{2i}, & x_2(t_f) = x_{2f}. \end{array} \tag{4.62}$$

This optimal control problem is the same one used in [4]. We use the same parameters in order to be able to compare two methods. Therefore, $k_1 = 1$, $k_2 = 1$, $m = 1$, $q_1 = 1$, $q_2 = 1$, $r = 1$, $t_f = 40$, $x_{1i} = 1$, $x_{2i} = 0$, $x_{1f} = 0.75$, and $x_{2f} = 0$.

Hamiltonian Boundary Value Problem: The Hamiltonian can be written as

$$\mathcal{H} = \frac{1}{2} \left(x_1^2 + x_2^2 + u^2 \right) + \lambda_1 x_2 + \lambda_2 \left(-x_1 - x_1^3 + u \right). \tag{4.63}$$

Since $\frac{\partial \mathcal{H}}{\partial u} = 0$ for the optimal control, $u^* = -\lambda_2$. Substituting this optimal control in Eq. (4.63), the first order necessary conditions for optimality are obtained

$$\begin{array}{l} \dot{x}_1 = x_2, \\ \dot{x}_2 - x_1 - x_1^3 - \lambda_2, \\ \dot{\lambda}_1 = -x_1 + \lambda_2 (1 + 3x_1^2), \\ \dot{\lambda}_2 = -x_2 - \lambda_1 \end{array} \tag{4.64}$$

with the boundary constraints

$$\begin{array}{ll} x_1(0) = x_{1i} = 1, & x_1(t_f) = x_{1f} = 0.75, \\ x_2(0) = x_{2i} = 0, & x_2(t_f) = x_{0f} = 0. \end{array} \tag{4.65}$$

Eqs. (4.64) and (4.65) constitute a two-point boundary value problem.

Composite Solution to the HBVP: For this problem the duration of the initial and terminal boundary layers are chosen as 15. Note that the dynamics in Eq. (4.64) have an equilibrium point at $(x_1, x_2, \lambda_1, \lambda_2) = (0, 0, 0, 0)$. Thus, the solution of the optimal control problem can be constructed as

$$x = \begin{cases} x_s(t), & 0 \leq t \leq 15 \\ x_{eq}(t), & 15 < t < 25 \\ x_u(t), & 25 \leq t \leq 40 \end{cases} . \tag{4.66}$$

Analysis of Lyapunov Exponents and Vectors: The compact region $\mathcal{X}$ can be chosen as an hyper-cube around the origin of the 4-dimensional phase space such that it includes the initial and final points, is large enough so that it provides long enough averaging times, and is not too large so that the behavior in $\mathcal{X}$ is uniform. After computing the Lyapunov exponents at points around the origin of the phase space it is concluded that $\mathcal{X} = \{(x_1, x_2, \lambda_1, \lambda_2) \in \mathcal{R}^4 \ : \ x_1 \in [-100, 100], \ x_2 \in [-100, 100], \ \lambda_1 \in [-100, 100], \ \lambda_2 \in [-100, 100]\}$ satisfies these requirements. The finite time Lyapunov exponents are calculated at several points in $\mathcal{X}$ for various averaging times. The finite time Lyapunov exponents vs. the averaging time plot shown in Fig. (4.3) are obtained by calculating the exponents at $(x_1, x_2, \lambda_1, \lambda_2) = (1, 0, 2, 0)$; and they are representative of the exponents at other points.

In this case T_{min} can be chosen as zero. There is a spectral gap around 1.5 between $\mu_2^+(T, x)$ and $\mu_3^+(T, x)$ (and between $\mu_2^-(T, x)$ and $\mu_3^-(T, x)$). At the same point the absolute values of the components of the finite time Lyapunov vectors are shown versus the averaging time in Fig. (4.4). As seen in Fig. (4.4) the components of the finite time

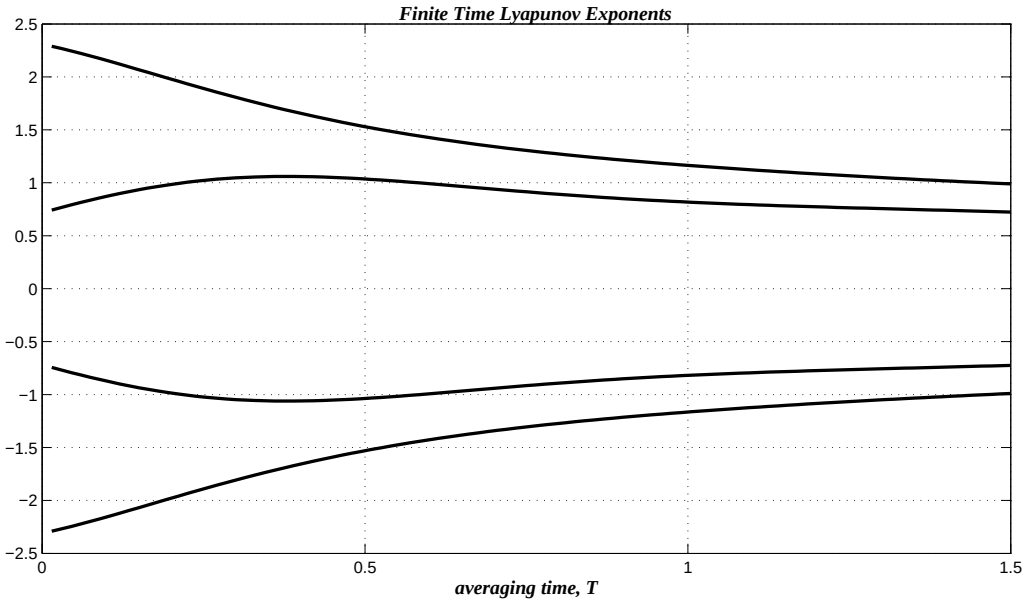

Figure 4.3: Finite time Lyapunov exponents vs. averaging time at $x = (1, 0, 2, 0)$.

Lyapunov vectors do not converge within the averaging time $T = 1.5$. Thus, the individual finite time Lyapunov vectors do not converge. However, in order to be able to apply the methodology developed in the previous section, only the convergence of the subspaces $L_2^+(T, x)$ and $L_2^-(T, x)$ is required. This is tested by solving the optimization problems

$$J_+^i(T)^* = \min_{a_{i1}^+,\ a_{i2}^+} \|l_i^+(T, x) - a_{i1}^+ l_1^+(T + \Delta T, x) - a_{i2}^+ l_2^+(T + \Delta T, x)\|,\ i = 1,\ 2 \qquad (4.67)$$

and

$$J_-^i(T)^* = \min_{a_{i1}^-,\ a_{i2}^-} \|l_i^-(T, x) - a_{i1}^- l_1^-(T + \Delta T, x) - a_{i2}^- l_2^-(T + \Delta T, x)\|,\ i = 1,\ 2, \qquad (4.68)$$

where ΔT is a pre-specified value and it is chosen as a small fraction of the averaging time. $J_+^i(T)^*$ and $J_-^i(T)^*$ should decrease toward zero with increasing T if the subspaces $L_2^+(T, x)$ and $L_2^-(T, x)$ converge. For the forward time vectors, the value of $J_+^i(T)^*$ versus the averaging time are shown in Fig. (4.5) for $i = 1,\ 2$. Fig. (4.5) indicates that the finite time subspace $L_2^+(T, x)$ converges, although the individual finite time vectors, $l_1^+(T, x)$ and $l_2^+(T, x)$ in $L_2^+(T, x)$, do not from Fig. (4.4). This optimization problem is solved for other

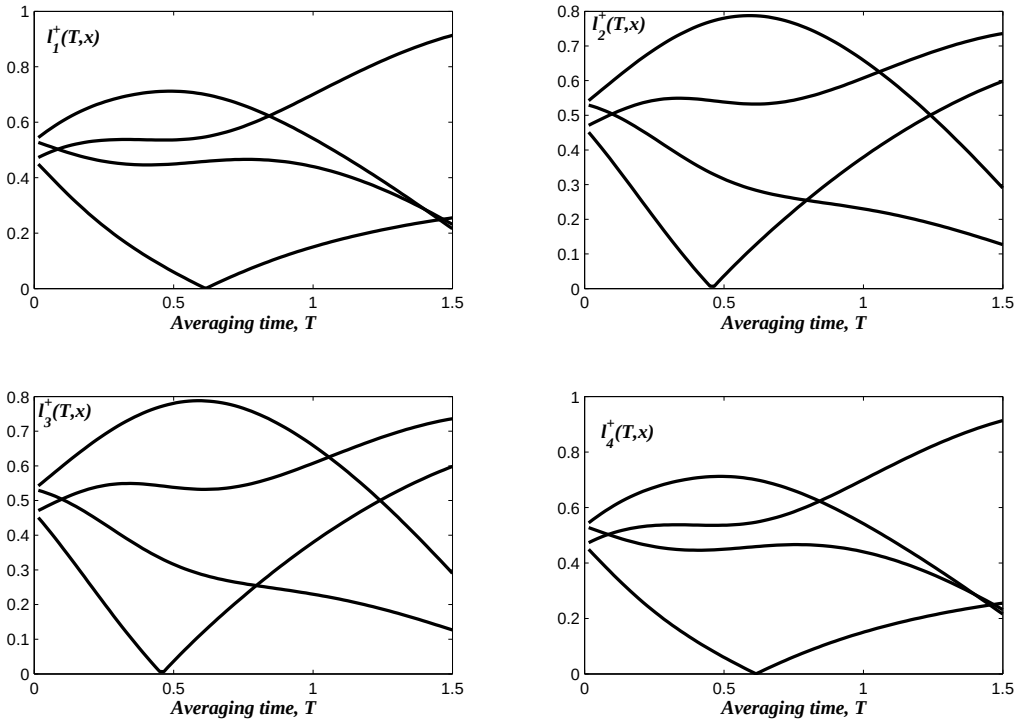

Figure 4.4: The absolute values of the components of the finite time Lyapunov vectors vs. averaging time at $x = (1, 0, 2, 0)$.

points in the region $\mathcal{X}$, and similar behavior is observed. Similar results are obtained for the backward time vectors.

Solution to the Optimal Control Problem: The initial boundary layer segment of the solution is computed by using the forward finite time Lyapunov vectors with an averaging time $T = 1.5$. The procedure is re-initialized every 0.2 units of time. The solution is shown in Fig. (4.6) along with the exact solution. (By the "exact solution", we mean the solution obtained by using the multi-purpose optimization software "GESOP" [56].) Note that the approximate dichotomic basis method is able to reproduce the optimal solution. The length of the initial boundary layer segment is chosen such that $\|x(t_{ibl}) - x_{eq}\|$ is less than a pre-specified matching tolerance. In our solution, the matching tolerance is 10^{-5} and is achieved with the specified re-initialization and averaging parameters. When solved

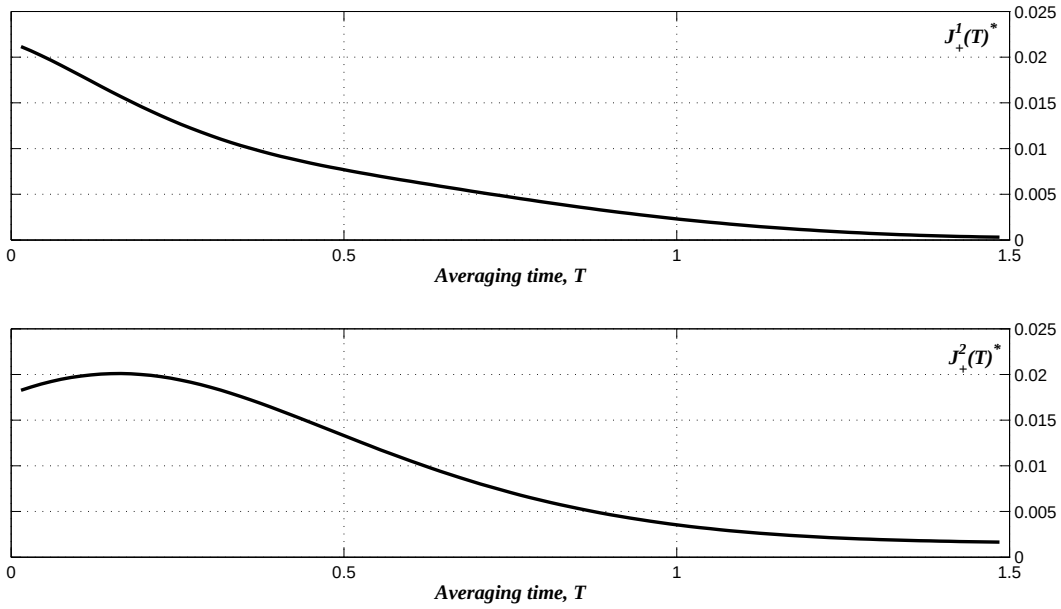

Figure 4.5: $J^1_+(T)^*$ and $J^1_+(T)^*$ vs. averaging time at $x = (1, 0, 2, 0)$.

with the iterative method developed by Rao and Mease, which utilizes the eigenvectors of the Jacobian matrix, the solution is obtained after 10 iterations with a matching tolerance 10^{-4} [4]. Note that the method with the finite time Lyapunov vectors as the approximate dichotomic basis achieved a smaller tolerance without iteration.

Similarly, the terminal boundary layer segment of the solution is computed by using the backward finite time Lyapunov vectors with an averaging time $T = 1.5$. The procedure is re-initialized every 0.2 units of time. The solution is shown in Fig. (4.7) with the exact solution.

The complete solution is obtained by adding the equilibrium segment between $t = 15$ and $t = 25$ and is shown in Fig. (4.8) along with the exact solution. The exact solution and the dichotomic basis method solution is visually indistinguishable.

With a smaller number of re-initializations, the matching of the boundary layers and the equilibrium segment within the prescribed tolerances is still achieved. In those cases there was a 5% mismatch between the peak value of the exact solution and that of the

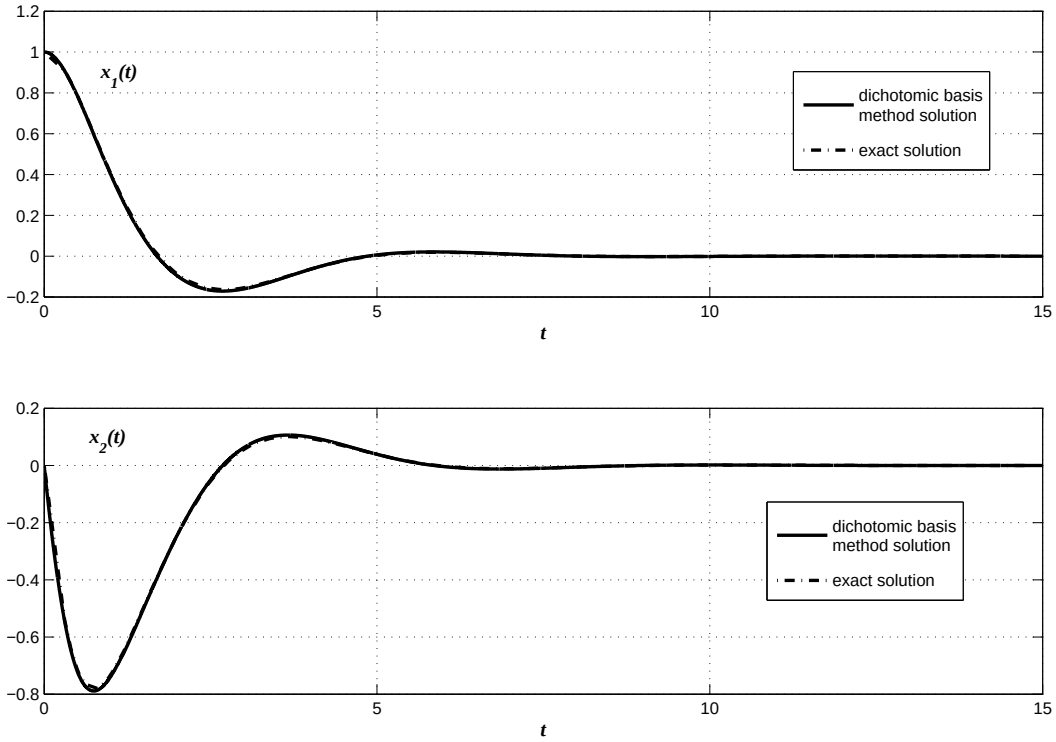

Figure 4.6: The initial boundary layer segment of the solution of the nonlinear spring-mass system optimal control problem.

dichotomic basis method solution, although the rest of the solution was on top of each other. This shows that the hyper-sensitivity of the system can be removed with a smaller number of re-initialization when sub-optimal solutions are acceptable.

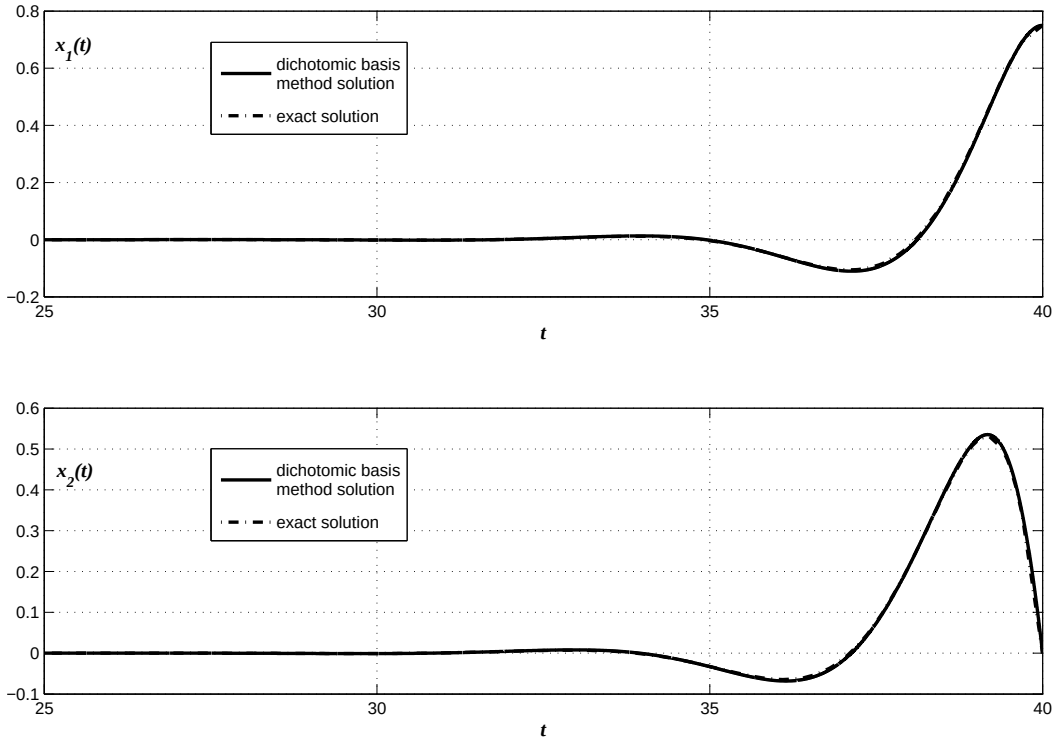

Figure 4.7: The terminal boundary layer segment of the solution of the nonlinear spring-mass system optimal control problem.

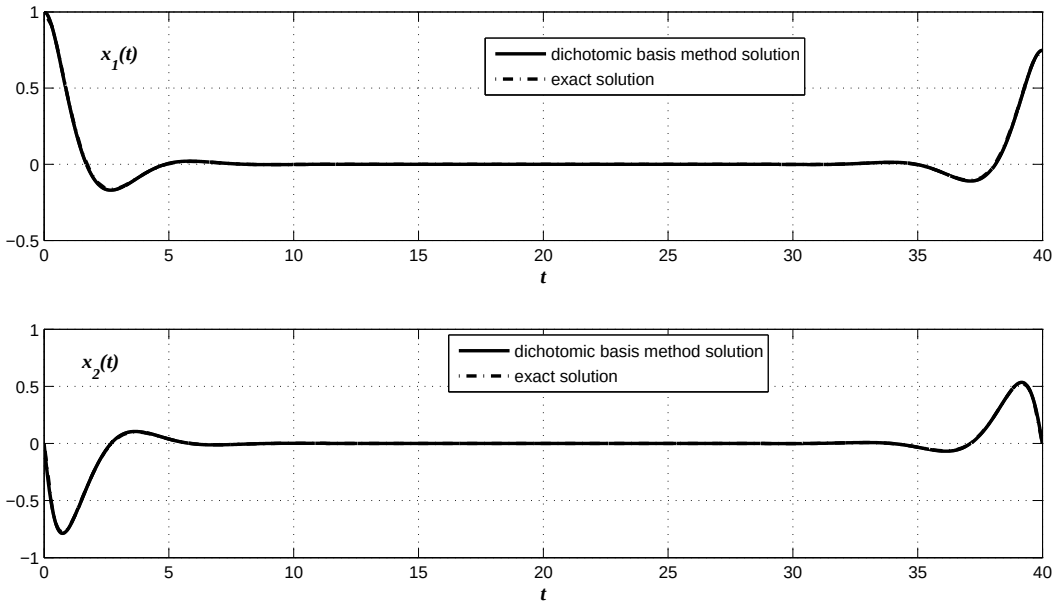

Figure 4.8: The composite solution of the nonlinear spring-mass system optimal control problem.

Chapter 5

Conclusion and Future Work

5.1 Conclusion

The purpose of this work was to identify the timescale structure of a general nonlinear system and the associated geometric structure. The main contribution of this thesis is the development of practical tools for understanding the timescale structure in the associated tangent space. The tools are finite time Lyapunov exponents and vectors. In the literature, the classical Lyapunov exponents and vectors, that are infinite time limits of the finite time exponents and vectors in certain cases, have found extensive use in the study of dynamical systems. However, we can only use the finite time versions in practical problems, because only require finite averaging times are possible. The key property of the finite time Lyapunov vectors is their exponentially fast convergence to the infinite time limits. Thus, they provide good approximations of their infinite time limits, when there exists a long enough averaging time relative to the spectral gap.

The motivation for this research was clarified by two simple examples in the first chapter: the geometric structure of a nonlinear system near an equilibrium point and an invariant manifold.

The second chapter introduced both the classical and finite time Lyapunov exponents and vectors. The timescale decomposition in the tangent space was developed based on

the subspaces determined by the appropriate Lyapunov vectors. The relations between finite time timescale information and its infinite time limit have been explained. The invariance of the distributions in terms of the infinite time Lyapunov vectors play a central role in proving a certain hypothesis in which the infinite time vectors were used. A weaker invariance property, that we call "practical invariance", was established for finite time Lyapunov vectors and for the appropriate distributions in terms of the finite time vectors. Some aspects about the computation of the Lyapunov exponents and vectors were mentioned.

The third chapter was devoted to the two-timescale nonlinear dynamical systems and the computation of the slow manifold in such systems, if the slow manifold exists. The existing methods for computing the slow manifold were studied in order to compare the advantages of the existing methods and the new method that is based on the finite time Lyapunov vectors. The development of the procedure for diagnosing a possibly existing two-timescale behavior was followed by the proposition of a new invariance based technique for computing the slow manifold. The method was compared with the already existing invariance based method that uses the eigenvectors of the Jacobian. The new method gave very promising results compared to an eigenvector-based method.

The fourth chapter dealt with the geometric structure in the state-costate space for a completely hyper-sensitive boundary value problem, that is induced by the first order necessary conditions for optimality in a boundary-layer type optimal control problem. The classical Lyapunov vectors were shown to be capable of identifying the geometric structure in the tangent space. The finite time Lyapunov vectors were proposed for identifying this structure approximately. Another invariance based method for locating the stable and unstable manifolds of the equilibrium point was developed.

5.2 Future Work

The difficulty in the computation of the Lyapunov exponents and vectors makes the application of the methods based on them challenging at this time. It is important to develop more effective methods for computing the Lyapunov exponents and vectors.

The method for solving the boundary-layer type optimal control problems was developed for completely hyper-sensitive boundary value problems. Extending the method to partially hyper-sensitive boundary value problems will broaden the applicability of the method.

Finally, although a step toward model reduction in the general nonlinear systems has been taken by understanding the timescale structure and computing the slow manifold, these tools do not lead to a general model reduction process at the time being, unless they are available analytically. The long term goal is to develop tools that enable model reduction based on the timescale structure.

Bibliography

[1] T.J. Kaper. An introduction to geometric methods and dynamical systems theory for singular perturbation problems. *Proceedings of Symposia in Applied Mathematics*, 56:85–131, 1999.

[2] R.E. O'Malley. *Singular Perturbation Methods for Ordinary Differential Equations.* Applied Mathematical Sciences 89. Springer- Verlag, New York, 1989.

[3] A.E. Bryson and Y.-C. Ho. *Applied Optimal Control : Optimization, Estimation, and Control.* Hemisphere Pub. Corp., Washington, 1975.

[4] A.V. Rao and K.D. Mease. Dichotomic basis approach to solving hyper-sensitive optimal control problems. *Automatica*, 35:633–642, 1999.

[5] A.V. Rao and K.D. Mease. Eigenvector approximate dichotomic basis method for solving hyper-sensitive optimal control problems. *Optimal Control Applications and Methods*, 21:1–19, 2000.

[6] C. Robinson. *Dynamical Systems: Stability, Symbolic Dynamics, and Chaos.* CRC Press, Boca Raton, 1994.

[7] J. Guckenheimer and P. Holmes. *Nonlinear Oscillations, Dynamical Systems, and Bifurcations of Vector Fields.* Applied Mathematical Sciences 42. Springer- Verlag, New York, 1983.

[8] S. Bharadwaj. *Geometric structure of multiple time-scale nonlinear dynamical systems.* PhD thesis, University of California, Irvine, 1999.

[9] M. Hirsch, C. Pugh, and M. Shub. *Invariant Manifolds.* Lecture Notes in Mathematics. Springer- Verlag, Heidelberg, 1977.

[10] S.H. Lam. Singular perturbation for stiff equations using numerical computations. *Lectures in Applied Mathematics*, 24:3–19, 1986.

[11] K.D. Mease, S. Bharadwaj, and S. Iravanchy. Timescale analysis for nonlinear dynamical systems. *Journal of Guidance, Control and Dynamics*, 26(2):318–330, 2003.

[12] K.D. Mease and U. Topcu. Two-timescale nonlinear dynamics: diagnosis and slow manifold determination. Under review.

[13] A. Isidori. *Nonlinear Control Systems.* Springer-Verlag, London, 3rd edition, 1995.

[14] A.M. Lyapunov. The general problem of stability of motion. *International Journal of Control*, 55(3):531–773, 1992.

[15] J.A. Vastano and R.D. Moser. Short-time lyapunov exponent analysis and the transition to chaos in Taylor-Couette flow. *Journal of Fluid Mechanics*, 233:83–118, 1991.

[16] R.M. Samelson. Lyapunov, Floquet, and singular vectors for baroclinic waves. *Nonlinear Processes in Geophysics*, 8:439–448, 2001.

[17] A. Trevisan and R. Legnani. Transient error growth and local predictability: a study in the Lorenz system. *Tellus*, 47A:103–117, 1995.

[18] W.E. Wiesel. Optimal pole placement in time-dependent linear systems. *Journal of Guidance, Control, and Dynamics*, 18(5):995–999, 1994.

[19] L. Barreira and Y.B. Pesin. *Lyapunov Exponents and Smooth Ergodic Theory*. University Lecture Series Vol.23. American Mathematical Society, Providence, Rhode Island, 2001.

[20] W. Hahn. *Stability of Motion*. Springer-Verlag, New York, 1967.

[21] A. Katok and B. Hasselblatt. *Introduction to the Modern Theory of Dynamical Systems*. Cambridge University Press, New York, 1995.

[22] S. Bharadwaj and K.D. Mease. A new invariance property of lyapunov characteristic directions. *Proceedings of the American Control Conference*, 6:3800–3804, 1999.

[23] U.M. Ascher, R.M.M. Mattheij, and R.D. Russell. *Numerical Solution of Boundary Value Problems for Ordinary Differential Equations*. SIAM, Philadelphia, 1995.

[24] R.A. Horn and C.R. Johnson. *Matrix Analysis*. Cambridge University Press, New York, 1985.

[25] I. Goldhirsch, P.L. Sulem, and S.A. Orszag. Stability and Lyapunov stability of dynamical systems: a differential approach and a numerical method. *Physica D*, 27:311–337, 1987.

[26] S. Iravanchy. *Computational methods for time-scale analysis of nonlinear dynamical systems*. PhD thesis, University of California, Irvine, 2003.

[27] K. Geist, U. Parlitz, and W. Lauterborn. Comparison of different methods for computing Lyapunov exponents. *Progress of Theoretical Physics*, 83(5):875–893, 1990.

[28] L. Dieci, R.D. Russell, and E.S. Van Vleck. On the computation of Lyapunov exponents for continuous dynamical systems. *SIAM Journal on Numerical Analysis*, 34(1):402–423, 1997.

[29] J. M. Greene and J.S. Kim. The calculation of Lyapunov spectra. *Physica D*, 24:213–225, 1987.

[30] E.J. McDonald and D.J. Higham. Error analysis of QR algorithms for computing Lyapunov exponents. *Electronic Transactions on Numerical Analysis*, 12:234–251, 2001.

[31] F. Christiansen and H.H. Rugh. Computing Lyapunov spectra with continuous Gram-Schmidt orthonormalization. *Nonlinearity*, 10:1063–1072, 1997.

[32] J.-L. Thiffeault. Derivatives and constraints in chaotic flow: asymptotic behaviour and a numerical method. *Physica D*, 172:139–161, 2002.

[33] N. Fenichel. Geometric singular perturbation theory for ordinary differential equations. *Journal of Differential Equations*, 31:53–98, 1979.

[34] P.V. Kokotovic, H.K. Khalil, and J. O'Reilly. *Singular Perturbation Methods in Control: Analysis and Design*. Academic Press, New York, 1986.

[35] D.S. Naidu and A.J. Calise. Singular perturbations and timescales in guidance and control of aerospace systems: A survey. *Journal of Guidance, Control and Dynamics*, 24(6):1057–1078, 2001.

[36] A.E. Bryson, M.N. Desai, and W.C. Hoffman. Energy-state approximation in performance optimization of supersonic aircraf. *Journal of Aircraft*, 6:481–488, 1969.

[37] H.J. Kelley, E.M. Cliff, and A.R. Weston. Energy state revisited. *Optimal Control Applications and Methods*, 7:175–200, 1986.

[38] H.J. Kelley. Aircraft maneuver optimization by reduced-order approximation. In C.T. Leondes, editor, *Control and Dynamic Systems*, pages 131–178. 1973.

[39] K.D. Mease. Multiple time-scales in nonlinear flight mechanics: Diagnosis and modeling. *Applied Mathematics and Computation*, 164:627–648, 2005.

[40] S.J. Fraser. The steady state and equilibrium approximations: A geometric picture. *Journal of Chemical Physics*, 88:4732–4738, 1988.

[41] M.R. Roussel and S.J. Fraser. Geometry of the steady-state approximation: perturbation and accelerated convergence methods. *Journal of Chemical Physics*, 93:1072–1081, 1990.

[42] U. Maas and S.B. Pope. Simplifying chemical kinetics: Intrinsic low-dimensional manifolds in composition space. *Combustion and Flame*, 88(3):239–264, 1992.

[43] H. G. Kaper and T. J. Kaper. Asymptotic analysis of two reduction methods for systems of chemical reactions. *Physica D*, 165:66–93, 2002.

[44] S.H. Lam and D.A. Goussis. The CSP method for simplifying kinetics. *International Journal of Chemical Kinetics*, 26:461–486, 1994.

[45] K.D. Mease. Geometry of computational singular perturbations. In A.J. Krener and D.Q. Mayne, editors, *Nonlinear Control System Design*, pages 855–861. Pergamon, Oxford, UK, 1996.

[46] A. Zagaris, H.G. Kaper, and T.J. Kaper. Analysis of the computational singular perturbation reduction method for chemical kinetics. *Journal of Nonlinear Science*, 14:59–91, 2004.

[47] D.A. Goussis, M. Valorina, F. Creta, and H.N. Najm. Inertial manifolds with CSP. In K.J. Bathe, editor, *Computational Fluid and Solid Mechanics*, pages 1–4. Elsevier Science, New York, 2003.

[48] M. J. Davis and R. T. Skodje. Geometric investigation of low-dimensional manifolds in systems approaching equilibrium. *Journal of Chemical Physics*, 111(3):859–874, 1999.

[49] H.K. Khalil. *Nonlinear Systems*. Prentice Hall, Upper Saddle River, N.J., 3rd edition, 2002.

[50] M. Valorani, D.A. Goussis, F. Creta, and H.N. Najm. Higher order corrections in the approximation of low dimensional manifolds and the construction of simplified problems with the CSP method. In print, 2004.

[51] J.H. Chow. A class of singularly perturbed nonlinear, fixed endpoint control problems. *Journal of Optimization Theory and Applications*, 29:231–251, 1979.

[52] R.J. Sacker and G.R. Sell. The spectrum of an invariant submanifold. *Journal of Differential Equations*, 38:135–160, 1980.

[53] V.I. Arnol'd. *Ordinary Differential Equations*. Springer-Verlag, Berlin, 1992.

[54] W.E. Wiesel. Continuous time algorithm for Lyapunov exponents I. *Physical Review E*, 47(5):3686–3691, 1993.

[55] H.G. Golub and C.F. Van Loan. *Matrix Computations*. The Johns Hopkins University Press, Baltimore, 3rd edition, 1996.

[56] Institute of Flight Mechanics and Control, University of Stuttgart, Stuttgart. *GESOP Software User Manual*, 2004.

[57] R. Eichhorn, S.J. Linz, and P. Hanggi. Transformation invariance of Lyapunov exponents. *Chaos, Solitons, and Fractals*, 12:1377–1383, 2001.

[58] W.E. Wiesel. Modal feedback control on chaotic trajectories. *Physical Review E*, 49(3):1990–1996, 1994.

Appendix A

Lyapunov Exponents and Constant Coordinate Transformations

It is well known that the infinite time Lyapunov exponents are invariant under coordinate and metric transformations [11, 57]. When the norm of the transformation is bounded above, the shift in the finite time Lyapunov exponent due to the transformation is bounded. In case the Lyapunov exponents converge with increasing averaging time, this shift decays with the averaging time as the averaging time tends to infinity.

Here, we develop the relation between the finite time Lyapunov exponents of two systems that are related with a constant coordinate transformation. These relations may be useful when the solution of a problem is obtained for scaled coordinate variables. In this case the transformation will be a diagonal matrix.

Let x and y be two coordinates related by a constant transformation $y = Tx$. Let the dynamics in x-coordinates be given by $\dot{x} = f(x)$. The linearized dynamics can be written as $\delta\dot{x} = \frac{\partial f}{\partial x}\delta x$. If the integration is initiated with $\Phi_x(0, x) = I$, the linearized dynamics give $\delta x = \Phi_x(t, x)\delta x_0$. In y-coordinates the nonlinear dynamics is found as $\dot{y} = Tf(x)$. The linearized dynamics are then $\delta\dot{y} = T\frac{\partial f}{\partial x}T^{-1}\delta y$.

The Lyapunov exponent in x-coordinates is defined as $\mu_x(t, x, v) = \frac{1}{t}ln\,\|\Phi_x(t, x)v\|$ where v is a unit vector without the loss of generality. Then, the Lyapunov exponent in

y-coordinates can be defined as $\mu_y(t,y,w) = \frac{1}{t} ln \frac{\|\Phi_y(t,x)w\|}{\|w\|}$ where $y = Tx$. The subscript of Φ denotes the coordinate frame in which it is defined. In order to find a relation between Lyapunov exponents in two coordinate frames let's write the difference between them

$$\mu_x(t,x,v) - \mu_y(t,y,w) = \frac{1}{t} ln \frac{\|\Phi_x(t,x)v\| \, \|w\|}{\|\Phi_y(t,y)w\|}. \tag{A.1}$$

In order to put this equation in a more useful form we need a relation between $\Phi_x(t,x)$ and $\Phi_y(t,y)$. By the linearized dynamics in x-coordinates $\delta x = \Phi_x(t,x)\delta x_0$. The same can be done in y-coordinates to yield to $\delta y = \Phi_y(t,y)\delta y_0$. Using the transformation $y = Tx$ and correspondingly $\delta y = T\delta y$ we can write $\delta x = T^{-1}\Phi_y(t,y)T\delta x_0$. By comparing last two equations for δx we can write $\Phi_y(t,y) = T\Phi_x(t,x)T^{-1}$. If we put this in Eq. (A.1) and use the relation $w = Tv$, we can write

$$\mu_x(t,x,v) - \mu_y(t,y,w) = \frac{1}{t} ln \frac{\|\Phi_x(t,x)v\| \, \|Tv\|}{\|T\Phi_x(t,x)v\|}. \tag{A.2}$$

Note that this expression requires information in x-coordinates and the transformation matrix. Thus, it can be used for computing the finite time Lyapunov exponents in y-coordinates.

Appendix B

The transients in μ vs. T plots

We have investigated what happens in the systems during the period of time that we call T_{min} and discarded in diagnosing the timescale behavior because it is not representative of the average expansion/contraction over longer periods of time. We start by interpreting what we see in the μ vs. T plots that appear in the analysis of each example. We will use the $2D$ nonlinear example used in Chapter (3) for which we have the analytical solution.

In Fig. (B.1), $\mu_2^+(T, 30)$ is the curve, which shows the finite time Lyapunov exponent of the vector, which has the largest Lyapunov exponent for the averaging time T at point x such that $x_1 = 30$. It does not show the finite time Lyapunov exponent of an individual vector. Each point on the curve corresponds to another vector. Other two curves in Fig. (B.1) show the finite time Lyapunov exponents of the vectors $l_2^+(0.05, 30)$ and $l_2^+(0.1, 30)$. Note that they touch the $\mu_2^+(T, 30)$ curve at time 0.05 and 0.1 respectively. This is because for the averaging time $T = 0.05$, $l_2^+(0.05, 30)$ is the vector that has the largest finite time Lyapunov exponent. Thus, the point on the $\mu_2^+(T, 30)$ curve at $T = 0.05$ corresponds to the Lyapunov exponent of that vectors. Similarly, $l_2^+(0.1, 30)$ is the vector which is supposed to have largest exponent for $T = 0.1$.

When the finite time Lyapunov exponents converge, all the finite time Lyapunov exponents approach their infinite time limits as the averaging time increases. Since the infinite

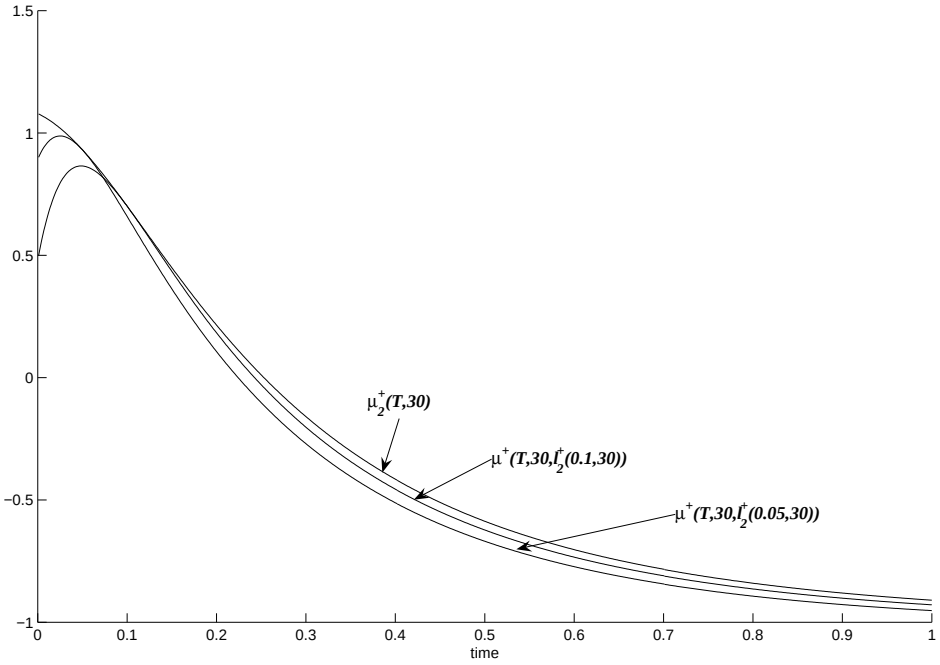

Figure B.1: Interpretation of μ vs. T plots.

time Lyapunov exponents are constant along the trajectories, the finite time Lyapunov exponents at different points on the same trajectory converge to the same value. However, they may feature different transient characteristics during the period $[0, T_{min}]$, because the Lyapunov exponents tend to the eigenvalues of $\frac{J(x)^T+J(x)}{2}$ as the averaging time tends to zero [58]. This feature is illustrated in Fig. (B.2) in which the finite time Lyapunov exponent $\mu_2^+(T,x)$ vs. the averaging time curves and the maximum eigenvalue of $\frac{J(x)^T+J(x)}{2}$ are shown at points with different x_1. Note that the $\mu_2^+(T,x)$ curves are bounded from above by the maximum eigenvalue of $\frac{J(x)^T+J(x)}{2}$ and $\mu_2^+(T,x)$ curves approach to -1 at each x_1 as the averaging time increases. Similarly, $\mu_2^+(T,x)$ curves are bounded from below by the minimum eigenvalue of $\frac{J(x)^T+J(x)}{2}$. Thus, the maximum and minimum eigenvalues of $\frac{J(x)^T+J(x)}{2}$ are bounds for the finite time Lyapunov exponents. But, they are tight only for very small averaging times.

Another question that comes up during the study of the transients is what is happening

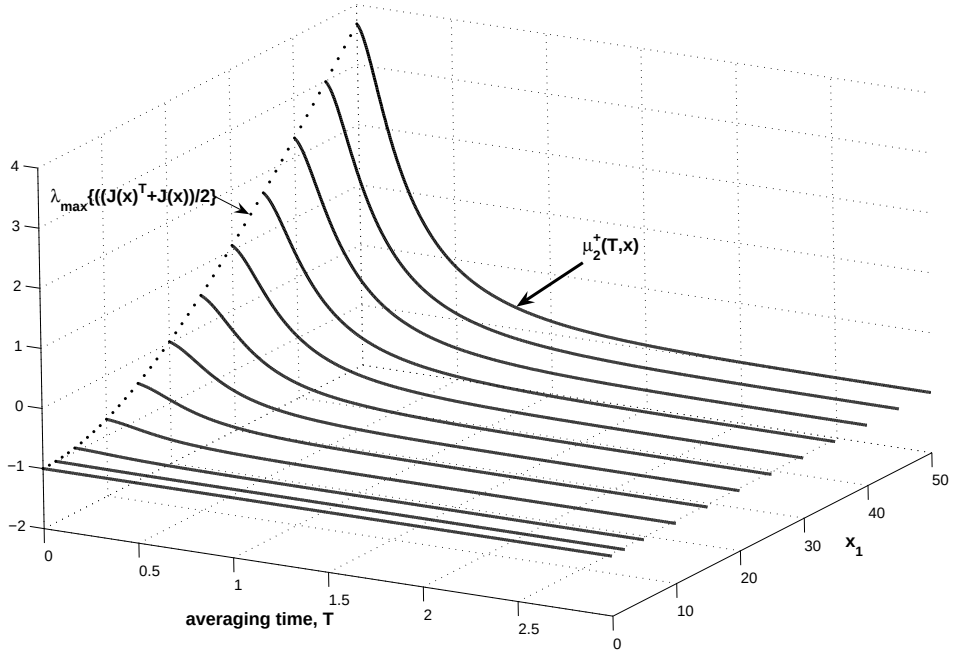

Figure B.2: $\mu_2^+(T,x)$ curves vs. T and x compared with the maximum eigenvalue of $\frac{J(x)^T+J(x)}{2}$.

during the transient period $[0, T_{min}]$? For example, what does a positive exponent for $T = 0.1$ mean although there is no positive exponents for longer averaging times? The answer is obvious from the definition of the finite time Lyapunov exponents: There are some directions in which the initial perturbations grow exponentially until $T = 0.1$. However, if that perturbation is propagated for a longer time the perturbation shrinks. This can be easily verified by taking a small initial perturbation in the direction of, e.g., $l_2^+(0.1, x)$, propagating both points x and $x + \epsilon l_2^+(0.1, x)$ for 0.1 units of time and comparing the final perturbation with the initial perturbation.

Appendix C

A refinement procedure for the new basis vectors

Although finite time Lyapunov vectors converge very quickly to infinite time vectors which identify the correct fast and slow directions, they can be made more accurate by using a refinement procedure without increasing the averaging times. The refinement technique proposed is the one used in Computational Singular Perturbation (CSP) method [44, 45]. The eigenvectors are used as the starting basis in CSP method. We propose to start with finite time Lyapunov vectors instead of eigenvectors.

For an LTV system in the singularly perturbed form

$$\begin{pmatrix} \dot{p} \\ \epsilon\dot{q} \end{pmatrix} = \begin{pmatrix} A_{11} & A_{12} \\ A_{21} & A_{22} \end{pmatrix} \begin{pmatrix} p \\ q \end{pmatrix}, p \in \mathcal{R}^{n^s},\ q \in \mathcal{R}^{n^f} \tag{C.1}$$

where $A_{ij}(t)$ satisfy $i)$ $Re\ \lambda(A_{22}(t)) \leq -c_1 < 0 \quad \forall t \in [0, T_c]$, $ii)$ $A_{ij}(t)$ is continuously differentiable and bounded on $[0, T_c]$, $iii)$ $\dot{A}_{12}(t)$, $\dot{A}_{21}(t)$, $\dot{A}_{22}(t)$ are bounded on $[0, T_c]$; then there exists an $\epsilon^* > 0$ such that for all $\epsilon \in (0, \epsilon^*)$ and there exist continuously differentiable matrices G and H, bounded on $[0, T_c]$, satisfying

$$\begin{aligned} \epsilon\dot{G} &= A_{22}G - A_{21} - \epsilon G(A_{11} - A_{12}G) \\ -\epsilon\dot{H} &= H\tilde{A}_1 - A_{12} - \epsilon\tilde{A}_2 H \end{aligned} \tag{C.2}$$

where $\tilde{A}_1 = A_{22} + \epsilon G A_{12}$ and $\tilde{A}_2 = A_{11} - A_{12}G$. Moreover, $G(t) = G_0(t) + O(\epsilon)$ and $H(t) = H_0(t) + O(\epsilon)$ where $G_0 = A_{22}^{-1}A_{21}$ and $H_0 = A_{12}A_{22}^{-1}$.

Then, the Lyapunov transformation

$$\begin{aligned}\begin{pmatrix} \tilde{p} \\ \tilde{q} \end{pmatrix} &= \begin{pmatrix} I_{n^s} - \epsilon H(t)G(t) & -\epsilon H(t) \\ G(t) & I_{n^{fc}+n^{fe}} \end{pmatrix} \begin{pmatrix} p \\ q \end{pmatrix} \\ &= T^{-1}(t) \begin{pmatrix} p \\ q \end{pmatrix}\end{aligned} \tag{C.3}$$

brings the original system into the form

$$\begin{aligned}\dot{\tilde{p}} &= [A_{11}(t) - A_{12}(t)G(t)]\tilde{p} \\ \epsilon\dot{\tilde{q}} &= [A_{22}(t) - \epsilon G(t)A_{12}(t)]\tilde{q}\end{aligned} \tag{C.4}$$

Then, $T(t) = \begin{pmatrix} I_{n^s} & \epsilon H(t) \\ -G(t) & I_{n^{fc}+n^{fe}} - \epsilon G(t)H(t) \end{pmatrix}$. Calculation of $G(t)$ and $H(t)$ in series form shows that higher-order approximations of $G(t)$ and $H(t)$ is a repetition of the first-order approximations. In theory, the series expressions for $G(t)$ and $H(t)$ can be used efficiently. But, in application first order approximations are more practical and lead to $T^{-1}(t) = \begin{pmatrix} I_{n^s} - \epsilon H_0 G_0 & -\epsilon H_0 \\ G_0 & I_{n^{fc}+n^{fe}} \end{pmatrix}$. This transformation, $A_{k+1} = A_k T^{-1}$ with A_1 is as in Eq.(C.1), will not bring the starting directions to the true fast and slow directions. Successive applications of this refinement turn them to the correct directions. This transformation holds for all ϵ, particularly for $\epsilon = 1$ for our purposes. Although the first assumption restricts the use of this procedure to the system having only fast stable behavior, there is an extension of this theorem which enables it to be used for systems with fast unstable modes [34].

Since we are also interested in Hamiltonian systems the condition on the eigenvalues of $A_{22}(t)$ being less than zero is too restrictive. In [34], it is shown that the same transformation can be used if $A_{22}(t)$ satisfies the following alternative assumption instead of the first assumption. Alternative assumption: There exists a nonsingular continuously differentiable matrix $W(t)$ such that

$$W^{-1}(t)A_{22}(t)W(t) = \begin{pmatrix} D_1(t) & 0 \\ 0 & D_2(t) \end{pmatrix} \quad \forall t \in [t_0, t_f] \tag{C.5}$$

where $Re\ \lambda(D_1(t)) \leq -c_1$ and $Re\ \lambda(D_2(t)) \geq c_2$. The assumption of the existence of the transformation $W(t)$ holds whenever the eigenvalues of a continuously differentiable matrix $A_{22}(t)$ are bounded away from the imaginary axis.